UNIVERSIDADE EVANGÉLICA DE GOIÁS – UniEVANGÉLICA
PROGRAMA DE PÓS-GRADUAÇÃO EM CIÊNCIAS FARMACÊUTICAS, FARMACOLOGIA E TERAPÊUTICA

Áureo Barbosa de Souza

ESTUDO TEÓRICO E EXPERIMENTAL DA TOXICOLOGIA DOS FUNGICIDAS TRIADIMEFON E TRIADIMENOL: DA ESTRUTURA MOLECULAR AOS IMPACTOS CITOGENÉTICOS

Anápolis-GO, 2026

ÁUREO BARBOSA DE SOUZA

ESTUDO TEÓRICO E EXPERIMENTAL DA TOXICOLOGIA DOS FUNGICIDAS TRIADIMEFON E TRIADIMENOL: DA ESTRUTURA MOLECULAR AOS IMPACTOS CITOGENÉTICOS

Dissertação apresentada à Universidade Evangélica de Goiás - UniEVANGÉLICA, para obtenção do Título de Mestre em Ciências Farmacêuticas, Farmacologia e Terapêutica.

Linha de Pesquisa: Farmacologia Clínica e Terapêutica, Farmacologia Básica e Experimental, Aspectos Fitoquímicos e Farmacológicos de Produtos Naturais e Sintéticos.

Orientador: Prof. Dr. Antônio Sérgio Nakao Aguiar

Anápolis-GO, 2026

S729

Souza, Áureo Barbosa de.

Estudo teórico e experimental da toxicologia dos fungicidas Triadimefon e Triadimenol: da estrutura molecular aos impactos citogenéticos / Áureo Barbosa de Souza - Anápolis: Universidade Evangélica de Goiás, 2026.

96 p.; il.

Orientador: Prof. Dr. Antônio Sérgio Nakao Aguiar.

Dissertação (mestrado) – Programa de pós-graduação em Ciências Farmacêuticas – Universidade Evangélica de Goiás, 2026.

1. Triazóis 2. *In Sílico* 3. Citogenicidade. 4. *Eisenia fetida* I. Aguiar, Antonio Sérgio Nakao. II. Título.

CDU 615

Catalogação na Fonte
Elaborado por Hellen Lisboa de Souza CRB1/1570

ÁUREO BARBOSA DE SOUZA

ESTUDO TEÓRICO E EXPERIMENTAL DA TOXICOLOGIA DOS FUNGICIDAS TRIADIMEFON E TRIADIMENOL: DA ESTRUTURA MOLECULAR AOS IMPACTOS CITOGENÉTICOS

Dissertação apresentada à Universidade Evangélica de Goiás - UniEVANGÉLICA, para obtenção do Título de Mestre em Ciências Farmacêuticas, Farmacologia e Terapêutica.

Linha de Pesquisa: Farmacologia Clínica e Terapêutica, Farmacologia Básica e Experimental, Aspectos Fitoquímicos e Farmacológicos de Produtos Naturais e Sintéticos.

Aprovada em_____

Banca examinadora

Documento assinado digitalmente
gov.br
ANTONIO SERGIO NAKAO DE AGUIAR
Data: 01/06/2026 09:20:50-0300
Verifique em https://validar.iti.gov.br

_____ _____

Prof. (Dr) (Antônio Sérgio Nakão de Aguiar)

Universidade Evangélica de Goiás (UniEvangélica)

Presidente

Documento assinado digitalmente
gov.br
LEONARDO LUIZ BORGES
Data: 01/06/2026 11:21:02-0300
Verifique em https://validar.iti.gov.br

_____

Prof. (Dr). (Leonardo L. Borges)

Pontifícia Universidade Católica de Goiás (PUC)

Documento assinado digitalmente
gov.br
LUCIMAR PINHEIRO ROSSETO
Data: 01/06/2026 09:30:20-0300
Verifique em https://validar.iti.gov.br

_____ _____

Prof. (Dra). (Lucimar Pinheiro Rosseto)

Universidade Evangélica de Goiás (UniEvangélica)

DEDICATÓRIA

Dedico este trabalho à minha família (esposa e filhos), pelo apoio incondicional, compreensão e incentivo ao longo desses dois anos de estudo.

Aos meus colegas de trabalho e a todos que, de alguma forma, contribuíram para que este objetivo fosse alcançado, oferecendo apoio, confiança e palavras de encorajamento, expresso minha sincera gratidão.

AGRADECIMENTOS

Agradeço, primeiramente, a Deus, pela vida, saúde e pela força necessária para superar os desafios ao longo desta trajetória acadêmica.

À minha família, pelo apoio incondicional, compreensão, incentivo constante e por acreditarem em mim mesmo nos momentos de maior dificuldade.

Ao meu orientador, professor (Dr) Antônio Sérgio Nakao Aguiar, pela dedicação, paciência, contribuições valiosas e pela orientação segura e incondicional ao longo do desenvolvimento deste trabalho, sem o trabalho incansável dele isso não seria possível.

Aos professores do programa de pós-graduação, pelos conhecimentos compartilhados e pela contribuição significativa para minha formação acadêmica e profissional.

Aos colegas de curso, pelo companheirismo, trocas de experiências e apoio durante essa caminhada.

Aos parceiros pesquisadores: Ronaldo G. Freitas Junior, Ana L. M. Monteiro, Leonardo R. de Almeida, Lucas D. Dias, Lucas B. Ribeiro de Carvalho, Hamilton B. Napolitano, Amanda Silva Fernandes, Marcelino Benvindo de Souza, Luciane Madureira de Almeida, Octavio Luiz Franco, Eliza Flávia Luiz Cardoso Bailão, Leonardo Luiz Borges. Obrigado pelo conhecimento compartilhado.

À Universidade Evangélica de Goiás e ao programa de pós-graduação, pela oportunidade de crescimento acadêmico e pelo suporte oferecido.

Nas pessoas de meus gestores Cristiano Veloso e Ulisses Martins, aqui representando à Fresenius Kabi Brasil, pela bolsa a mim concedida, sem ela eu não teria conseguido ingressar e concluir o mestrado em ciências farmacêuticas.

Por fim, a todos que, direta ou indiretamente, contribuíram para a realização deste trabalho, minha sincera gratidão.

“Na natureza nada se cria, nada se perde, tudo se transforma.”
Antoine Lavoisier

LISTA DE FIGURAS

LISTA DE ABREVIATURAS

Acetil-CoA	Acetil Coenzima A
AChE	Acetilcolinesterase
ADME	Absorção, Distribuição, Metabolismo e Excreção
Ars	Aromatic Rings
CIF	Crystallographic Information File
CSD	Cambridge Structural Database
DFT	Density Functional Theory
DMIs	Demethylation Inhibitors
FF-MAS	Follicle Fluid-Meiosis Activating Sterol
FRAC	Fungicide Resistance Action Committee
FTs	Fungicidas Triazólicos
HBAs	Hydrogen Bond Acceptors
HBDs	Hydrogen Bond Donors
HOMO	Highest Occupied Molecular Orbital
IC	Inhibitory Concentration
LDM	Lanosterol Desmetilase
LUMO	Lowest Unoccupied Molecular Orbital
MEP	Molecular Electrostatic Potential
KS	Kohn-Sham
PDB	Protein Data Bank
QTAIM	Quantum theory of atoms in molecules
SBI	Sterol Biosynthesis Inhibitors
SFP	Shared Feature Pharmacophore
TF	Triadimefon
TN	Triadimenol

RESUMO

A necessidade de conciliar a produtividade agrícola com a proteção ambiental e a saúde pública tem se tornado cada vez mais evidente, especialmente diante do uso intensivo de agrotóxicos e de seus potenciais efeitos adversos, como desregulação endócrina, toxicidade hepática e impactos negativos sobre organismos não alvo. O presente estudo investigou a reatividade química, as interações supramoleculares, os efeitos citogenotóxicos e o perfil ecotoxicológico de fungicidas triazólicos, amplamente utilizados na agricultura e comercializados predominantemente como misturas estereoisoméricas, o que aumenta a complexidade da avaliação de riscos ambientais e biológicos. A metodologia adotada baseou-se em uma abordagem computacional integrada, utilizando ferramentas de Mecânica Quântica fundamentadas na Teoria do Funcional de Densidade para a determinação de descritores de reatividade global e local, incluindo orbitais de fronteira (ocupado de maior energia e desocupado de menor energia) e funções de Fukui. A análise do estado sólido foi conduzida por meio das técnicas de Superfície de *Hirshfeld*, Teoria Quântica de Átomos em Moléculas (QTAIM) e Orbitais Naturais de Ligação, permitindo uma caracterização detalhada das interações intermoleculares na estrutura do cristal. Os efeitos citogenotóxicos em linfócitos humanos foram investigados por meio do teste de exclusão do azul de tripan e do ensaio cometa. Complementarmente, utilizaram-se as ferramentas *BioTransformer e DIGEP-Pred* para elucidar as vias metabólicas de destoxificação desses xenobióticos e avaliar seus efeitos na transcrição gênica, respectivamente. Adicionalmente, realizaram-se predições farmacocinéticas e toxicológicas (*in silico*) de parâmetros farmacocinéticos, bem como de toxicidade ambiental e humana, empregando-se os servidores *SwissADME e ProTox-3.0*. Os resultados, organizados em três artigos científicos com foco nos fungicidas triadimefon e triadimenol, evidenciaram diferenças significativas na reatividade química e no comportamento biológico desses compostos. Observou-se que a biotransformação do triadimefon em seu metabólito estereoisomérico triadimenol, caracterizada pela substituição do grupo carbonila por uma hidroxila e pela introdução de novos centros quirais, promove alterações sistemáticas no potencial eletrostático molecular e nos índices de reatividade. Essas variações estruturais fundamentam o comportamento distinto de ambos os compostos em sistemas biológicos observados experimentalmente, incluindo danos ao DNA em linfócitos humanos e efeitos genotóxicos em organismos como *Eisenia fetida* (Savigny). Em conjunto, os resultados obtidos em ensaios biológicos indicam que a integração da mecânica quântica com ferramentas *in silico* constitui uma estratégia robusta para a compreensão da toxicodinâmica desses fungicidas. Embora sejam necessárias investigações adicionais, a exposição a esses fungicidas triazólicos, em concentrações ambientalmente relevantes, induziu significativamente quebras nas cadeias de DNA em linfócitos, além de resultar na redução da biomassa de *Eisenia fetida* (Savigny), indicando efeitos subletais associados ao estresse metabólico. Ao integrar mecânica quântica, toxicologia preditiva e experimental, este trabalho poderá apoiar em novos estudos, aprimoramento de análises de risco, desenvolvimento de práticas agroquímicas mais seguras e sustentáveis, alinhadas à proteção da saúde humana e ambiental.

Palavras-chave: Triazóis; *In Silico*; Citogenicidade, *Eisenia fetida*,

ABSTRACT

The need to reconcile agricultural productivity with environmental protection and public health has become increasingly evident, especially in light of the intensive use of pesticides and their potential adverse effects, such as endocrine disruption, hepatic toxicity, and negative impacts on non-target organisms. This study investigated the chemical reactivity, supramolecular interactions, cytogenotoxic effects, and ecotoxicological profile of triazole fungicides, widely used in agriculture and predominantly marketed as stereoisomeric mixtures, which increases the complexity of environmental and biological risk assessment. The methodology adopted was based on an integrated computational approach, using Quantum Mechanics tools grounded in Density Functional Theory to determine global and local reactivity descriptors, including frontier orbitals (highest occupied and lowest unoccupied) and Fukui functions. Solid-state analysis was conducted through Hirshfeld Surface techniques, Quantum Theory of Atoms in Molecules (QTAIM), and Natural Bond Orbitals, allowing detailed characterization of intermolecular interactions in the crystal structure. Cytogenotoxic effects in human lymphocytes were investigated using the trypan blue exclusion test and the comet assay. Additionally, BioTransformer and DIGEP-Pred tools were employed to elucidate detoxification metabolic pathways of these xenobiotics and to assess their effects on gene transcription, respectively. Pharmacokinetic and toxicological predictions (*in silico*) of pharmacokinetic parameters, as well as environmental and human toxicity, were performed using SwissADME and ProTox-3.0 servers. The results, organized into three scientific articles focusing on the fungicides triadimefon and triadimenol, revealed significant differences in the chemical reactivity and biological behavior of these compounds. It was observed that the biotransformation of triadimefon into its stereoisomeric metabolite triadimenol, characterized by the substitution of the carbonyl group with a hydroxyl and the introduction of new chiral centers, promotes systematic changes in the molecular electrostatic potential and reactivity indices. These structural variations underpin the distinct behavior of both compounds in biological systems observed experimentally, including DNA damage in human lymphocytes and genotoxic effects in organisms such as *Eisenia fetida* (Savigny). Altogether, the results obtained in biological assays indicate that the integration of quantum mechanics with *in silico* tools constitutes a robust strategy for understanding the toxicodynamics of these fungicides. Although further investigations are necessary, exposure to these triazole fungicides at environmentally relevant concentrations significantly induced DNA strand breaks in lymphocytes, as well as reduced the biomass of *Eisenia fetida* (Savigny), indicating sublethal effects associated with metabolic stress. By integrating quantum mechanics, predictive toxicology, and experimental approaches, this work may support new studies, improve risk analyses, and foster the development of safer and more sustainable agrochemical practices aligned with the protection of human and environmental health.

Keywords: Triazoles; *In silico*; Cytogenicity; *Eisenia fetida*

SUMÁRIO

1. INTRODUÇÃO

A agricultura desempenha um papel fundamental na economia global, figurando no Brasil como uma das principais bases para a diversificação produtiva. Para garantir rendimentos elevados e estabilidade na produção, o uso de agrotóxicos (defensivos agrícolas ou pesticidas) tornou-se uma prática amplamente difundida, apesar de seus efeitos nocivos serem documentados há mais de cinquenta anos. Atualmente, o país consolida-se como um dos líderes mundiais no consumo desses insumos químicos, com um volume estimado em cerca de 500 mil toneladas anuais, abrangendo classes como herbicidas, inseticidas e fungicidas (Botelho *et al*., 2020).

Essas substâncias, concebidas para prevenir, destruir ou mitigar infestações de pragas, desempenham um papel determinante na proteção das culturas contra insetos, ervas daninhas e fungos (Cassal *et al*., 2014). No entanto, sua natureza como moléculas bioativas está associada à possibilidade de efeitos adversos ou tóxicos, dependendo da dose e do organismo exposto (Roman *et al*., 2021). Essa toxicidade é inerente à sua função: são agentes biocidas desenvolvidos para eliminar organismos indesejados. Contudo, o uso intensivo e contínuo desses compostos gera alta contaminação ambiental. A pulverização em sistemas abertos inviabiliza medidas efetivas de contenção, resultando na degradação de matrizes como o solo, a água e o ar, além de promover a exposição indevida de seres humanos e da fauna local (Botelho *et al*., 2020).

Os defensivos podem ser classificados conforme sua função, composição química e modo de ação, destacando-se os inseticidas, herbicidas, fungicidas, rodenticidas, nematicidas, entre outros (Pauly Ribas; Santos Matsumura, 2009; Peres; Moreira, 2003). Dentre as classes mais utilizadas no Brasil, os fungicidas representam 16,1% do total. Especificamente, os Fungicidas Triazólicos (FTs), ou Inibidores da Desmetilação (DMIs - *Demethylation inhibitors*), constituem uma classe essencial na proteção de culturas como cereais, frutas e vegetais, devido ao seu amplo espectro de ação sistêmica (Liu *et al*., 2024; Lv *et al*., 2017; Roman *et al*., 2021). Estima-se que os FTs detenham entre 20% e 25% do mercado global de fungicidas (Ishii, 2023; Wang *et al*., 2024).

O mecanismo de ação dos FTs reside na inibição da enzima lanosterol 14α-desmetilase, essencial para a biossíntese do ergosterol, componente vital da membrana celular fúngica (Nasonov; Yakuba, 2024; Shi *et al*., 2024; Sun *et al*., 2023). Embora eficazes contra patógenos, a estabilidade química e a baixa biodegradabilidade desses compostos conferem-lhes uma persistência ambiental que levanta sérias preocupações sobre os impactos em organismos não

alvo (Roman et al., 2021; Zou *et al*., 2024). No solo, a aplicação desses fungicidas, mesmo em doses recomendadas, pode afetar drasticamente a microbiota e a atividade enzimática (Wang *et al*., 2025). Estudos indicam que inibidores da biossíntese de esteróis (SBI - *Sterol Biosynthesis Inhibitors*) reduzem a abundância e a diversidade de microrganismos edáficos[1].

Ademais, a baixa adsorção de triazóis como flutriafol, miclobutanil e triadimenol, aliada à sua persistência, representa um risco significativo de lixiviação para águas subterrâneas (Aliste *et al*., 2021). Ecossistemas aquáticos são severamente impactados; resíduos de tebuconazole, por exemplo, são frequentemente detectados em águas superficiais, perturbando funções ecológicas essenciais. Além disso, os DMIs impactam as comunidades microbianas do néctar floral, favorecendo o crescimento bacteriano em detrimento de leveduras, o que pode alterar a dinâmica de polinização (Botelho et al., 2020; Quevedo-Caraballo; Roldán; Álvarez-Pérez, 2024).

Sob a ótica da saúde pública, os FTs são classificados como potencialmente tóxicos, com resíduos detectados em alimentos e matrizes ambientais (Chen *et al*., 2024). Evidências toxicológicas apontam para efeitos adversos como toxicidade hepática, reprodutiva e desregulação endócrina (Heise *et al*., 2018; Wang *et al*., 2024). A exposição ao tebuconazol e hexaconazol pode induzir disfunções tireoidianas e cardiovasculares em estágios iniciais de desenvolvimento (Liu *et al*., 2024), enquanto o triadimefon (TF) apresenta potencial teratogênico comprovado *in vitro* (Li *et al*., 2019).

Um risco emergente e alarmante é a correlação entre o uso de azóis agrícolas e o desenvolvimento de resistência em fungos patogênicos humanos, como o *Aspergillus fumigatus*, dificultando o tratamento de aspergilose invasiva (Ishii, 2023). A avaliação de risco dos FTs é complexa devido à quiralidade e aos efeitos de mistura enantiomérica. Cerca de 84% dos FTs são quirais e introduzidos no ambiente como misturas de enantiômeros (Chen *et al*., 2024). Visto que a toxicidade e a degradação desses fungicidas são determinadas pela sua estereoquímica, a negligência da quiralidade resulta na subestimação dos riscos reais associados a cada enantiômero (Zhang *et al*., 2018). Por fim, a exposição combinada a diferentes agrotóxicos pode gerar efeitos sinérgicos ou aditivos, exigindo que a toxicologia de misturas considere que compostos com modos de ação semelhantes podem atuar conjuntamente, mesmo em doses baixas (Heise *et al*., 2018; Knebel *et al*., 2018).

Nessa perspectiva, os fungicidas triadimefon e triadimenol foram selecionados como modelos de estudo devido à sua estereoquímica, estreita relação metabólica e expressiva

[1] Refere-se ao que é próprio ou relativo ao solo. Microrganismos edáficos são aqueles que compõem a microbiota do solo, sendo essenciais para a ciclagem de nutrientes e o equilíbrio do ecossistema terrestre.

presença em sistemas agrícolas brasileiros. A redução do triadimefon ao triadimenol, tanto no ambiente quanto em organismos vivos, torna a investigação conjunta dessas duas moléculas essencial para melhor compreender o ciclo de contaminação e a progressão da toxicidade. Além disso, a relevância desses compostos reside em sua estabilidade química e no histórico de detecção frequente em matrizes de solo e água, o que demanda uma análise mais detalhada de suas propriedades moleculares e de seus impactos em diferentes níveis biológicos.

Apesar dos avanços na elucidação do comportamento químico e biológico desses compostos, observa-se uma lacuna científica na integração de dados de reatividade química com respostas biológicas específicas em organismos da edafofauna[2] e células humanas. A maioria dos estudos foca ou na caracterização química isolada ou em ensaios macroscópicos, carecendo de uma abordagem multidisciplinar que conecte as propriedades moleculares *in silico* aos efeitos citotóxicos e ecotoxicológicos. Diante disso, este trabalho norteia-se pela hipótese de que as diferenças estruturais entre o triadimefon e seu metabólito triadimenol conferem perfis de reatividade química distintos, os quais se correlacionam diretamente com variações na estabilidade genômica de linfócitos humanos e na integridade de organismos bioindicadores do solo.

Este estudo utilizou ferramentas computacionais para a análise da reatividade química e propriedades toxicológicas de fungicidas triazólicos, ao passo que examinou o comportamento citotóxico e ecotoxicológico desses compostos. Para isso, utilizou-se cálculos de mecânica quântica baseados na Teoria do Funcional de Densidade (DFT - *Density Functional Theory*) e ensaios *in silico* para o triadimefon e o triadimenol, ao mesmo tempo em que empregou ensaios biológicos com linfócitos humanos e *Eisenia fetida* para a análise do perfil de toxicidade. O conjunto desses dados fornece insights sobre as interações moleculares e os impactos biológicos desses compostos.

[2] Refere-se ao conjunto de animais que vivem e habitam no solo.

2. OBJETIVOS

2.1. Objetivo geral

Avaliar a reatividade química, as interações intermoleculares, bem como os efeitos tóxicos dos fungicidas triazólicos triadimefon e triadimenol, por meio de ensaios *in silico, in vitro* e *in vivo.*

2.2. Objetivos específicos

- Determinar os descritores de reatividade química do triadimefon e do triadimenol utilizando métodos de mecânica quântica;
- Avaliar as interações dos arranjos supramoleculares entre as moléculas estudadas e seus alvos biológicos;
- Investigar os efeitos citogenotóxicos do triadimefon e triadimenol em linfócitos humanos;
- Avaliar os efeitos genotóxicos, mutagênicos e na biomassa de minhocas da espécie *Eisenia fetida.*

3. EMBASAMENTO TEÓRICO

3.1. Os fungicidas

Na agricultura moderna, os pesticidas constituem ferramentas essenciais para salvaguardar a produtividade e a qualidade das culturas, suprimindo pressões bióticas como insetos, fitopatógenos e plantas daninhas (Aliste *et al*., 2021). No entanto, devido à sua natureza bioativa inerente, concebida para mitigar diversas espécies, tais compostos apresentam toxicidade intrínseca (Roman *et al*., 2021). Esses agentes químicos, naturais ou sintéticos, interagem com sistemas biológicos influenciando processos fisiológicos e patológicos. Na agricultura, são estrategicamente classificados em três grandes grupos: inseticidas, herbicidas e fungicidas.

Os fungicidas, especificamente, podem ser categorizados conforme o princípio de controle, mobilidade na planta, alvo biológico, modo de ação e composição química (GARCIA, 1999). Quanto ao princípio de controle, as estratégias dividem-se em: preventiva; que antecede o aparecimento da doença; curativa; que atua na eliminação do fungo após a infecção; e erradicante; utilizada para suprimir a infecção existente e impedir sua disseminação.

Sob a ótica da mobilidade, os fungicidas são classificados como: de contato; que agem restritamente no local de aplicação, ou sistêmicos; que são absorvidos e translocados internamente pelos tecidos vegetais (FRAC, 2024). O modo de ação, por sua vez, define a forma como o composto interfere no metabolismo fúngico, incluindo a inibição da biossíntese de esteróis, a síntese de proteínas e ácidos nucleicos, ou a interrupção da respiração celular (Bartlett *et al*., 2002; Leroux, 2007).

O Comitê de Ação à Resistência a Fungicidas (FRAC – *Fungicide Resistance Action Committee*) cataloga diversos compostos organizados em grupos de acordo com o seu modo de ação, mecanismo de resistência e estrutura química. Essa classificação é fundamental para o manejo integrado de doenças, permitindo a alternância de princípios ativos para evitar a seleção de populações fúngicas resistentes. As principais classes de fungicidas utilizadas atualmente, seus alvos biológicos e exemplos de grupos químicos estão sintetizados no Quadro 1.

Quadro 1 - Classificação dos fungicidas segundo o FRAC 2025.

Modo de Ação (MoA)	Código FRAC	Grupo Químico	Alvo Biológico
A: Síntese de Ácidos Nucleicos	4	Fenilamidas	Síntese de RNA
B: Mitose e Divisão Celular	1	Benzimidazóis	Montagem de β-tubulina
C: Respiração	7	Carboxamidas (SDHI)	Succinato desidrogenase
	11	Estrobilurinas (QoI)	Citocromo bc1 (sítio Qo)
	21	Quinonas (QiI)	Citocromo bc1 (sítio Qi)
D: Síntese de Proteínas	2	Anilinopirimidinas	Biossíntese de aminoácidos
E: Transdução de Sinal	13	Quinofenos	Via de sinalização osmótica
F: Lipídios e Membrana	28	Carbamatos	Integridade da membrana
G: Biossíntese de Esteróis	3	Triazóis (DMI)	Biossíntese de Ergosterol
H: Biossíntese de Parede Celular	40	CAA	Síntese de celulose
I: Síntese de Melanina	16.1	MBI-R (Redutase)	Redução da melanina
	16.2	MBI-D (Desidratase)	Desidratação da melanina
M: Ação Multissítio	M01 a M12	Inorgânicos, Nitrilas, ditiocarbamatos	Inibição multienzimática
P: Indutores de Defesa da Planta	P01 a P08	Benzotiadiazóis, Fosfonatos	Indução de Resistência
BM: Biológicos	BM	Agentes Microbianos e Extratos	Múltiplos processos

Fonte: Adaptado de FRAC (2025).

Dentre as classes de sítio de ação específico destacadas no Quadro 1, as estrobilurinas (Grupo 11) derivam de compostos naturais encontrados no fungo *Strobilurus tenacellus*. Sua estrutura básica inclui a subunidade metoxiacrilato (Figura 1), essencial para a atividade biológica. Esse grupo liga-se ao sítio de ação no complexo III da cadeia de transporte de elétrons mitocondrial, inibindo a respiração celular do patógeno (Bartlett *et al*., 2002).

Figura 1 - Estrutura química da azoxistrobina e do grupo funcional metoxiacrilato

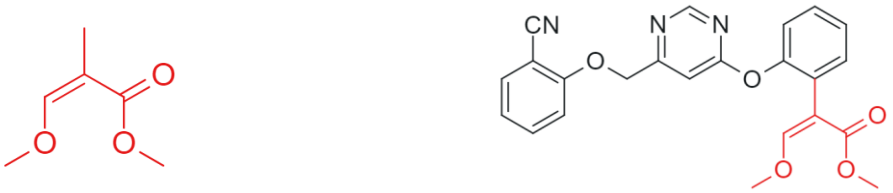

Metoxiacrilato Azoxistrobina

Fonte: Elaborado pelo autor (2025)

Os ditiocarbamatos, apresentam o grupo funcional (-NCS_2), frequentemente formando complexos metálicos com zinco e manganês, Figura 2 (Sarker; Hogarth, 2021). Classificados como fungicidas de contato, atuam inibindo enzimas vitais envolvidas no metabolismo do enxofre e na biossíntese de lipídios (Bansal, 2022).

Figura 2 - Estrutura química do fungicida Ziram e do grupo funcional ditiocarbamato

Ditiocarbamato Ziram

Fonte: Elaborado pelo autor (2025)

Os carbamatos, são identificados pelo grupo funcional ($R_1O(C=O)NR_2R_3$), derivado do ácido carbâmico (NH_2COOH), Figura 3. Embora atuem na proteção fúngica, são amplamente conhecidos por inibir a enzima acetilcolinesterase (AChE), resultando em neurotoxicidade em insetos-alvo (Fukuto, 1990; Lee; Barron, 2016).

Figura 3 - Estrutura molecular do valifenalato e do grupo funcional carbamato

Carbamato Valifenalato

Fonte: Elaborado pelo autor (2025)

Semelhantemente, os benzoimidazóis Figura 4, agem na inibição da síntese de microtúbulos. Ao ligarem-se à tubulina, impedem a divisão celular e o crescimento fúngico (Brent, 1995; Ma; Michailides, 2005). Já as anilinopirimidinas Figura 5, comumente sistêmicas, combinam uma anilina ($C_6H_5NH_2$) com uma pirimidina ($C_4H_4N_2$), atuando como inibidores da biossíntese de metionina (Mahfoudh *et al.,* 2017; FRAC, 2024).

Figura 4 - Estrutura química do benomil e do grupo funcional anel benzoimidazol

Benzoimidazol Benomil

Fonte: Elaborado pelo autor (2025)

Figura 5 - Estruturas químicas do pirimetanil e dos grupos funcionais anilina e pirimidina

Anilina Piridina Pirimetanil

Fonte: Elaborado pelo autor (2025)

3.1.1. Fungicidas triazólicos e o mecanismo DMI

Entre os defensivos, os fungicidas triazólicos destacam-se pela eficácia sistêmica e amplo espectro de ação (Klittich, 2014). Indispensáveis desde a década de 1970, são amplamente empregados em culturas de trigo, milho e hortaliças para controlar ferrugens e oídio[3] (Nagappan; Deresinski, 2007). Segundo o Frac Code List 2024, esta classe pertence aos inibidores de desmetilação, FRAC G1 (DMI), atuando na interrupção da biossíntese do ergosterol (Heise *et al*., 2018; Mercadante *et al*., 2014). O ergosterol é vital para a integridade das membranas fúngicas; sua inibição acarreta defeitos estruturais que culminam na morte do fungo (Peyton; Gallagher; Hashemzadeh, 2015).

Dentro da grande classe dos Inibidores da Biossíntese de Esteróis (SBI), o FRAC subdivide os compostos de acordo com o sítio específico de inibição na via do ergosterol, conforme detalhado no Quadro 2.

Quadro 2 - Classe Inibidores da Biossíntese de Esteróis (SBI), segundo FRAC (2025) continua.

Sítio de Ação	Grupo Químico	Moléculas Ativas
G1: DMI (Inibidores de Desmetilação no C14)	Triazóis	Azaconazol, Bitertanol, Bromuconazol, Ciproconazol, Diclobutrazol, Difenoconazol, Diniconazol, Diniconazol-M, Epoxiconazol, Etaconazol, Fenbuconazol, Fluquinconazol, Flusilazol, Flutriafol, Hexaconazol, Imibenconazol, Ipconazol, Metconazol, Miclobutanil, Penconazol, Propiconazol, Simeconazol, Tebuconazol, Tetraconazol, Triadimefon, Triadimenol, Triticonazol, Uniconazol, Iprentrifluconazol, Mefentrifluconazol.
	Triazolintiona	Protioconazol.
	Imidazóis	Imazalil, Oxpoconazol, Pefurazoato, Procloraz, Triflumizol.
	Pirimidinas	Fenarimol, Nuarimol. Fenarimol, Nuarimol.
	Piridinas	Pirifenox, Pirisoxazol.
	Piperazinas	Triforina.

[3] O oídio (também conhecido como "mofo branco" ou "cinza") é uma das doenças fúngicas mais comuns e reconhecíveis em plantas.

Quadro 2 - Classe Inibidores da Biossíntese de Esteróis (SBI), segundo FRAC (2025) continuação.

Sítio de Ação	Grupo Químico	Moléculas Ativas
G2: Aminas (Δ14-redutase e Δ8→Δ7-isomerase)	Morfolinas Piperidinas Spiroquetalaminas	Aldimorfe, Dodemorfe, Fenpropimorfe, Tridemorfe. Fenpropidina, Piperalin. Espiroxamina.
G3: Inibidores da 3-Keto Redutase	Hidroxianilidas Amino-pirazolinonas	Fenhexamida. Fenpirazamina.
G4: Inibidores da Esqualeno Epoxidase	Alilaminas	Terbinafina, Naftifina.
	Tiocarbamatos	Piributicarbe.

Fonte: Adaptado de FRAC (2025).

Como observado no Quadro 2, os triazóis compõem o grupo mais numeroso dos DMIs (G1). Quimicamente, os triazóis são compostos heterocíclicos de cinco membros contendo três átomos de nitrogênio (Figura 6), ocorrendo como 1,2,3-triazóis (frequentemente farmacológicos) ou 1,2,4-triazóis (majoritariamente agrícolas) (Zhang, 2019).

Figura 6 - Isômeros do anel triazol: representação das formas 1,2,3-triazol e 1,2,4-triazol

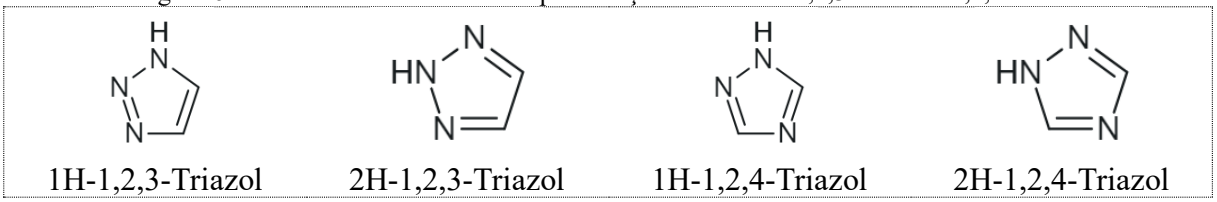

Fonte: Elaborado pelo autor (2025)

Os derivados 1,2,4-triazólicos possuem alta afinidade pela enzima lanosterol 14α-desmetilase (CYP51). O mecanismo envolve a inibição desta monooxigenase do citocromo P450, etapa crucial na formação da membrana celular (Monk *et al.*, 2020). Entre os principais representantes estão o triadimefon (TF) e seu metabólito triadimenol (TN).

Figura 7 - Relação estrutural entre o (TF) e seu principal metabólito, o (TN)

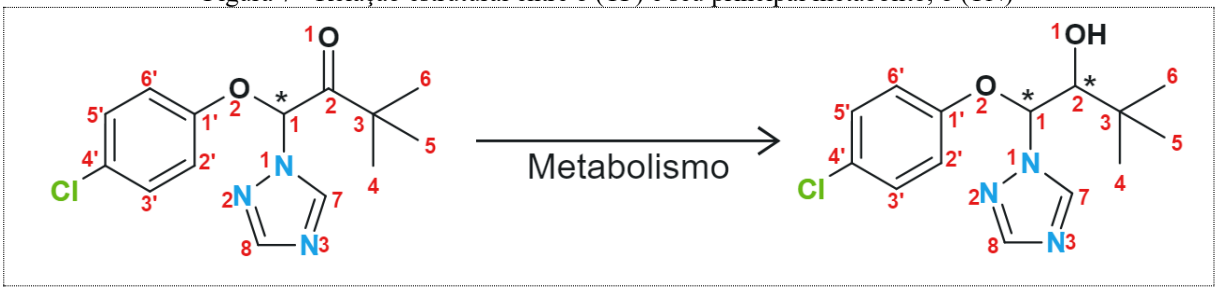

Fonte: Elaborado pelo autor (2025)

O TF possui um centro quiral (*C1), existindo como enantiômeros S-(+) e R-(−). Sua biotransformação em TN introduz um segundo centro quiral (Figura 7), gerando quatro estereoisômeros organizados em dois pares diastereoisoméricos (Figura 8), TN-A (1R,2S e 1S,2R) e TN-B (1R,2R e 1S,2S) (Kenneke *et al*., 2008). Essa assimetria estereoquímica é determinante: o estereoisômero 1S,2R pode apresentar atividade fungicida até 1000 vezes superior aos demais, enquanto o diastereisômero A demonstra maior toxicidade para mamíferos com base nos valores de DL_{50} oral em ratos (Burden *et al*., 1987; Li *et al*., 2014).

Figura 8 - Estruturas dos quatro estereoisômeros do triadimenol organizados por relações de diastereoisometria.

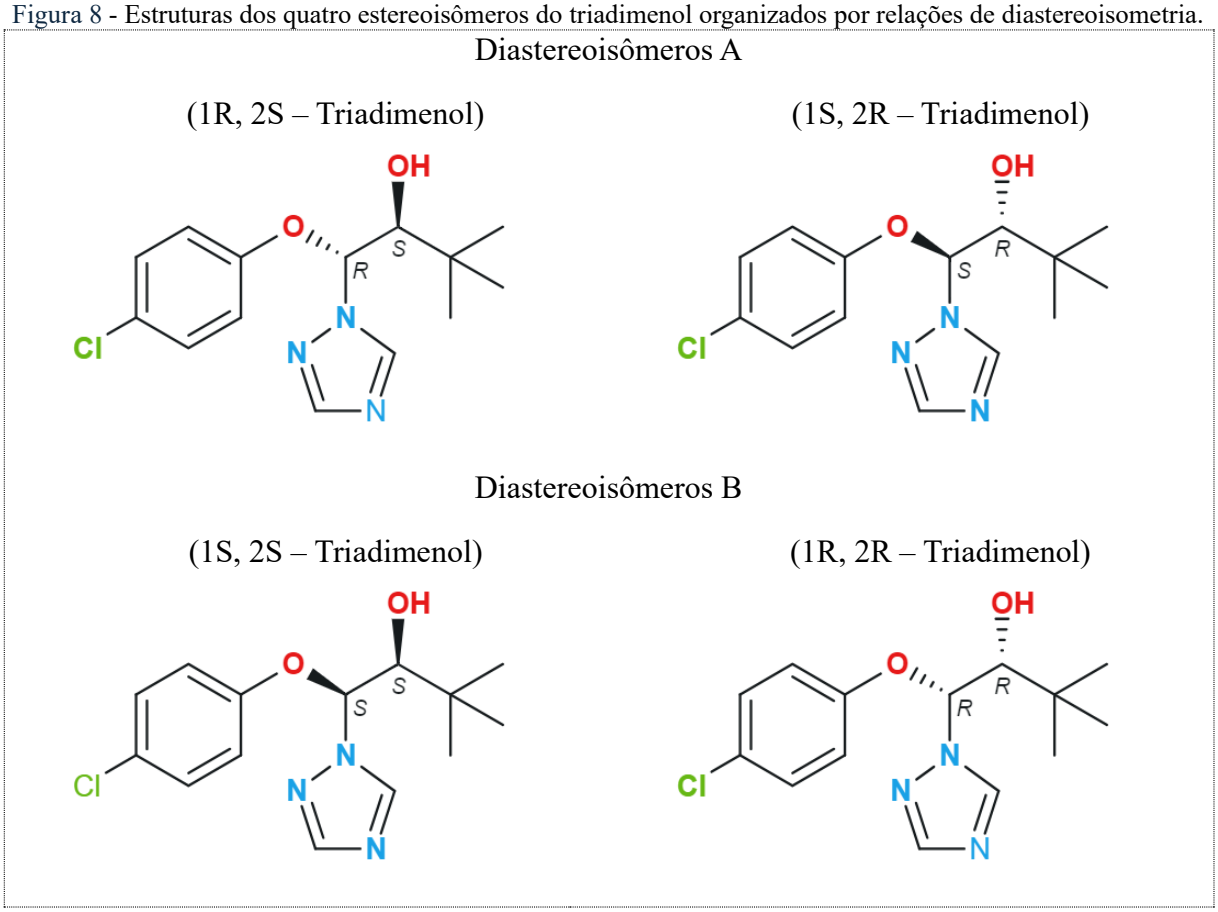

Fonte: Elaborado pelo autor (2025)

3.2. Enzima lanosterol 14α – desmetilase

A enzima lanosterol 14α-desmetilase (LDM), também conhecida como CYP51 ou *Erg11p* (Kaluzhskiy *et al*., 2021), é o alvo biológico primário dos antifúngicos azólicos (imidazóis e triazóis). Em leveduras e diversos patógenos fúngicos, a LDM (Figura 9) atua como uma monooxigenase citocromo P450 pertencente à família CYP51, a qual é altamente conservada sob o ponto de vista evolutivo (Debeljak; Fink; Rozman, 2003; Keniya *et al*., 2018;

Monk *et al*., 2020). Notadamente, esta é a única família do citocromo P450 presente em todos os reinos biológicos (bactérias, fungos, plantas e animais), sendo considerada a ancestral das demais famílias P450. A conservação da sequência de aminoácidos entre as CYP51 eucarióticas é elevada, especialmente nas regiões responsáveis pelo reconhecimento do substrato (Monk *et al*., 2020; Tyndall *et al*., 2016).

Figura 9 - Estrutura cocristalizada do lanosterol ligado à enzima lanosterol 14α-desmetilase, extraída da *Saccharomyces cerevisiae*.

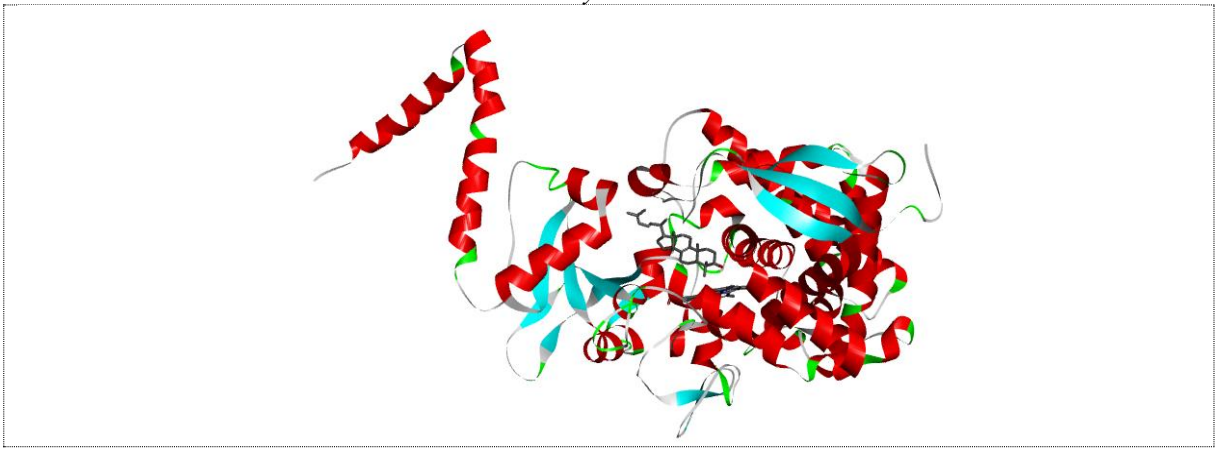

Fonte: Elaborado pelo autor (2025)

A LDM desempenha um papel essencial na via de biossíntese de esteróis, catalisando a remoção oxidativa do grupo metila na posição C14 (14-metil). Embora o substrato comum inicial da biossíntese seja a Acetil Coenzima A (Acetil-CoA), os intermediários variam conforme o organismo: animais e plantas possuem, respectivamente, o lanosterol e o cicloartenol como metabólitos intermediários, enquanto fungos podem utilizar o ergosterol intermediário como precursor (Figura 9) (Kaluzhskiy *et al*., 2021; Monk *et al*., 2020; Tyndall *et al*., 2016).

Figura 10 - Estruturas químicas dos substratos da via de biossíntese de esteróis em animais, plantas e fungos.

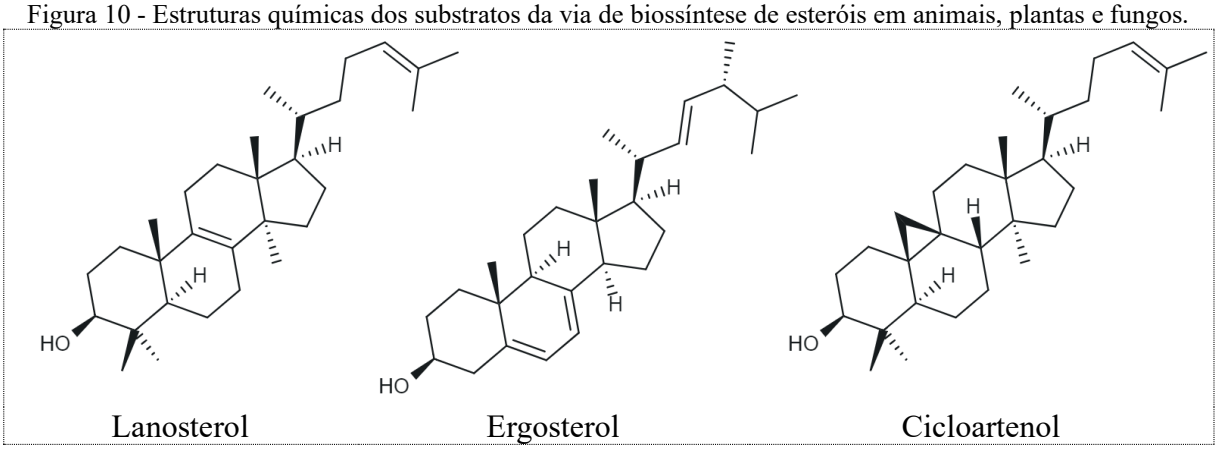

Fonte: Elaborado pelo autor (2025)

O produto da reação de desmetilação em fungos é um precursor do ergosterol, ao passo que, em humanos, é um precursor do colesterol. Em mamíferos, a enzima também converte o lanosterol em 4,4-dimetil-5-colesta-8,14,24-trieno-3-ol, conhecido como esterol ativador da meiose do fluido folicular (*FF-MAS - Follicle Fluid-Meiosis Activating Sterol*), que atua como sinalizador reprodutivo (Kaluzhskiy *et al*., 2021; Keniya *et al*., 2018). A reação ocorre em três etapas sucessivas de monooxigenação (Figura 10): o grupo metila é convertido em álcool, seguido por aldeído e, finalmente, removido na forma de ácido fórmico (Debeljak; Fink; Rozman, 2003).

A região catalítica da enzima possui um sítio de ligação centralizado e profundamente embutido, que inclui um anel de porfirina contendo ferro (heme). O ferro heme representa o principal ponto de interação dos azóis; um dos átomos de nitrogênio do anel azólico do composto bioativo coordena-se ao ferro do grupo heme, bloqueando a ativação do oxigênio e a subsequente biossíntese de ergosterol. Esse bloqueio resulta na depleção de ergosterol e no acúmulo de esteróis tóxicos na membrana celular fúngica, levando à lise e morte do microrganismo (Emami; Tavangar; Keighobadi, 2017; Keniya *et al*., 2018; Monk *et al*., 2020).

Figura 11 - Esquema do mecanismo de desmetilação de esterol (Lanosterol) pela LDM (CYP51)

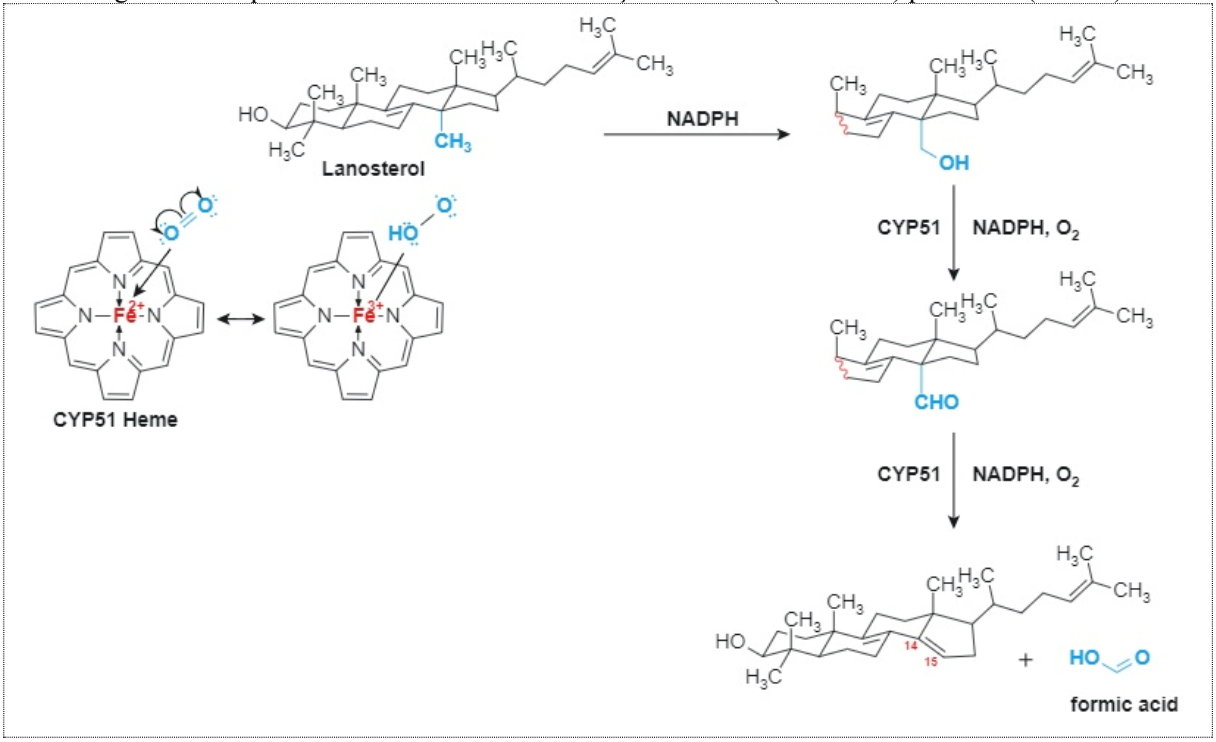

Fonte: Elaborado pelo autor (2025)

Do ponto de vista da biologia estrutural, a LDM opera como um complexo de isolamento catalítico. Sua arquitetura molecular permite que o grupo heme permaneça

profundamente embutido, acessível apenas através de canais de acesso hidrofóbicos que filtram a entrada de substratos. Esta organização protege a célula de espécies reativas de oxigênio geradas durante a catálise e garante a especificidade enzimática. Quando um inibidor azólico ocupa este espaço, ele não apenas bloqueia o sítio ativo, mas interrompe toda a dinâmica de fluxo de membrana, levando ao colapso da homeostase lipídica do fungo (Debeljak; Fink; Rozman, 2003; Kaluzhskiy *et al*., 2021; Monk *et al*., 2020).

3.3. Teoria do funcional de densidade (DFT)

A Teoria do Funcional Densidade (DFT) é uma das abordagens mais populares na mecânica quântica para descrever as propriedades eletrônicas de sistemas complexos (Parr; Weitao, 1995). Nesse método, as características do sistema são determinadas pela aplicação de funcionais baseados na densidade eletrônica. A ideia inicial de descrever a estrutura eletrônica em termos da densidade $\rho(\mathbf{r})$, em vez de funções de onda eletrônicas individuais, foi proposta independentemente por Llewellyn Thomas e Enrico Fermi (Parr; Weitao, 1995). No entanto, esse método não produziu previsões quantitativas precisas, pois só era válido para cargas nucleares infinitas. Baseados nas ideias de Thomas-Fermi, o físico Pierre Hohenberg (Hohenberg; Kohn, 1964) e o químico Walter Sham (Kohn; Sham, 1965) demonstraram que é possível determinar, de maneira exata, problemas quânticos por meio da densidade eletrônica. O método Kohn-Sham (KS) é uma variante operacional do método HF, que leva em consideração a construção de um sistema não interagente que reproduz a mesma densidade do problema original. Resolver esse tipo de sistema é relativamente mais simples, pois a função de onda pode ser representada exatamente como um determinante de Slater de orbitais.

A DFT é fundamentada em dois teoremas propostos por Hohenberg e Kohn, os quais são aplicáveis a sistemas compostos por um número arbitrário de elétrons confinados em uma caixa, sujeitos a um potencial externo $v(\mathbf{r})$ e à repulsão coulombiana mútua.

1° Teorema: O potencial externo $v(\mathbf{r})$ é um funcional da densidade $\rho(\mathbf{r})$. Este teorema estabelece que a densidade pode ser a variável fundamental na determinação da estrutura eletrônica. Consequentemente, o conhecimento da densidade implica conhecer tanto a função de onda quanto o potencial externo. Isso possibilita a determinação do hamiltoniano do sistema e, por conseguinte, de todos os observáveis no estado fundamental,

$$\rho\,(\boldsymbol{r}) \Longrightarrow \psi \;\Longrightarrow\; v\,(\boldsymbol{r}) \;\Longrightarrow \text{observáveis.} \qquad (01)$$

Seja o hamiltoniano eletrônico $He = T + V + U$, onde a energia cinética total é,

$$T = \frac{1}{2}\int \boldsymbol{\nabla}\psi^*(\boldsymbol{r}) \cdot \boldsymbol{\nabla}\psi(\boldsymbol{r})d\boldsymbol{r}, \tag{02}$$

a energia potencial proveniente do potencial externo é,

$$V = \int \upsilon(\boldsymbol{r})\psi^*(\boldsymbol{r})\psi(\boldsymbol{r})d\boldsymbol{r}, \tag{03}$$

e o termo de repulsão colombiana é,

$$U = \frac{1}{2}\int \frac{1}{|\boldsymbol{r}-\boldsymbol{r}'|}\ \psi^*(\boldsymbol{r})\psi^*(\boldsymbol{r}')\psi(\boldsymbol{r})\psi(\boldsymbol{r}')d\boldsymbol{r}d\boldsymbol{r}'. \tag{04}$$

Supondo, por simplicidade, que o estado fundamental é não degenerado, a densidade eletrônica neste estado é dada por,

$$\rho\ (\boldsymbol{r}) = \int \psi^*(\boldsymbol{r})\psi(\boldsymbol{r})d\boldsymbol{r}. \tag{05}$$

Supondo também que o potencial $\upsilon'(\mathbf{r})$ esteja associado ao hamiltoniano $He\ ' = T + V' + U$, cujo estado fundamental ψ' e energia total E', dê origem à mesma densidade eletrônica $\rho(\mathbf{r})$.

Para que ψ seja diferente de ψ', $\upsilon'(\mathbf{r}) - \upsilon(\mathbf{r})$ não precisa ser, necessariamente, uma constante e as funções de onda satisfazem diferentes equações de Schrödinger. A energia do estado fundamental é mínima para a função de onda exata desse estado, garantindo que as desigualdades,

$$\mathrm{E}' = \langle\psi'|H_e'|\psi'\rangle < \langle\psi|H_e'|\psi\rangle = \langle\psi|H_e + V' - V|\psi\rangle, \tag{06}$$

$$E' < E\ + \int [\upsilon'(\boldsymbol{r}) - \upsilon(\boldsymbol{r})]\rho(\boldsymbol{r})d\boldsymbol{r} \tag{07}$$

e,

$$E < E'\ + \int [\upsilon(\boldsymbol{r}) - \upsilon'(\boldsymbol{r})]\rho(\boldsymbol{r})d\boldsymbol{r} \tag{08}$$

sejam válidas, de acordo com o princípio variacional. Entretanto, ao assumir que a densidade seja igual para $\upsilon'(\mathbf{r}) \neq \upsilon(\mathbf{r})$, surge uma inconsistência decorrente da necessidade de ψ ser obrigatoriamente diferente de ψ'. Isso pode ser observado ao somar as desigualdades (07) e (08),

$$E' + E < E + E'.$$

Assim, a exigência de unicidade para $\rho(\mathbf{r})$ implica que $\psi = \psi'$ e $\upsilon'(\mathbf{r}) - \upsilon(\mathbf{r})$ seja constante. Portanto, o potencial externo é um funcional único da densidade eletrônica.

2° Teorema: A energia do estado fundamental é mínima para densidade $\rho(\mathbf{r})$ exata. O segundo teorema de Hohenberg-Kohn estabelece um critério para determinar a densidade do estado fundamental. A energia do estado fundamental é um funcional da densidade eletrônica, em que o valor mínimo é alcançado para a densidade exata.
Seja o functional,

$$E_\upsilon[\rho(\boldsymbol{r})] \equiv \int \upsilon(\boldsymbol{r})\rho(\boldsymbol{r})d\boldsymbol{r} + F[\rho(\boldsymbol{r})], \tag{09}$$

onde $F[\rho(\mathbf{r})] = \langle\psi|T + U|\psi\rangle$ é denominado funcional universal. Pelo método variacional, o funcional $\epsilon\upsilon$ da função de onda ψ',

$$E_\upsilon[\psi] = \langle\psi'|V|\psi'\rangle + \langle\psi'|T + U|\psi'\rangle, \tag{10}$$

é mínimo para o estado fundamental ψ. Se ψ' for o estado fundamental associado ao potencial externo $\upsilon'(\mathbf{r})$, é válida a relação

$$E_\upsilon[\psi'] = \int \upsilon(\boldsymbol{r})\rho'(\boldsymbol{r})d\boldsymbol{r} + F[\rho'(\boldsymbol{r})] > E_\upsilon[\psi'] = \int \upsilon(\boldsymbol{r})\rho(\boldsymbol{r})d\boldsymbol{r} + F[\rho(\boldsymbol{r})], \tag{11}$$

de maneira que $\epsilon[\rho'(\mathbf{r})] > \epsilon[\rho(\mathbf{r})]$. Se $F[\rho(\mathbf{r})]$ for um funcional conhecido, o problema de determinar a densidade e a energia do estado fundamental de um sistema eletrônico, sob um dado potencial externo, é simplificado para a minimização do funcional $E\upsilon[\rho(\mathbf{r})]$. Uma vez que as interações de Coulomb são de longo alcance, é conveniente separar essa interação do funcional universal,

$$F[\rho(r) = \frac{1}{2}\int \rho(\boldsymbol{r})\rho'(\boldsymbol{r})\,|\boldsymbol{r} - \boldsymbol{r}'|\,d\boldsymbol{r}d\boldsymbol{r}' + G[\rho(\boldsymbol{r})] \tag{12}$$

e definir o funcional $G[\rho(\mathbf{r})]$ que deve estar relacionado às energias cinética, de troca e correlação dos elétrons. Até este ponto, o desenvolvimento da teoria é preciso, mesmo considerando a aproximação de Born-Oppenheimer. Contudo, não há uma forma analítica conhecida para o funcional $G[\rho(\mathbf{r})]$, e, por conseguinte, são necessárias aproximações para viabilizar a determinação da densidade eletrônica do estado fundamental.

Kohn e Sham foram pioneiros ao propor uma abordagem para determinar a estrutura eletrônica de sistemas multieletrônicos, utilizando a minimização do funcional Ev. Em sua proposta, eles sugeriram que a densidade do estado fundamental de um sistema com elétrons interagentes seja igual à densidade do estado fundamental de um sistema fictício com elétrons não interagentes em um potencial efetivo. Assim, o funcional universal $G[\rho(\mathbf{r})]$ é dado por:

$$G[\rho(\boldsymbol{r})] = T_S[\rho(\boldsymbol{r})] + Exc[\rho(\boldsymbol{r})] \tag{13}$$

onde $Ts[\rho(\mathbf{r})]$ é a energia cinética do sistema não interagente com densidade $\rho(\mathbf{r})$ e $Exc[\rho(\mathbf{r})]$ é a energia de troca e correlação de um sistema interagente de mesma densidade. Deste modo, o funcional energia a ser minimizado é,

$$E_v[\rho(\boldsymbol{r})] = \int v(\boldsymbol{r})\rho(\boldsymbol{r})d\boldsymbol{r} + \frac{1}{2}\int \frac{\rho(\boldsymbol{r})\rho(\boldsymbol{r}')}{|\boldsymbol{r}-\boldsymbol{r}'|}d\boldsymbol{r}d\boldsymbol{r}' + T_S[\rho(\boldsymbol{r})] + \int \rho(\boldsymbol{r})Exc[\rho(\boldsymbol{r})]d\boldsymbol{r} \tag{14}$$

A densidade eletrônica exata é um extremo do funcional energia Ev e a carga eletrônica total do sistema de N elétrons é fixa, de maneira que,

$$\int v(\boldsymbol{r})\rho(\boldsymbol{r})d\boldsymbol{r} = N, \tag{15}$$

seja um vínculo. De acordo com o método variacional, a inclusão deste vínculo deve fornecer

$$\int \delta\rho(\boldsymbol{r})\left(\frac{\delta T_S}{\delta\rho(\boldsymbol{r})} + v(\boldsymbol{r}) + \int \frac{\rho(\boldsymbol{r}')}{|\boldsymbol{r}-\boldsymbol{r}'|}d\boldsymbol{r}' + v_{xc}[\rho(\boldsymbol{r})] - \mu\right)d\boldsymbol{r} = 0, \tag{16}$$

onde μ é o multiplicador de Lagrange e $v_{xc}[\rho(r)] = \frac{\delta E_{xc}}{\delta \rho(r)}$ é o potencial de troca e correlação. No formalismo da DFT, energia cinética do sistema fictício não interagente (em unidades atômicas) é dado pela expressão:

$$T_s[\rho(\boldsymbol{r})] = -\frac{1}{2}\sum_i \int \psi_{\mathrm{i}}^* \nabla^2 \psi_{\mathrm{i}}\, d^3\boldsymbol{r}, \tag{17}$$

e da proposta de Kohn-Sham, decorre que a densidade do estado fundamental é,

$$\rho(\boldsymbol{r}) = \sum_{\mathrm{i}=1}^{N} |\psi_{\mathrm{i}}(\boldsymbol{r})|^2 \tag{18}$$

A solução da equação de minimização que deve resultar em $\rho(\mathbf{r})$ pode ser obtida da equação de Schrödinger de uma partícula, uma vez que no sistema fictício, os elétrons não interagem. Desta maneira, a equação de autovalor resultante do método de Kohn-Sham é,

$$\hat{h}^{KS}\psi_{\mathrm{i}}(\boldsymbol{r}) = \left(-\frac{1}{2}\nabla^2 + v^{KS}[\rho(\boldsymbol{r})]\right)\psi_{\mathrm{i}}(\boldsymbol{r}) = \epsilon_{\mathrm{i}}\psi_{\mathrm{i}}(\boldsymbol{r}), \tag{19}$$

onde $\hat{h}^{KS}$ é o hamiltoniano de Kohn-Sham e

$$v^{KS} = v(\boldsymbol{r}) + \int \frac{\rho(\boldsymbol{r}')}{|\boldsymbol{r}-\boldsymbol{r}'|} d\boldsymbol{r}' + v_{xc}[\rho(\boldsymbol{r})] \tag{20}$$

é o potencial efetivo de Kohn-Sham. É importante salientar que esses orbitais ψi não representam as funções de onda do sistema interagente, assim como ϵi não corresponde ao autovalor de energia do sistema real. A igualdade está presente apenas na densidade do estado fundamental, $\rho(\mathbf{r})$, nos sistemas real e fictício.

Para determinar a densidade eletrônica, é necessário resolver a equação de Kohn Sham, (19). No entanto, como v^{KS} depende de $\rho(\mathbf{r})$, não é possível resolver a equação diretamente. A solução de (19) ocorre por meio de um cálculo auto consistente, onde, a partir de uma densidade inicial ρ^j, o potencial efetivo de Kohn-Sham v^{KS} é calculado, e as funções de onda $\psi_{\mathrm{i}}(\mathbf{r})$ são determinadas ao resolver a equação de Kohn-Sham. Em seguida, a densidade do estado fundamental ρj+1 é calculada a partir desses orbitais. A densidade ρj+1 é comparada à densidade inicial, e caso $\rho^{j+1} = \rho^j$, o cálculo converge, e ρ^{j+1} pode ser utilizada para

determinar os observáveis físicos. Caso contrário, se não houver convergência, ρ^{j+1} é usada para calcular o potencial efetivo, e o ciclo de auto consistência é reiniciado. Esse processo continua até que o cálculo atinja a convergência. A densidade eletrônica inicial é arbitrária e, normalmente, consiste em uma distribuição aleatória. Para calcular o potencial efetivo de Kohn Sham, é necessário, a priori, aproximar o funcional de troca e correlação Exc, cuja forma analítica é desconhecida.

4. METODOLOGIA

A etapa inicial deste estudo compreendeu uma prospecção bibliográfica nas bases de dados Google Acadêmico, SciELO, Portal de Periódicos CAPES, Scopus, *Web of Science* e *Science Direct*, além de consultas ao *Protein Data Bank* (PDB) para identificação de estruturas macromoleculares pertinentes. O levantamento visou mapear as discussões científicas sobre fungicidas e delimitar uma classe específica para investigação. Inicialmente, foram selecionados cinco compostos: miclobutanil, tebuconazol, epoxiconazol, protioconazol e ciproconazol. No entanto, o escopo foi refinado com base nos critérios do Comitê de Ação à Resistência a Fungicidas (FRAC), que classifica os compostos conforme o modo de ação e o alvo biológico. A partir desse referencial, a pesquisa restringiu-se à classe dos triazóis, selecionando-se especificamente o triadimefon (TF) e o triadimenol (TN) devido à sua relevante estereoquímica, considerando que o segundo é o principal metabólito do primeiro.

4.1. Análise do estado sólido

As estruturas cristalográficas dos compostos TF e TN foram obtidas a partir do *Cambridge Structural Database* (CSD) (Nowell; Walker; Anderson. N. H., 1982; Spitzer; Kopf; Nickless, 1982), considerando a presença de grupos funcionais associados à atividade antifúngica, como os triazóis (Huang *et al*., 2022). Os dados estruturais, obtidos no formato *crystallographic information file* (CIF), serviram de base para as análises geométricas e do arranjo supramolecular. As representações moleculares, tabelas e figuras foram elaboradas com os softwares *Mercury* versão 3.8 (Macrae *et al*., 2020) e GIMP.

A análise das interações intermoleculares foi realizada por meio de superfícies de *Hirshfeld*, utilizando as configurações d_{norm} e *shape index*, bem como os respectivos gráficos de impressão digital 2D, obtidos com o programa *Crystal Explorer* versão 21.5 (Spackman *et al*., 2021). Essas análises permitiram a identificação e a caracterização detalhada das regiões de contato molecular, incluindo interações envolvendo sistemas π (Spackman; Jayatilaka, 2009). Considerando a presença de centros quirais, foram selecionadas configurações específicas dos compostos TF e TN para fins de discussão.

A natureza e a estabilidade das interações intermoleculares foram investigadas por meio da Teoria Quântica de Átomos em Moléculas (QTAIM - *Quantum Theory of Atoms in Molecules*) (Bader, 1985, 1994) e da análise de Orbitais Naturais de Ligação (NBO - *Natural Bonding Orbitals*) (Weinhold; Landis, 2001, 2012). Os cálculos quânticos foram realizados no

âmbito da Teoria do Funcional da Densidade (DFT) (Hohenberg; Kohn, 1964; Kohn; Sham, 1965) empregando o funcional M06-2X (Zhao; Truhlar, 2008) em combinação com o conjunto de bases 6-311++G(d,p), conforme implementado no software *Gaussian* 16 (Frisch *et al*., 2016). As geometrias iniciais foram construídas a partir das estruturas experimentais e otimizadas, sendo realizadas análises de frequência para assegurar a obtenção de mínimos verdadeiros na superfície de energia potencial.

Os parâmetros topológicos da QTAIM foram obtidos com o programa *Multiwfn* 3.5 (Lu; Chen, 2012), enquanto as interações hiperconjugativas foram avaliadas por meio da análise NBO, utilizando teoria de perturbação de segunda ordem para estimar as energias de estabilização associadas às interações do tipo doador–aceptor (Alabugin; Gilmore; Peterson, 2011).

4.2. Estudo de modelagem molecular

A caracterização da reatividade química dos compostos TF e TN foi realizada através da Teoria do Funcional da Densidade (DFT). As geometrias de estado fundamental foram determinadas via busca conformacional por varredura relaxada (*relaxed scan*), utilizando o nível de teoria (M06-2X/6-311++G(d,p)).

A partir das energias dos orbitais moleculares de fronteira (HOMO - *Highest Occupied Molecular Orbital* e LUMO - *Lowest Unoccupied Molecular Orbital*) (Zhang; Musgrave, 2007), foram calculados descritores de reatividade global, tais como dureza química (resistência à deformação da nuvem eletrônica), potencial químico (tendência de escape eletrônico) (Pearson, 1992, 2005) e o índice de eletrofilicidade global (capacidade de estabilização energética ao receber carga) (Parr; Szentpály; Liu, 1999).

Adicionalmente, a distribuição espacial da densidade de carga foi analisada através de mapas de Potencial Eletrostático Molecular (MEP - *Molecular Electrostatic Potential*) (Sjoberg; Politzer, 1990; Weinstein *et al*., 1981) para a identificação de sítios nucleofílicos e eletrofílicos. De forma complementar, a reatividade local foi mapeada por meio das Funções de Fukui (Fukui, 1982; Li; Evans, 1995), permitindo a predição precisa dos centros susceptíveis a ataques nucleofílicos, eletrofílicos e radicalares.

4.3. Previsão de toxicidade e modelagem de farmacóforos

Em colaboração com pesquisadores do Grupo de Química Teórica e Estrutural de Anápolis, Goiás, Brasil, da Universidade Estadual de Goiás, foi realizada a modelagem farmacofórica dos diferentes isômeros dos fungicidas frente aos ligantes-alvo da lanosterol 14α-desmetilase (família CYP51), utilizando-se o software *LigandScout* v4.5. O programa identificou combinações de características farmacofóricas compartilhadas, incluindo doadores de ligação de hidrogênio (*Hydrogen Bond Donors* – HBDs), aceitadores de ligação de hidrogênio (*Hydrogen Bond Acceptors* – HBAs), grupos carregados positiva e negativamente, regiões hidrofóbicas (*Hydrophobic* – HyPho) e anéis aromáticos (*Aromatic Rings* – ARs). Esses farmacóforos foram integrados ao processo de alinhamento para o desenvolvimento do modelo de farmacóforo de características compartilhadas (SFP - *Shared Feature Pharmacophore*).

Uma revisão da literatura foi realizada nas bases de dados *Binding* DB para identificar compostos com atividade antagonista da lanosterol 14α-desmetilase. Um total de cinco compostos com os menores valores de concentração inibitória (IC_{50}), os quais incluem BDBM24656, BDBM25806, BDBM25807, BDBM25808 e BDBM25809, compuseram o conjunto de dados utilizado no cálculo dos modelos farmacofóricos.

Para a caracterização do perfil farmacocinético, realizou-se um estudo dos parâmetros de absorção, distribuição, metabolismo e excreção (ADME) empregando a ferramenta *SwissADME online* (http://www.swissadme.ch/) (Daina; Michielin; Zoete, 2017; Salah *et al*., 2024). Adicionalmente, a predição de toxicidade química foi realizada com o auxílio do servidor *ProTox-3.0*, (Banerjee *et al*., 2024) (https://tox.charite.de/protox3/), aplicando-se os parâmetros de toxicidade ao componente com maior potencial de atividade biológica.

A avaliação de potenciais efeitos tóxicos ocorreu por meio de predições computacionais; a toxicidade cardíaca foi avaliada pelo servidor *Pred-hERG* (Braga *et al*., 2015; Sanches *et al*., 2024) (https://predherg.labmol.com.br/) e a toxicidade cutânea utilizando o *Pred-Skin* (Alves *et al*., 2018; Borba *et al*., 2021) (https://predskin.labmol.com.br/). Adicionalmente, a toxicidade ambiental foi investigada empregando o servidor *ADMETSAR* (Cheng *et al*., 2012; Yang *et al*., 2019) (https://lmmd.ecust.edu.cn/admetsar2/), contemplando parâmetros como toxicidade para *Tetrahymena pyriformis*, abelhas, peixes, bem como o potencial de biodegradação.

4.4. Avaliação da citogenotoxicidade, genotoxiocidade e mutagenicidade

A investigação dos efeitos citogenotóxicos, genotóxicos e mutagênicos dos fungicidas triadimefon (TF) e triadimenol (TN) foi viabilizada por meio de uma rede de cooperação

científica multi-institucional. Os procedimentos experimentais foram centralizados no Laboratório de Biotecnologia da Universidade Estadual de Goiás (UEG), Campus Central, em estreita colaboração com o Programa de Pós-Graduação em Conservação de Recursos Naturais do Cerrado do Instituto Federal Goiano (IF Goiano – Urutaí) e o Laboratório de Novos Materiais da Universidade Evangélica de Goiás (UniEVANGÉLICA). Adicionalmente, o suporte computacional para predição de metabólitos contou com a parceria do S-Inova Biotech da Universidade Católica de Dom Bosco (UCDB) e do Centro de Análises Proteômicas e Bioquímicas da Universidade Católica de Brasília (UCB).

A metodologia abrangeu modelos biológicos complementares, iniciando-se pela avaliação ecotoxicológica *in vivo* com anelídeos da espécie *Eisenia fetida*. Esses organismos foram expostos a solos contaminados com concentrações ambientalmente relevantes de TF (0,006 a 0,024 mg/kg) e TN (1,5 a 6,0 mg/kg), além de misturas binárias, por períodos de 7, 14 e 21 dias. Para quantificar a genotoxicidade e mutagenicidade nesse modelo, procedeu-se à coleta do fluido celômico para a realização do ensaio cometa, analisando a integridade do DNA, e do teste de micronúcleo, para identificação de danos cromossômicos permanentes.

Paralelamente, a citogenotoxicidade foi avaliada *in vitro* em linfócitos de sangue periférico humano, coletados sob aprovação do Comitê de Ética em Pesquisa da UEG (CAAE nº 66860023.1.0000.8113). As células foram submetidas ao teste de exclusão de Azul de Trypan para monitoramento da viabilidade celular e ao ensaio cometa para detecção de quebras na cadeia de DNA após exposição aguda aos triazóis. Esta abordagem permitiu comparar a sensibilidade de um organismo sentinela[4] ambiental com o potencial de dano em células humanas.

Por fim, o potencial metabólico e a regulação da expressão gênica foram preditos através dos servidores *BioTransformer e DIGEP-Pred*. Essa análise *in silico* permitiu correlacionar os danos observados nos modelos biológicos com as rotas de biotransformação (sistema citocromo P450) e possíveis mecanismos de estresse oxidativo inerentes aos xenobióticos estudados, conferindo robustez aos dados experimentais obtidos nos ensaios com anelídeos e linfócitos. Para o detalhamento dos procedimentos metodológicos completos, consultar os Manuscritos 2 e 3 no item Resultados e Discussão desta dissertação.

[4] Organismo utilizado como indicador biológico para monitorar a saúde de um ecossistema ou a eficácia de um processo.

5. RESULTADOS E DISCUSSÃO

Os resultados aqui apresentados são frutos de uma construção científica coletiva, integrando pesquisadores e laboratórios da Universidade Estadual de Goiás (UEG – Campus Central), especificamente do Grupo de Química Teórica e Estrutural de Anápolis, além do Instituto Federal Goiano (IF Goiano – Urutaí), da Universidade Evangélica de Goiás (UniEVANGÉLICA) e da Pontifícia Universidade Católica de Goiás (PUC Goiás). Contamos, também, com a participação do S-Inova Biotech (UCDB) e do Centro de Análises Proteômicas e Bioquímicas (UCB), que colaboraram com o suporte computacional. Tal rede de cooperação investigou os fungicidas triadimefon (TF) e triadimenol (TN) sob diferentes perspectivas, unindo a química teórica aos ensaios com sistemas biológicos complexos, organizados em três manuscritos articulados.

No Artigo 01 (submetido à *Results in Chemistry*), a aplicação da Teoria do Funcional da Densidade (DFT) revelou que o triadimefon e o triadimenol possuem perfis de reatividade distintos. A análise dos orbitais moleculares de fronteira (HOMO e LUMO) permitiu a determinação de descritores de reatividade globais e locais. A análise da dureza química e do índice de eletrofilicidade global indicou que o TF, por possuir um caráter eletrofílico mais acentuado em regiões específicas da molécula, apresenta uma tendência intrínseca a interagir com centros nucleofílicos biológicos. O mapeamento de sítios de reatividade locais corroborou essa percepção, sugerindo que a estabilidade eletrônica e a distribuição de carga nestes fungicidas são fatores importantes para a sua persistência e potencial de interação com macromoléculas.

Esses *insights* da química teórica apresentaram alinhamento direto aos achados experimentais dos Artigos 02 e 03. No estudo com linfócitos humanos (Artigo 02, publicado na *Drug and Chemical Toxicology*), observou-se que a exposição aguda aos triazóis resultou em danos significativos na integridade do DNA, detectados pelo ensaio cometa. De forma complementar, a investigação com a espécie sentinela *Eisenia fetida* (Artigo 03, submetido à *Environmental Toxicology and Pharmacology*) revelou que a toxicidade evolui de quebras na cadeia de DNA para danos cromossômicos permanentes, evidenciados pela formação de micronúcleos.

A discussão integrada destes dados sugere que a genotoxicidade observada não é meramente casual, mas sim influenciada pela estereoquímica dos compostos. Enquanto a modelagem eletrônica do Artigo 01 mostrou a "disponibilidade" da molécula para reagir, os ensaios biológicos confirmaram que essa reatividade se traduz em estresse celular. As predições

metabólicas discutidas nos manuscritos reforçam que a biotransformação, mediada pelo sistema citocromo P450, pode ser o elo entre a estrutura molecular e o dano genômico, onde a conformação espacial dos isômeros de triadimenol desempenha um papel chave na afinidade enzimática.

Embora reconheçamos as limitações de cada modelo isolado, a corroboração dos resultados teóricos e experimentais oferece uma visão mais nítida dos riscos. Em conjunto, os achados sugerem que o perfil eletrônico e a quiralidade do TF e do TN estão intimamente associados aos efeitos citogenotóxicos e mutagênicos observados. Esta abordagem multidisciplinar, portanto, não apenas caracteriza o perigo destes contaminantes, mas contribui com subsídios importantes para futuras revisões em protocolos de avaliação de risco ambiental e ocupacional, visando uma proteção mais eficaz da saúde humana e dos ecossistemas.

5.1. Artigo 1: Predição da toxicidade de fungicidas triazóis: uma perspectiva molecular sobre o triadimefon e o triadimenol

5.1.1. Resumo

Contexto: Fungicidas triazóis, como o triadimefon e seu metabólito estereoisomérico, triadimenol, permanecem como agroquímicos fundamentais. No entanto, sua estereoquímica pode afetar a reatividade de forma, o reconhecimento intermolecular e a ecotoxicidade de diferentes maneiras, com impactos potenciais em espécies não alvo. Objetivo: Este estudo emprega métodos computacionais para descrever descritores estruturais e eletrônicos, quantificar interações supramoleculares e prever desfechos toxicológicos *in silico* para triadimefon e seu estereoisômero individual, triadimenol. Métodos: Cálculos de teoria do funcional da densidade foram empregados para otimizar as geometrias moleculares e calcular descritores de reatividade no nível de teoria M06-2X/6-311++G(d,p). As interações intermoleculares foram comparadas usando análise de superfícies de Hirshfeld, teoria quântica de átomos em moléculas e análise de orbitais naturais de ligação. Descritores de reatividade química foram calculados para avaliar sítios reativos. Modelagem farmacofórica foi realizada para verificar o potencial dos seis isômeros em interagir com o alvo lanosterol 14α-desmetilase. A toxicidade foi prevista usando modelos computacionais disponíveis online. Resultados: Diferenças significativas foram encontradas entre as propriedades eletrônicas e interações intermoleculares de triadimefon e triadimenol, devido à presença de grupos funcionais -OH ou -CO-. Essas variações influenciam o potencial eletrostático molecular, descritores de

reatividade e energias de interação, afetando seu comportamento biológico. Os resultados da modelagem farmacofórica sugerem que apenas os isômeros 1R-TF, 1S,2R-TN e 1S,2S-TN demonstraram potencial de interação com o alvo lanosterol 14α-desmetilase. As previsões de toxicidade revelaram que alguns estereoisômeros de triadimenol exibem maior potencial de efeitos adversos em organismos não alvo quando comparados ao triadimefon. Conclusão: Os achados destacam o papel crucial da estereoquímica na modulação do comportamento químico e da toxicidade de fungicidas triazóis. Além disso, o uso de métodos *in silico* mostra-se eficaz na predição de perfis ecotoxicológicos desses compostos e apoia o desenvolvimento de práticas agroquímicas mais seguras e sustentáveis.

5.1.2. Introdução

Na agricultura moderna, os pesticidas são ferramentas essenciais que protegem o rendimento e a qualidade ao suprimir insetos-praga, doenças das plantas e ervas daninhas(Aliste *et al*., 2021). No entanto, devido à sua natureza bioativa inerente, projetada para eliminar diversas espécies, esses compostos são tóxicos (Roman *et al*., 2021). Entre as diferentes classes, os fungicidas triazóis se destacam por sua eficácia sistêmica, amplo espectro de ação e propriedades físico-químicas favoráveis (Klittich, 2014; Singh, 2002). Desde sua introdução na década de 1970, os fungicidas triazóis tornaram-se ferramentas indispensáveis para o manejo de doenças fúngicas em todo o mundo. Graças à sua atividade de amplo espectro, alta eficácia, rápida ação, efeitos duradouros e forte absorção e translocação sistêmica, esses compostos são amplamente empregados em culturas como trigo, milho, frutas, hortaliças e plantas ornamentais para controlar ferrugens, oídios e para regular o crescimento das plantas (Li *et al*., 2022; Nagappan; Deresinski, 2007; Thompson; Wiederhold, 2010).

Os triazóis representam uma classe significativa de compostos heterocíclicos devido ao seu amplo espectro de atividades biológicas. Sua estrutura central consiste em um heterociclo de cinco membros contendo três átomos de nitrogênio, que podem ocorrer em duas formas isoméricas distintas, dependendo da posição dos átomos de nitrogênio: 1,2,3-triazóis e 1,2,4-triazóis (Zhang, 2019). Derivados de 1,2,3-triazóis demonstraram propriedades farmacológicas notáveis, incluindo atividades antibacterianas potentes (Marepu; Yeturu; Pal, 2018; Ramírez-Villalva *et al*., 2017; Ratnakar Reddy *et al*., 2014; Venugopala *et al*., 2020), anticâncer (Németh-Rieder *et al*., 2023; Ratnakar Reddy *et al*., 2014) e antitumorais (Deng *et al*., 2022; Wang *et al*., 2022), tornando-os valiosos na química medicinal. Por outro lado, os derivados de 1,2,4-triazóis são amplamente empregados na agricultura como agentes fungicidas (Nagappan; Deresinski,

2007; Thompson; Wiederhold, 2010), principalmente devido à sua alta eficácia e seletividade contra uma ampla gama de fungos fitopatogênicos. Os fungicidas 1,2,4-triazóis apresentam estabilidade eletrônica e alta afinidade pela lanosterol 14α-desmetilase (CYP51), a enzima-alvo responsável pela biossíntese do ergosterol. Seu mecanismo de ação envolve a inibição dessa monooxigenase do citocromo P450, que catalisa a desmetilação do lanosterol – uma etapa crucial na formação das membranas celulares fúngicas (Monk *et al*., 2020).

Entre eles, triadimefom (TF), triadimenol (TN), diniconazol, hexaconazol, miclobutanil e tebuconazol apresentam quiralidade devido a um ou mais estereocentros, influenciando sua atividade biológica e comportamento ambiental (De Albuquerque *et al*., 2018). O TF [1-(4-clorofenoxi)-1-(1,2,4-triazol-1-il)-3,3-dimetil-butano-2-ona] contém um único centro quiral (*C1) e existe como um par de enantiômeros S-(+) e R-(−) (Kurihara *et al*., 1997). Sua biotransformação leva ao TN [1-(4-clorofenoxi)-1-(1,2,4-triazol-1-il)-3,3-dimetil-butano-2-ol], seu principal metabólito em plantas, solos e animais. Enquanto o TF possui um único centro quiral, o TN apresenta dois, dando origem a quatro estereoisômeros – (1R,2S), (1S,2R), (1R,2R) e (1S,2S) – que se organizam em dois pares diastereoméricos: TN-A e TN-B (Kenneke *et al*., 2008; Li *et al*., 2014). Essas variações estruturais afetam significativamente as propriedades físico-químicas e toxicológicas. Notavelmente, o estereoisômero 1S,2R apresenta até 1000 vezes maior atividade fungicida do que seus equivalentes, e o diastereômero A é marcadamente mais tóxico para mamíferos, com base nos valores de DL_{50} oral em ratos (Burden *et al*., 1987; Kenneke *et al*., 2010). Essa assimetria estereoquímica é essencial para compreender o desempenho biológico, o perfil toxicológico e o destino ambiental desses compostos.

Figura 12. Fórmulas estruturais do Triadimefom e de seu metabólito Triadimenol. O asterisco (*) indica o carbono quiral presente em suas estruturas químicas.

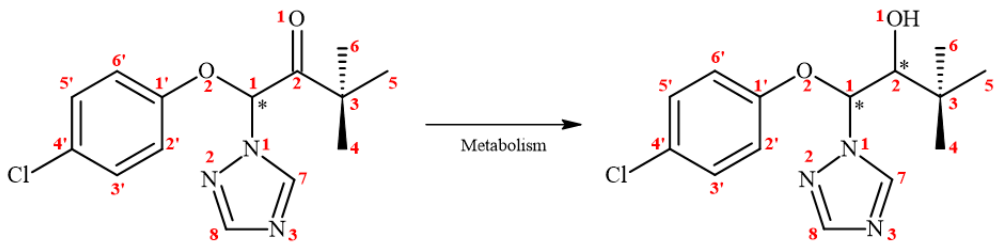

Triadimefon Triadimenol

Dado o uso agrícola extensivo de TF e TN e as preocupações ecotoxicológicas associadas, este estudo elucida suas características eletrônicas e supramoleculares por meio de um fluxo de trabalho computacional abrangente. Foram previstos perfis toxicológicos utilizando modelos *in silico* informados por padrões de interação intermolecular e descritores

de reatividade, com o objetivo de resolver diferenças específicas entre estereoisômeros e antecipar potenciais impactos em organismos não alvo. Os resultados destinam-se a orientar um uso mais seguro e racional desses fungicidas, além de apoiar avaliações regulatórias que incorporem considerações estereoquímicas.

5.1.3. Conclusão

Os resultados destacam que diferenças estereoquímicas entre triadimefon e triadimenol influenciam diretamente suas propriedades eletrônicas, interações supramoleculares e perfis toxicológicos. Alguns estereoisômeros de triadimenol mostraram maior potencial de toxicidade em organismos não alvo do que o triadimefon. Esses achados reforçam a importância de considerar a estereoquímica em avaliações regulatórias e demonstram que métodos computacionais *in silico* são ferramentas eficazes para prever perfis ecotoxicológicos e apoiar práticas agrícolas mais seguras e sustentáveis.

5.2. Artigo 2: Dano no DNA induzido pelos fungicidas triadimefon, triadimenol e sua mistura em linfócitos humanos: citogenotoxicidade e análise computacional das vias metabólicas

5.2.1. Resumo

Triadimefon (TF) e triadimenol (TN) são fungicidas triazólicos amplamente utilizados para prevenir infecções fúngicas em cereais, frutas e outras culturas de importância econômica. Seus efeitos nocivos em organismos não alvo já foram relatados. Este estudo investigou os efeitos citogenotóxicos de TF e TN, isolados e combinados, em concentrações ambientalmente relevantes (TF: 0,006; 0,012; e 0,024 mg/ml; TN: 1,5; 3,0; e 6,0 mg/ml; e 0,012 mg/ml TF + 3,0 mg/ml TN) em linfócitos humanos, utilizando o teste de exclusão por azul de tripano e o ensaio do cometa. Adicionalmente, ferramentas *in silico*, *BioTransformer e DIGEP-Pred*, foram empregadas para elucidar vias metabólicas de detoxificação desses xenobióticos e avaliar seus possíveis efeitos na transcrição gênica. A exposição a TF e TN, isolados ou em combinação, não afetou a viabilidade dos linfócitos nas concentrações testadas. Contudo, ambos os compostos induziram aumento na porcentagem de quebras de fitas de DNA após o tratamento. As previsões *in silico* sugeriram que a interação com isoformas do citocromo P450 (CYP1A2, CYP2A6, CYP2C9 e CYP2D6) diferiu para cada composto analisado. A predição de expressão

gênica indicou que TF e TN podem regular positivamente genes envolvidos em alterações hormonais, risco de Alzheimer e progressão do câncer (SF1, SPON1, ADGRF5 e RORB), enquanto podem regular negativamente um gene associado a alterações no ritmo cardíaco e neurotoxicidade (HCN1). Em conclusão, nossos achados reforçam que os fungicidas triazólicos TF e TN, embora eficazes na agricultura, podem representar riscos à estabilidade genômica em humanos, destacando a importância de estudos de biomonitoramento em populações expostas.

5.2.2. Introdução

Os pesticidas são amplamente utilizados na agricultura moderna para proteger as culturas contra pragas, fungos e doenças (Boros, Roman e Isvoran, 2024). Os fungicidas, uma classe primária de pesticidas, desempenham papel crucial no controle de infecções fúngicas que comprometem a produtividade agrícola (Zubrod *et al*., 2019). Entre eles, os triazóis constituem uma classe importante devido à sua atividade de amplo espectro e propriedades sistêmicas, que inibem a biossíntese de ergosterol e impedem a formação de membranas celulares fúngicas (Dong *et al*., 2023). Apesar de sua eficácia, os triazóis têm sido associados a efeitos adversos em organismos não alvo, levantando preocupações quanto à segurança toxicológica e às possíveis consequências ambientais de longo prazo (Boros, Roman e Isvoran, 2024; Tofan *et al*., 2023; Zarn, Brüschweiler e Schlatter, 2003).

O triadimefon (TF) é um fungicida triazólico utilizado principalmente no controle da ferrugem e do oídio (Han *et al*., 2024). Diversos efeitos adversos em organismos não alvo já foram relatados para esse composto, incluindo neurotoxicidade, hepatotoxicidade, toxicidade cardiovascular, estresse oxidativo e efeitos teratogênicos (Zarn, Brüschweiler e Schlatter, 2003). O TF demonstrou provocar alterações no desenvolvimento de organismos aquáticos, como malformações nos arcos branquiais de anfíbios e comprometimento da embriogênese em zebrafish (Hou *et al*., 2022).

O triadimenol (TN), principal metabólito do TF, é amplamente utilizado como fungicida para controlar infecções fúngicas em culturas agrícolas (Zhang *et al*., 2018). Assim como o TF, o TN tem sido associado a efeitos genotóxicos, incluindo formação de micronúcleos e aberrações cromossômicas em diferentes tipos celulares (Rasgele, 2025), além de estresse oxidativo em girinos (Zhang *et al*., 2018). Ademais, o TN induziu toxicidade no desenvolvimento, no sistema endócrino e na reprodução de mamíferos (Zarn, Brüschweiler e Schlatter, 2003).

Embora TF e TN não sejam geralmente comercializados como mistura, sua proximidade química e metabólica sugere que a coexposição é possível (Garrison, Avants e Jones, 2011; Hou *et al*., 2022). A alta estabilidade, baixa biodegradabilidade e facilidade de transporte de TF e TN contribuem para sua persistência diferencial em solos e águas. Consequentemente, essa persistência aumenta a ocorrência de exposições sequenciais ou simultâneas, ressaltando a necessidade de investigar os possíveis efeitos genotóxicos sinérgicos ou aditivos que podem resultar dessas coexposições (Hou *et al*., 2022; Zhang *et al*., 2018). Dada a classificação estabelecida de TF e TN como possíveis carcinógenos humanos (Hou *et al*., 2022) e sua associação com diversos desfechos toxicológicos, é relevante investigar seu potencial de induzir danos ao DNA em células humanas. A exposição humana a esses compostos pode ocorrer por meio do manuseio ocupacional ou pela ingestão de resíduos alimentares (Pedroso *et al*., 2022). Já foi relatado que a exposição ocupacional a pesticidas pode levar a efeitos genotóxicos, incluindo trocas de cromátides-irmãs, formação de micronúcleos, aberrações cromossômicas, adutos de DNA e quebras de fitas. Esses efeitos têm potencial para comprometer os sistemas nervoso, respiratório, reprodutivo e imunológico, aumentando o risco de câncer (Ahmad *et al*., 2024; Pedroso *et al*., 2022).

Embora diversos estudos tenham descrito a citotoxicidade e a genotoxicidade de TF e TN em organismos aquáticos e modelos mamíferos, pouco se sabe sobre seus efeitos em células humanas. Além disso, nenhum estudo avaliou ainda o impacto combinado de TF e TN em linfócitos humanos. Os linfócitos de sangue periférico humano são tipos celulares relevantes que refletem a exposição sistêmica e a estabilidade genômica (Antoniou *et al*., 2023). O uso de linfócitos como modelo fornece uma correlação apropriada entre achados *in vitro* e exposição humana real, apoiando a extrapolação para riscos ocupacionais e dietéticos potenciais (Lebailly *et al*., 2015). Diante da persistência ambiental e da possível coocorrência de TF e TN, é necessária uma avaliação abrangente que incorpore exposições individuais e combinadas.

O ensaio do cometa é um método rápido, simples e sensível capaz de detectar quebras de fitas de DNA (simples e duplas, sítios lábeis em meio alcalino e ligações DNA-proteína) em células individuais. Esse ensaio tem sido amplamente utilizado para avaliar efeitos genotóxicos induzidos por agentes químicos em diferentes tipos celulares e condições experimentais (Calderón-Segura *et al*., 2012; Ramos *et al*., 2021; Sasikala *et al*., 2023). Além disso, é comumente empregado em estudos de biomonitoramento humano como biomarcador de exposição a agentes genotóxicos (Ladeira *et al*., 2024; Ramos *et al*., 2021). A previsão das características metabólicas induzidas por TF e TN fornece uma abordagem poderosa para elucidar possíveis mecanismos de ação tóxica. Ao investigar como esses compostos perturbam

vias bioquímicas essenciais, podemos identificar biomarcadores precoces de efeitos adversos, prever toxicidade crônica e estabelecer bases para uma avaliação de risco mais robusta (Hasselgren e Myatt, 2018; Loiodice, Nogueira da Costa e Atienzar, 2019).

Assim, este trabalho teve como objetivo investigar a citogenotoxicidade de TF e TN, isolados e combinados, em concentrações ambientalmente relevantes, em linfócitos humanos. Além disso, ferramentas *in silico* foram utilizadas para elucidar vias metabólicas de detoxificação desses xenobióticos e avaliar seus possíveis efeitos na transcrição gênica. Em síntese, este estudo vinculou a investigação toxicológica *in vitro* e *in silico* de TF e TN à exposição real, permitindo políticas baseadas em evidências e apoiando o desenvolvimento de alternativas de menor risco.

5.2.3. Conclusão

Nossos resultados demonstraram que o triadimefon (TF) e o triadimenol (TN), individualmente ou em combinação, induziram danos ao DNA em linfócitos humanos em concentrações ambientalmente relevantes, apesar de não afetarem a viabilidade celular. As análises *in silico* revelaram interações distintas com isoformas do citocromo P450 e previram alterações na expressão gênica associadas à regulação hormonal, neurotoxicidade e progressão do câncer. Esses achados reforçam que os fungicidas triazólicos, embora eficazes na agricultura, podem representar riscos à estabilidade genômica em humanos. Portanto, estudos de biomonitoramento em populações expostas são essenciais, e pesquisas adicionais são necessárias para esclarecer as implicações de longo prazo da exposição a esses compostos.

5.3. Artigo 3: Efeito genotóxico, mutagênico e na biomassa de *eisenia fetida* expostas ao fungicida triadimefon e triadimenol

5.3.1. Resumo

Triadimefon e triadimenol são fungicidas sistêmicos de amplo espectro amplamente utilizados na agricultura. No presente estudo, avaliamos os efeitos genotóxicos, mutagênicos e na biomassa de minhocas da espécie *Eisenia fetida* expostas ao triadimefon, triadimenol e à mistura de ambos. As minhocas foram expostas por 7, 14 e 21 dias a diferentes concentrações de triadimefon (0,006; 0,12; e 0,24 mg/kg) e triadimenol (1,5; 3; e 6 mg/kg). Aos 14 e 21 dias, a perda de peso ultrapassou 20%, chegando a mais de 40% nas maiores concentrações de ambos

os triazóis. Em relação aos biomarcadores ecotoxicológicos, efeitos genotóxicos foram detectados nas maiores concentrações dos fungicidas, isolados e em mistura, especialmente após 14 e 21 dias de exposição. Em contraste, um leve aumento mutagênico foi observado apenas na maior concentração de triadimefon. Além disso, a exposição de *E. fetida* aos fungicidas triazólicos promoveu redução significativa da biomassa a partir do 14º dia, indicando efeitos subletais associados ao estresse metabólico. Esses resultados reforçam a necessidade de monitoramento do impacto ambiental dos triazóis, pois mesmo em concentrações ambientalmente relevantes podem induzir danos genotóxicos em organismos modelo do solo.

5.3.2. Introdução

Os pesticidas são amplamente utilizados na agricultura comercial e contribuíram significativamente para o aumento da produtividade agrícola ao controlar pragas e doenças, garantindo a segurança alimentar para uma população global em constante crescimento (Lammertyn *et al*., 2024). Contudo, o uso excessivo ou inadequado pode levar ao acúmulo de resíduos no ambiente e comprometer a qualidade do solo, a biodiversidade e a saúde humana. Entre esses compostos, os pesticidas triazólicos constituem uma classe de fungicidas sistêmicos contendo a molécula 1,2,4-triazol (Liu *et al*., 2014). Devido ao seu amplo espectro e versatilidade, os triazóis são amplamente utilizados como fungicidas ou agentes medicinais e representam o segundo maior grupo de fungicidas mundialmente (Tang *et al*., 2024).

Introduzidos no mercado em meados da década de 1970 por empresas como a Ciba-Geigy®, os compostos triazólicos são absorvidos pelas plantas e distribuídos em sua estrutura, proporcionando proteção duradoura (Nasonov e Yakuba, 2024; Sun *et al*., 2023). Seu mecanismo de ação baseia-se na inibição da biossíntese de ergosterol, componente essencial das membranas celulares fúngicas, por meio da enzima lanosterol 14α-desmetilase (CYP51), um citocromo P450 monooxigenase. Dada sua ampla aplicação, é essencial compreender suas propriedades químicas, que influenciam diretamente o comportamento ambiental, a persistência, a atividade biológica e o potencial ecotoxicológico (Malik *et al*., 2024).

Neste contexto, o presente estudo investigou os fungicidas triazólicos triadimefon e triadimenol, moléculas heterocíclicas com diferentes centros quirais e potenciais toxicológicos. Apesar de sua eficácia agrícola, estudos relatam efeitos adversos em organismos silvestres e classificam ambos como possíveis carcinógenos humanos (Li *et al*., 2017; Zhang *et al*., 2020). As minhocas da espécie *Eisenia fetida* foram escolhidas como bioindicadores devido à sua reconhecida sensibilidade a poluentes do solo e relevância em avaliações ecotoxicológicas

(Zhou *et al*., 2016; Rico *et al*., 2016). Assim, este trabalho buscou avaliar os efeitos genotóxicos, mutagênicos e na biomassa de *E. fetida* expostas a triadimefon, triadimenol e à mistura, em diferentes tempos e concentrações, utilizando biomarcadores genéticos como o ensaio do cometa e o teste de micronúcleo.

5.3.3. Conclusão

Em síntese, a exposição de *Eisenia fetida* aos fungicidas triazólicos triadimefon e triadimenol resultou em redução significativa da biomassa, especialmente após 14 e 21 dias, indicando efeitos subletais associados ao estresse metabólico. Os biomarcadores genéticos demonstraram que ambos os compostos induzem danos ao DNA, com maior intensidade para o triadimefon, enquanto a mutagenicidade foi observada apenas na maior concentração desse fungicida após 21 dias. A análise integrada (PCA) evidenciou que os efeitos genotóxicos e mutagênicos são dependentes da concentração, do tipo de composto e do tempo de exposição, sugerindo risco genético elevado em exposições prolongadas. Esses resultados reforçam a necessidade de monitoramento ambiental dos triazóis e de estudos adicionais que integrem biomarcadores genéticos e bioquímicos, visando compreender melhor os mecanismos de toxicidade e os impactos de longo prazo desses fungicidas em organismos do solo.

6. CONSIDERAÇÕES FINAIS

Este trabalho demonstrou, por meio de uma abordagem multidisciplinar que integra a química teórica, a modelagem molecular e a toxicologia experimental, que os riscos ambientais e biológicos dos fungicidas triadimefon (TF) e triadimenol (TN) estão intrinsecamente associados às suas propriedades moleculares e estereoquímicas. A principal contribuição deste estudo reside na demonstração de que a toxicidade não é uniforme entre estereoisômeros; as variações nos índices de reatividade química e nas interações não covalentes revelaram níveis de risco distintos para organismos não alvo. Tais achados preenchem uma lacuna na compreensão mecanística desses xenobióticos, reforçando a necessidade crítica de que processos regulatórios considerem explicitamente a quiralidade das moléculas na avaliação de risco.

A investigação evidenciou que tanto o TF quanto o TN possuem capacidade de induzir quebras nas cadeias de DNA em concentrações ambientalmente relevantes sem provocar morte celular imediata, caracterizando um risco genotóxico significativo. Este fenômeno alerta para os perigos da exposição crônica e o potencial acúmulo de danos genômicos em populações expostas. Ademais, as predições de interação com enzimas do citocromo P450 sugerem que estes agroquímicos podem atuar como interferentes metabólicos, extrapolando o dano celular direto e apontando para possíveis desequilíbrios endócrinos.

Não obstante as contribuições alcançadas, o estudo apresenta limitações, como o foco em modelos biológicos específicos (*in vitro* humano e *in vivo* com anelídeos) e a dependência de predições computacionais para as rotas metabólicas, que, embora robustas, representam simplificações de sistemas biológicos complexos.

Como perspectivas para trabalhos futuros, aponta-se a necessidade de validação experimental direta dos metabólitos previstos *in silico* e a ampliação desta metodologia para outros fungicidas inibidores da desmetilação (DMIs). Tais passos são fundamentais para consolidar o uso de ferramentas computacionais na predição de toxicidade e fornecer subsídios mais precisos para a revisão de protocolos de segurança ambiental e ocupacional, visando um manejo agrícola verdadeiramente sustentável e seguro para a saúde humana.

REFERÊNCIAS BIBLIOGRÁFICAS

AGUILAR-BAÑUELOS, José Antonio *et al.* Environmental exposure to pesticides is associated with oxidative stress, oxidative DNA damage, and elevated interleukin-8 in a child population. **Environmental Toxicology and Pharmacology**, v. 114, p. 104656, mar. 2025.

AHMAD, Md Faruque *et al.* Pesticides impacts on human health and the environment with their mechanisms of action and possible countermeasures. **Heliyon**, v. 10, n. 7, p. e29128, abr. 2024.

ALABUGIN, Igor V.; GILMORE, Kerry M.; PETERSON, Paul W. Hyperconjugation. **WIREs Computational Molecular Science**, v. 1, n. 1, p. 109–141, 21 jan. 2011.

ALISTE, Marina *et al.* Risk Assessment of 1,2,4-Triazole-Typed Fungicides for Groundwater Pollution Using Leaching Potential Indices. **Water, Air, and Soil Pollution**, v. 232, n. 11, 1 nov. 2021.

ALVES, Vinicius M. *et al.* A Perspective and a New Integrated Computational Strategy for Skin Sensitization Assessment. **ACS Sustainable Chemistry & Engineering**, v. 6, n. 3, p. 2845–2859, 5 mar. 2018.

ANTONIOU, Evangelia E. *et al.* Micronuclei in human peripheral blood and bone marrow as genotoxicity markers: A systematic review and meta-analysis. **Mutation Research/Genetic Toxicology and Environmental Mutagenesis**, v. 891, p. 503689, out. 2023.

BADER, R. F. W. Atoms in molecules. **Accounts of Chemical Research**, v. 18, n. 1, p. 9–15, 1 jan. 1985.

BADER, R. F. W.; ESSÉN, H. The characterization of atomic interactions. **The Journal of Chemical Physics**, v. 80, n. 5, p. 1943–1960, 1 mar. 1984.

BADER, R. F. W.; NGUYEN-DANG, T. T.; TAL, Y. A topological theory of molecular structure. **Reports on Progress in Physics**, v. 44, n. 8, p. 893–948, 1 ago. 1981.

BADER, Richard F. W. **Atoms in Molecules: A Quantum Theory**. 1. ed. Ontario: Clarendon Press, 1994.

BANERJEE, Priyanka *et al.* ProTox 3.0: a webserver for the prediction of toxicity of chemicals. **Nucleic Acids Research**, v. 52, n. W1, p. W513–W520, 5 jul. 2024.

BANSAL, O. P. Health Impacts of the Carbamate and Dithiocarbamate Pesticides: A Review. **International Journal of Scientific and Research Publications (IJSRP)**, v. 12, n. 2, p. 366, 24 fev. 2022.

BARBIERI, Geovana F. *et al.* Herbicide mixtures: interactions and modeling. **Advances in Weed Science**, v. 40, n. spe1, 12 dez. 2022.

BARTLETT, Dave W. *et al.* The strobilurin fungicides. **Pest Management Science**, v. 58, n. 7, p. 649–662, 23 jul. 2002.

BERNSTEIN, Joel *et al.* Patterns in Hydrogen Bonding: Functionality and Graph Set Analysis in Crystals. **Angewandte Chemie International Edition in English**, v. 34, n. 15, p. 1555–1573, 18 ago. 1995.

BORBA, Joyce V. B. *et al.* Pred-Skin: A Web Portal for Accurate Prediction of Human Skin Sensitizers. **Chemical Research in Toxicology**, v. 34, n. 2, p. 258–267, 15 fev. 2021.

BOROS, Bianca-Vanesa; ROMAN, Diana-Larisa; ISVORAN, Adriana. Evaluation of the Aquatic Toxicity of Several Triazole Fungicides. **Metabolites**, v. 14, n. 4, p. 197, 2 abr. 2024.

BOTELHO, Matheus Gabriel Lopes *et al.* Agrotóxicos na agricultura: agentes de danos ambientais e a busca pela agricultura sustentável. **Research, Society and Development**, v. 9, n. 8, p. e396985806, 9 jul. 2020.

BOUZIANA, Stella D. Clinical relevance of clopidogrel-proton pump inhibitors interaction. **World Journal of Gastrointestinal Pharmacology and Therapeutics**, v. 6, n. 2, p. 17, 2015.

BRAGA, Rodolpho C. *et al.* Pred-hERG: A Novel web-Accessible Computational Tool for Predicting Cardiac Toxicity. **Molecular Informatics**, v. 34, n. 10, p. 698–701, 20 out. 2015.

BRENT, K. J. .. **Fungicide resistance in crop pathogens: how can it be managed?** *[S.l.]*: GIFAP, 1995.

BURDEN, Raymond S. *et al.* Comparative activity of the enantiomers of triadimenol and paclobutrazol as inhibitors of fungal growth and plant sterol and gibberellin biosynthesis. **Pesticide Science**, v. 21, n. 4, p. 253–267, 28 jan. 1987.

CALDERÓN-SEGURA, María Elena *et al.* Evaluation of Genotoxic and Cytotoxic Effects in Human Peripheral Blood Lymphocytes Exposed *In Vitro* to Neonicotinoid Insecticides News. **Journal of Toxicology**, v. 2012, p. 1–11, 2012.

CAMBRIDGE CRYSTALLOGRAPHIC DATA CENTRE. **The Cambridge Structural Database (CSD)**. Cambridge, 2023. Disponível em: https://www.ccdc.cam.ac.uk/.

CAMPANI, Tommaso *et al.* Toxicity of Four Commercial Fungicides, Alone and in Combination, on the Earthworm *Eisenia fetida*: A Field Experiment. **Toxics**, v. 13, n. 3, p. 209, 14 mar. 2025.

CASSAL, Vivian Brusius *et al.* AGROTÓXICOS: UMA REVISÃO DE SUAS CONSEQUÊNCIAS PARA A SAÚDE PÚBLICA. **Revista Eletrônica em Gestão, Educação e Tecnologia Ambiental**, v. 18, n. 1, 7 abr. 2014.

CHEN, Wenchan *et al.* Sterol demethylation inhibitor fungicide resistance in Colletotrichum siamense from chili is caused by mutations in CYP51A and CYP51B. **Phytopathology Research**, v. 4, n. 1, p. 41, 10 nov. 2022.

CHEN, Yewen *et al.* Computational simulations uncover enantioselective metabolism of chiral triazole fungicides by human CYP450 enzymes: A case study of tebuconazole. **Ecotoxicology and Environmental Safety**, v. 284, 1 out. 2024.

CHENG, Feixiong *et al.* admetSAR: A Comprehensive Source and Free Tool for Assessment of Chemical ADMET Properties. **Journal of Chemical Information and Modeling**, v. 52, n. 11, p. 3099–3105, 26 nov. 2012.

COLLINS, Andrew R. The Comet Assay for DNA Damage and Repair: Principles, Applications, and Limitations. **Molecular Biotechnology**, v. 26, n. 3, p. 249–261, 2004.

CROWELL, Susan Ritger *et al.* Development and application of a physiologically based pharmacokinetic model for triadimefon and its metabolite triadimenol in rats and humans. **Toxicology Letters**, v. 205, n. 2, p. 154–162, ago. 2011.

DA SILVA, Hélio Elias *et al.* Genotoxic and mutagenic evaluation in *Eisenia fetida* annelids exposed to iron ore tailings from the region of Brumadinho, MG, Brazil. **Environmental Toxicology and Pharmacology**, v. 102, p. 104247, set. 2023.

DAINA, Antoine; MICHIELIN, Olivier; ZOETE, Vincent. SwissADME: a free web tool to evaluate pharmacokinetics, drug-likeness and medicinal chemistry friendliness of small molecules. **Scientific Reports**, v. 7, n. 1, p. 42717, 3 mar. 2017.

DE ALBUQUERQUE, Nayara Cristina Perez *et al.* Metabolism studies of chiral pesticides: A critical review. **Journal of Pharmaceutical and Biomedical Analysis**, v. 147, p. 89–109, jan. 2018.

DEAS, A. H. B.; CLIFFORD, D. R. Metabolism of the 1,2,4-triazolylmethane fungicides, triadimefon, triadimenol, and diclobutrazol, by Aspergillus niger (van Tiegh.). **Pesticide Biochemistry and Physiology**, v. 17, n. 2, p. 120–133, abr. 1982.

DEAS, A. H. B.; CLIFFORD, D. R. Reductive and oxidative metabolism of triazolylmethanes by two basidiomycete fungi. **Pesticide Biochemistry and Physiology**, v. 22, n. 3, p. 276–284, dez. 1984.

DEBELJAK, Nataša; FINK, Martina; ROZMAN, Damjana. Many facets of mammalian lanosterol 14α-demethylase from the evolutionarily conserved cytochrome P450 family CYP51. **Archives of Biochemistry and Biophysics**, v. 409, n. 1, p. 159–171, jan. 2003.

DENG, Peng *et al.* Synthesis and Antitumor Activity of Erlotinib Derivatives Linked With 1,2,3-Triazole. **Frontiers in Pharmacology**, v. 12, 17 jan. 2022.

DI RENZO, Francesca *et al.* Citral, an inhibitor of retinoic acid synthesis, attenuates the frequency and severity of branchial arch abnormalities induced by triazole-derivative fluconazole in rat embryos cultured *in vitro*. **Reproductive Toxicology**, v. 24, n. 3–4, p. 326–332, nov. 2007.

DI, Yuan *et al.* Structure, Function, Regulation and Polymorphism of Human Cytochrome P450 2A6. **Current Drug Metabolism**, v. 10, n. 7, p. 754–780, 1 set. 2009.

DIKILITAS, Murat *et al.* **EVALUATION OF GENOTOXICITY OF ENVIRONMENTALLY FRIENDLY PESTICIDES ON HIGHER CELLS USING THE SINGLE CELL GEL ELECTROPHORESIS (SCGE) ASSAY**. *[S.l.: S.n.]*. Disponível em: <www.sigma.com>.

DJOUMBOU-FEUNANG, Yannick *et al.* BioTransformer: a comprehensive computational tool for small molecule metabolism prediction and metabolite identification. **Journal of Cheminformatics**, v. 11, n. 1, p. 2, 5 dez. 2019.

DOMINGO, Luis R. *et al.* Quantitative characterization of the global electrophilicity power of common diene/dienophile pairs in Diels–Alder reactions. **Tetrahedron**, v. 58, n. 22, p. 4417–4423, maio 2002.

DONG, Zhan *et al.* The widespread presence of triazole fungicides in greenhouse soils in Shandong Province, China: A systematic study on human health and ecological risk assessments. **Environmental Pollution**, v. 328, p. 121637, jul. 2023.

DÜCKER, Christof; BROCKMÖLLER, Jürgen. How precise is quantitative prediction of pharmacokinetic effects due to drug-drug interactions and genotype from *in vitro* data? A comprehensive analysis on the example CYP2D6 and CYP2C19 substrates. **Pharmacology & Therapeutics**, v. 217, p. 107629, jan. 2021.

EMAMI, Saeed; TAVANGAR, Pegah; KEIGHOBADI, Masoud. An overview of azoles targeting sterol 14α-demethylase for antileishmanial therapy. **European Journal of Medicinal Chemistry**, v. 135, p. 241–259, jul. 2017.

EMAMIAN, Saeedreza *et al.* Exploring Nature and Predicting Strength of Hydrogen Bonds: A Correlation Analysis Between Atoms-in-Molecules Descriptors, Binding Energies, and Energy Components of Symmetry-Adapted Perturbation Theory. **Journal of Computational Chemistry**, v. 40, n. 32, p. 2868–2881, 15 dez. 2019.

FERNANDES, Amanda Silva *et al.* Tellimagrandin-I and camptothin a exhibit chemopreventive effects in *Salmonella enterica* serovar Typhimurium strains and human lymphocytes. **Journal of Toxicology and Environmental Health, Part A**, v. 87, n. 5, p. 185–198, 3 mar. 2024.

FERRI, Giovanni Maria *et al.* Lymphocytes DNA damages and exposure to chlorpyrifos, deltamethrin, penconazole, copper oxicloride. **Biomarkers**, v. 24, n. 2, p. 186–198, 17 fev. 2019.

FOTAKIS, George; TIMBRELL, John A. *In vitro* cytotoxicity assays: Comparison of LDH, neutral red, MTT and protein assay in hepatoma cell lines following exposure to cadmium chloride. **Toxicology Letters**, v. 160, n. 2, p. 171–177, jan. 2006.

FRAC. **FRAC Code List ©* 2024: Fungal control agents sorted by cross-resistance pattern and mode of action (including coding for FRAC Groups on product labels)**. *[S.l.: S.n.]*.

FRISCH, M. J. *et al.* **Gaussian 16, Revision C.01**. Wallingford, CTGaussian, Inc., , 2016.

FUKUI, Kenichi. Role of Frontier Orbitals in Chemical Reactions. **Science**, v. 218, n. 4574, p. 747–754, 19 nov. 1982.

FUKUTO, T. R. Mechanism of action of organophosphorus and carbamate insecticides. **Environmental Health Perspectives**, v. 87, p. 245–254, jul. 1990.

GAO, Minling *et al.* Effect on enzymes and histopathology in earthworm (*Eisenia fetida*) induced by triazole fungicides. **Environmental Toxicology and Pharmacology**, v. 35, n. 3, p. 427–433, maio 2013.

GARCIA, A. Fungicidas I: utilização no controle químico de doenças e sua ação contra os fitopatógenos. 1999.

GARRISON, Arthur W.; AVANTS, Jimmy K.; JONES, W. Jack. Microbial Transformation of Triadimefon to Triadimenol in Soils: Selective Production Rates of Triadimenol Stereoisomers Affect Exposure and Risk. **Environmental Science & Technology**, v. 45, n. 6, p. 2186–2193, 15 mar. 2011.

G.C. MONTEIRO, Mônica Bartira da Silva, Luan Fernando Ormond Sobreira Rodrigues, entre outros. Influência da aplicação de fungicidas sistêmicos na cultura de couve-flor. **Brazilian Applied Science Review (BASR)**, p. 1073–1082, 2019.

GHASEMI, Mahshid *et al.* The MTT Assay: Utility, Limitations, Pitfalls, and Interpretation in Bulk and Single-Cell Analysis. **International Journal of Molecular Sciences**, v. 22, n. 23, p. 12827, 26 nov. 2021.

GILLI, Gastone; GILLI, Paola. **The Nature of the Hydrogen Bond**. *[S.l.]*: Oxford University Press, 2009.

GOETZ, Amber K. *et al.* Disruption of Testosterone Homeostasis as a Mode of Action for the Reproductive Toxicity of Triazole Fungicides in the Male Rat. **Toxicological Sciences**, v. 95, n. 1, p. 227–239, jan. 2007.

HAN, Lei *et al.* Dissipation and residue of triadimefon in *Rosa roxburghii*. **Food Additives & Contaminants: Part A**, v. 41, n. 8, p. 914–922, 2 ago. 2024.

HASSELGREN, Catrin; MYATT, Glenn J. Computational Toxicology and Drug Discovery. *In*: *[S.l.: S.n.]*. p. 233–244.

HAZUKOVÁ, Radka *et al.* Oxidative DNA Damage and Arterial Hypertension in Light of Current ESC Guidelines. **International Journal of Molecular Sciences**, v. 25, n. 23, p. 12557, 22 nov. 2024.

HEISE, T. *et al.* Hepatotoxic combination effects of three azole fungicides in a broad dose range. **Archives of Toxicology**, v. 92, n. 2, p. 859–872, 1 fev. 2018.

HOHENBERG, P.; KOHN, W. Inhomogeneous Electron Gas. **Physical Review**, v. 136, n. 3B, p. B864–B871, 9 nov. 1964.

HOU, Lin *et al.* Triadimefon in aquatic environments: occurrence, fate, toxicity, and ecological risk. **Environmental Sciences Europe**, v. 34, n. 1, p. 12, 21 dez. 2022.

HOW, Chun Ming; LI, Shang-Wei; LIAO, Vivian Hsiu-Chuan. Chronic exposure to triadimenol at environmentally relevant concentration adversely affects aging biomarkers in Caenorhabditis elegans associated with insulin/IGF-1 signaling pathway. **Science of The Total Environment**, v. 640–641, p. 485–492, nov. 2018.

HUANG, Tao *et al.* A comprehensive review of 1,2,4-triazole fungicide toxicity in zebrafish (Danio rerio): A mitochondrial and metabolic perspective. **Science of The Total Environment**, v. 809, p. 151177, fev. 2022.

ISHII, Hideo. New chemical fungicides in relation to risk for resistance development. **Tropical Plant Pathology**, v. 49, n. 1, p. 18–35, 19 jul. 2023.

JACENIK, Damian; KARAGIANNIDIS, Ioannis; BESWICK, Ellen J. Th2 cells inhibit growth of colon and pancreas cancers by promoting anti-tumorigenic responses from macrophages and eosinophils. **British Journal of Cancer**, v. 128, n. 2, p. 387–397, 19 jan. 2023.

JIANG, Jinhua *et al.* Toxicological analysis of triadimefon on endocrine disruption and oxidative stress during rare minnow (Gobiocypris rarus) larvae development. **Environmental Science and Pollution Research**, v. 24, n. 34, p. 26681–26691, 27 dez. 2017.

KALUZHSKIY, Leonid *et al.* Human Lanosterol 14-Alpha Demethylase (CYP51A1) Is a Putative Target for Natural Flavonoid Luteolin 7,3′-Disulfate. **Molecules**, v. 26, n. 8, p. 2237, 13 abr. 2021.

KENIYA, Mikhail V. *et al.* Heterologous Expression of Full-Length Lanosterol 14α-Demethylases of Prominent Fungal Pathogens Candida albicans and Candida glabrata Provides Tools for Antifungal Discovery. **Antimicrobial Agents and Chemotherapy**, v. 62, n. 11, nov. 2018.

KENNEKE, John F. *et al.* Mechanistic Investigation of the Noncytochrome P450-Mediated Metabolism of Triadimefon to Triadimenol in Hepatic Microsomes. **Chemical Research in Toxicology**, v. 21, n. 10, p. 1997–2004, 20 out. 2008.

KENNEKE, John F. *et al.* Integration of metabolomics and *in vitro* metabolism assays for investigating the stereoselective transformation of triadimefon in rainbow trout. **Chirality**, v. 22, n. 2, p. 183–192, 5 fev. 2010.

KLITTICH, Carla J. R. Fungicide Mobility and the Influence of Physical Properties. *In*: *[S.l.: S.n.]*. p. 95–109.

KNEBEL, Constanze *et al.* Unexpected Effects of Propiconazole, Tebuconazole, and Their Mixture on the Receptors CAR and PXR in Human Liver Cells. **Toxicological Sciences**, v. 163, n. 1, p. 170–181, 1 maio 2018.

KOHN, W.; SHAM, L. J. Self-Consistent Equations Including Exchange and Correlation Effects. **Physical Review**, v. 140, n. 4A, p. A1133–A1138, 15 nov. 1965.

KOLENIČOVÁ, Simona *et al.* Genotoxicity testing of bovine lymphocytes exposed to epoxiconazole using alkaline and neutral comet assay. **Caryologia**, v. 73, n. 4, p. 99–109, 2020.

KONG, Zhiqiang *et al.* Stereoselective behaviors of the fungicide triadimefon and its metabolite triadimenol during malt storage and beer brewing. **Journal of Hazardous Materials**, v. 400, p. 123238, dez. 2020.

KURIHARA, N. *et al.* Pesticides Report 37: Chirality in synthetic agrochemicals: Bioactivity and safety consideration (Technical Report). **Pure and Applied Chemistry**, v. 69, n. 9, p. 2007–2026, 1 jan. 1997.

LADEIRA, Carina *et al.* The Comet Assay as a Tool in Human Biomonitoring Studies of Environmental and Occupational Exposure to Chemicals—A Systematic Scoping Review. **Toxics**, v. 12, n. 4, p. 270, 5 abr. 2024.

LAGUNIN, Alexey *et al.* DIGEP-Pred: web service for *in silico* prediction of drug-induced gene expression profiles based on structural formula. **Bioinformatics**, v. 29, n. 16, p. 2062–2063, 15 ago. 2013.

LAMMERTYN, Sofía *et al.* Earthworm injury test for in-situ biomonitoring of pesticides in biobeds. **Chemosphere**, v. 363, p. 142923, set. 2024.

LANGER, T.; WOLBER, G. Pharmacophore definition and 3D searches. **Drug Discovery Today: Technologies**, v. 1, n. 3, p. 203–207, dez. 2004.

LEBAILLY, Pierre *et al.* DNA damage in B and T lymphocytes of farmers during one pesticide spraying season. **International Archives of Occupational and Environmental Health**, v. 88, n. 7, p. 963–972, 3 out. 2015.

LEE, Sehan; BARRON, Mace G. A mechanism-based 3D-QSAR approach for classification and prediction of acetylcholinesterase inhibitory potency of organophosphate and carbamate analogs. **Journal of Computer-Aided Molecular Design**, v. 30, n. 4, p. 347–363, 7 abr. 2016.

LEROUX, Pierre. Chemical Control of Botrytis and its Resistance to Chemical Fungicides. *In*: **Botrytis: Biology, Pathology and Control**. Dordrecht: Springer Netherlands, 2007. p. 195–222.

LEROUX, Pierre *et al.* Mutations in the *CYP51* gene correlated with changes in sensitivity to sterol 14α-demethylation inhibitors in field isolates of *Mycosphaerella graminicola*. **Pest Management Science**, v. 63, n. 7, p. 688–698, 18 jul. 2007.

LI, Chaofeng *et al.* Toxicity, bioactivity of triazole fungicide metconazole and its effect on mycotoxin production by Fusarium verticillioides: New perspective from an enantiomeric level. **Science of The Total Environment**, v. 828, p. 154432, jul. 2022.

LI, Jitong *et al.* Tissue distribution and metabolism of triadimefon and triadimenol enantiomers in Chinese lizards (Eremias argus). **Ecotoxicology and Environmental Safety**, v. 142, p. 284–292, ago. 2017.

LI, Ning *et al.* Heart Rate Mystery Unveiled: Sex Differences in Human Sinoatrial Node Genes and Female Tachycardia. **Circulation: Arrhythmia and Electrophysiology**, v. 18, n. 5, maio 2025.

LI, Yan; EVANS, Jeremy N. S. The Fukui Function: A Key Concept Linking Frontier Molecular Orbital Theory and the Hard-Soft-Acid-Base Principle. **Journal of the American Chemical Society**, v. 117, n. 29, p. 7756–7759, 1 jul. 1995.

LI, Yinghong *et al.* Degradation of triadimefon and residue levels of metabolite triadimenol: tracing rapeseed from harvesting and storage to household oil processing. **Journal of the Science of Food and Agriculture**, v. 99, n. 4, p. 1484–1491, 15 mar. 2019.

LI, Yuanbo *et al.* Chiral fungicide triadimefon and triadimenol: Stereoselective transformation in greenhouse crops and soil, and toxicity to Daphnia magna. **Journal of Hazardous Materials**, v. 265, p. 115–123, jan. 2014.

LI, Zhaoyang *et al.* Enantioselective degradation, abiotic racemization, and chiral transformation of triadimefon in soils. **Environmental Science and Technology**, v. 45, n. 7, p. 2797–2803, 1 abr. 2011.

LIANG, Hongwu *et al.* Stereoselective transformation of triadimefon to metabolite triadimenol in wheat and soil under field conditions. **Journal of Hazardous Materials**, v. 260, p. 929–936, set. 2013.

LIU, Chunlan *et al.* Myclobutanil induces cardiotoxicity in developing zebrafish larvae by initiating oxidative stress and apoptosis: The protective role of curcumin. **Ecotoxicology and Environmental Safety**, v. 279, 1 jul. 2024.

LIU, Tiantian *et al.* Stereoselective Bioaccumulation and Metabolite Formation of Triadimefon in *Tubifex tubifex*. **Environmental Science & Technology**, v. 48, n. 12, p. 6687–6693, 17 jun. 2014.

LOIODICE, Simon; NOGUEIRA DA COSTA, Andre; ATIENZAR, Franck. Current trends in *in silico* , *in vitro* toxicology, and safety biomarkers in early drug development. **Drug and Chemical Toxicology**, v. 42, n. 2, p. 113–121, 4 mar. 2019.

LU HONGWEI, QIU Yurong, ZHANG Shanying, REN Saihao, ZHANG Yu, WANG Meng, LIANG Xiaoyu. Translocation and enrichment behavior of triadimefon and its metabolite triadimenol in rubber trees[J]. **Chinese Journal of Pesticide Science**, v. 25, n. 2, p. 444–452, 2023.

LU, Tian; CHEN, Feiwu. Multiwfn: A multifunctional wavefunction analyzer. **Journal of Computational Chemistry**, v. 33, n. 5, p. 580–592, 15 fev. 2012.

LV, Xuan *et al.* Effects of triazole fungicides on androgenic disruption and CYP3A4 enzyme activity. **Environmental Pollution**, v. 222, p. 504–512, 2017.

MA, Zhonghua; MICHAILIDES, Themis J. Advances in understanding molecular mechanisms of fungicide resistance and molecular detection of resistant genotypes in phytopathogenic fungi. **Crop Protection**, v. 24, n. 10, p. 853–863, out. 2005.

MACRAE, Clare F. *et al. Mercury 4.0* : from visualization to analysis, design and prediction. **Journal of Applied Crystallography**, v. 53, n. 1, p. 226–235, 1 fev. 2020.

MADEIRA, Pedro P. *et al.* Polarity of Aqueous Solutions. **Liquids**, v. 4, n. 1, p. 107–116, 12 jan. 2024.

MAHFOUDH, Mafakher *et al.* Recent Approaches to the Synthesis of Pyrimidine Derivatives. **European Journal of Organic Chemistry**, v. 2017, n. 20, p. 2856–2865, 26 maio 2017.

MALIK, Nisar Ahmad *et al.* **Fungicide-albumin interactions: unraveling the complex relationship—a comprehensive review**. **Biophysical Reviews**Springer Science and Business Media Deutschland GmbH, , 1 ago. 2024.

MAREPU, Nagaraju; YETURU, Sunandamma; PAL, Manojit. 1,2,3-Triazole fused with pyridine/pyrimidine as new template for antimicrobial agents: Regioselective synthesis and identification of potent N-heteroarenes. **Bioorganic & Medicinal Chemistry Letters**, v. 28, n. 20, p. 3302–3306, nov. 2018.

MATTA, Chérif F.; BADER, Richard F. W. Atoms-in-molecules study of the genetically encoded amino acids. III. Bond and atomic properties and their correlations with experiment including mutation-induced changes in protein stability and genetic coding. **Proteins: Structure, Function, and Bioinformatics**, v. 52, n. 3, p. 360–399, 15 ago. 2003.

MCKINNON, Joshua J.; SPACKMAN, Mark A.; MITCHELL, Anthony S. Novel tools for visualizing and exploring intermolecular interactions in molecular crystals. **Acta Crystallographica Section B Structural Science**, v. 60, n. 6, p. 627–668, 1 dez. 2004.

MENEGOLA, E. *et al.* Study on the common teratogenic pathway elicited by the fungicides triazole-derivatives. **Toxicology *in Vitro***, v. 19, n. 6, p. 737–748, set. 2005.

MERCADANTE, R. *et al.* Identification and Quantification of Metabolites of the Fungicide Tebuconazole in Human Urine. **Chemical Research in Toxicology**, v. 27, n. 11, p. 1943–1949, 17 nov. 2014.

MISHRA, C. S. K.; SAMAL, Suryasikha; SAMAL, Rashmi Rekha. Evaluating earthworms as candidates for remediating pesticide contaminated agricultural soil: A review. **Frontiers in Environmental Science**, v. 10, 25 out. 2022.

MONK, Brian C. *et al.* Architecture of a single membrane spanning cytochrome P450 suggests constraints that orient the catalytic domain relative to a bilayer. **Proceedings of the National Academy of Sciences**, v. 111, n. 10, p. 3865–3870, 11 mar. 2014.

MONK, Brian C. *et al.* Fungal Lanosterol 14α-demethylase: A target for next-generation antifungal design. **Biochimica et Biophysica Acta (BBA) - Proteins and Proteomics**, v. 1868, n. 3, p. 140206, mar. 2020.

NAGAPPAN, V.; DERESINSKI, S. Posaconazole: A Broad-Spectrum Triazole Antifungal Agent. **Clinical Infectious Diseases**, v. 45, n. 12, p. 1610–1617, 15 dez. 2007.

NAKANISHI, Waro; HAYASHI, Satoko; NARAHARA, Kenji. Atoms-in-Molecules Dual Parameter Analysis of Weak to Strong Interactions: Behaviors of Electronic Energy Densities versus Laplacian of Electron Densities at Bond Critical Points. **The Journal of Physical Chemistry A**, v. 112, n. 51, p. 13593–13599, 25 dez. 2008.

NAKANISHI, Waro; HAYASHI, Satoko; NARAHARA, Kenji. Polar Coordinate Representation of $H_b(r_c)$ versus $(\hbar^2/8m)\nabla^2\rho_b(r_c)$ at BCP in AIM Analysis: Classification

and Evaluation of Weak to Strong Interactions. **The Journal of Physical Chemistry A**, v. 113, n. 37, 17 set. 2009.

NASONOV, A. I.; YAKUBA, G. V. Apple Scab: Resistance to Chemical Fungicides. **Biology Bulletin Reviews**, v. 14, n. S1, p. S17–S30, 20 dez. 2024.

NÉMETH-RIEDER, Alexandra *et al.* Synthesis and *In Vitro* Anticancer Evaluation of Flavone—1,2,3-Triazole Hybrids. **Molecules**, v. 28, n. 2, p. 626, 7 jan. 2023.

NOWELL, I. W.; WALKER, P. E.; ANDERSON. N. H. Structure of 1-(4-chlorophenoxy)-3,3-dimethyl-1-(1,2,4-triazol-1-yl)-2-butanone. **Acta Crystallographica Section B Structural Crystallography and Crystal Chemistry**, v. 38, n. 6, p. 1857–1859, 15 jun. 1982.

OLIVE, Peggy L.; BANÁTH, Judit P. The comet assay: a method to measure DNA damage in individual cells. **Nature Protocols**, v. 1, n. 1, p. 23–29, 27 jun. 2006.

PANINI, Piyush *et al.* Solvatomorphism in Miconazole: The Role of Weak C–H···Cl Hydrogen Bonds and C–Cl···Cl–C Halogen Interactions in Similarities and Differences in the Crystal Packing. **Crystal Growth & Design**, v. 22, n. 4, p. 2703–2724, 6 abr. 2022.

PARR, Robert G.; SZENTPÁLY, László v.; LIU, Shubin. Electrophilicity Index. **Journal of the American Chemical Society**, v. 121, n. 9, p. 1922–1924, 1 mar. 1999.

PARR, Robert G.; WEITAO, Yang. **Density-Functional Theory of Atoms and Molecules**. *[S.l.]*: Oxford University Press, 1995.

PAULY RIBAS, Priscila; SANTOS MATSUMURA, Aida Terezinha. A química dos agrotóxicos: impacto sobre a saúde e meio ambiente. **Revista Liberato**, v. 10, n. 14, p. 149–158, 2009.

PEARSON, Ralph G. The electronic chemical potential and chemical hardness. **Journal of Molecular Structure: THEOCHEM**, v. 255, p. 261–270, mar. 1992.

PEARSON, Ralph G. Chemical hardness and density functional theory. **Journal of Chemical Sciences**, v. 117, n. 5, p. 369–377, set. 2005.

PEDROSO, Thays Millena Alves *et al.* Cancer and occupational exposure to pesticides: a bibliometric study of the past 10 years. **Environmental Science and Pollution Research**, v. 29, n. 12, p. 17464–17475, 19 mar. 2022.

PERES, Frederico; MOREIRA, Josino Costa. **É veneno ou é remédio? Agrotóxicos, saúde e ambiente**. *[S.l.]*: Editora FIOCRUZ, 2003.

PÉREZ, Patricia *et al.* Quantitative characterization of the global electrophilicity pattern of some reagents involved in 1,3-dipolar cycloaddition reactions. **Tetrahedron**, v. 59, n. 17, p. 3117–3125, abr. 2003.

PETRICCA, Sabrina *et al.* Oxidative Stress, Cytotoxic and Inflammatory Effects of Azoles Combinatorial Mixtures in Sertoli TM4 Cells. **Antioxidants**, v. 12, n. 6, p. 1142, 24 maio 2023.

PEYTON, L. R.; GALLAGHER, S.; HASHEMZADEH, M. Triazole antifungals: A review. **Drugs of Today**, v. 51, n. 12, p. 705, 2015.

PICININI, Edson Clodoveu; FERNANDES, José Maurício Cunha. Efeito do tratamento de sementes com fungicida sobre o controle de doenças na parte aérea do trigo. **Fitopatologia Brasileira**, v. 28, n. 5, p. 515–520, out. 2003.

QUEVEDO-CARABALLO, Sergio; ROLDÁN, Alejandra; ÁLVAREZ-PÉREZ, Sergio. Demethylation Inhibitor Fungicides Have a Significantly Detrimental Impact on Population Growth and Composition of Nectar Microbial Communities. **Microbial Ecology**, v. 87, n. 1, 1 dez. 2024.

RAMÍREZ-VILLALVA, Alejandra *et al.* Synthesis and antifungal activity of novel oxazolidin-2-one-linked 1,2,3-triazole derivatives. **MedChemComm**, v. 8, n. 12, p. 2258–2262, 2017.

RAMOS, Jheneffer Sonara Aguiar *et al.* Multi-biomarker responses to pesticides in an agricultural population from Central Brazil. **Science of The Total Environment**, v. 754, p. 141893, fev. 2021.

RASGELE, Pinar Goc. Comparative Assessment of Short- and Long-Term Effects of Triadimenol Fungicide on Danio rerio Erythrocytes Using the Micronucleus and Erythrocyte Nuclear Abnormality Assays. **Toxics**, v. 13, n. 3, p. 199, 11 mar. 2025.

RATNAKAR REDDY, K. *et al.* Synthesis of novel 1,2,3-triazole/isoxazole functionalized 2H-Chromene derivatives and their cytotoxic activity. **Bioorganic & Medicinal Chemistry Letters**, v. 24, n. 7, p. 1661–1663, abr. 2014.

RAY, Arpita *et al.* Evaluation of toxic effects of a triazole fungicide, difenoconazole in a freshwater fish model. **Ecotoxicology**, v. 34, n. 8, p. 1368–1383, 1 out. 2025.

REFFSTRUP, Trine Klein; LARSEN, John Christian; MEYER, Otto. Risk assessment of mixtures of pesticides. Current approaches and future strategies. **Regulatory Toxicology and Pharmacology**, v. 56, n. 2, p. 174–192, mar. 2010.

REYNOLDS, Chandra A. *et al.* Sequence variation in SORL1 and dementia risk in Swedes. **neurogenetics**, v. 11, n. 1, p. 139–142, 4 fev. 2010.

RJIBA-TOUATI, Karima *et al.* Genotoxic damage and apoptosis in rat glioma (F98) cell line following exposure to bromuconazole. **NeuroToxicology**, v. 94, p. 108–116, jan. 2023.

ROMAN, Diana Larisa *et al.* Effects of Triazole Fungicides on Soil Microbiota and on the Activities of Enzymes Found in Soil: A Review. **Agriculture**, v. 11, n. 9, p. 893, 17 set. 2021.

ROMAN, Diana Larisa *et al.* The Effects of the Fungicide Myclobutanil on Soil Enzyme Activity. **Agriculture**, v. 13, n. 10, p. 1956, 7 out. 2023.

ROUABHI, Mohamed *et al.* BBSome ablation in SF1 neurons causes obesity without comorbidities. **Molecular Metabolism**, v. 48, p. 101211, jun. 2021.

SABOTIČ, Jerica *et al.* A guide to the use of bioassays in exploration of natural resources. **Biotechnology Advances**, v. 71, p. 108307, mar. 2024.

SALAH, Eman Mohamed *et al.* Chemical composition and antifungal activity of Teucrium Leucocladum Boiss. essential oils growing in Egypt using two different techniques. **Future Journal of Pharmaceutical Sciences**, v. 10, n. 1, p. 51, 28 mar. 2024.

SANCHES, Igor H. *et al.* Enhancing hERG Risk Assessment with Interpretable Classificatory and Regression Models. **Chemical Research in Toxicology**, v. 37, n. 6, p. 910–922, 17 jun. 2024.

SARKER, Jagodish C.; HOGARTH, Graeme. Dithiocarbamate Complexes as Single Source Precursors to Nanoscale Binary, Ternary and Quaternary Metal Sulfides. **Chemical Reviews**, v. 121, n. 10, p. 6057–6123, 26 maio 2021.

SASIKALA, S. *et al.* Predicting the relationship between pesticide genotoxicity and breast cancer risk in South Indian women in *in vitro* and *in vivo* experiments. **Scientific Reports**, v. 13, n. 1, p. 9712, 15 jun. 2023.

SCHMIDT, F. *et al.* Combination effects of azole fungicides in male rats in a broad dose range. **Toxicology**, v. 355–356, p. 54–63, 29 abr. 2016.

SHAO, Yuting *et al.* Evaluation of the toxicity of 1-butyl-3-methyl imidazolium tetrafluoroborate using earthworms (*Eisenia fetida*) in two soils. **Science of The Total Environment**, v. 686, p. 946–958, out. 2019.

SHI, San Jun *et al.* Highly sensitive time-resolved fluorescent microspheres lateral flow immunoassay for the quantitative detection of triadimefon and its metabolite residues in fruits and vegetables. **Mikrochimica acta**, v. 191, n. 11, p. 670, 1 nov. 2024.

SINGH, Neera. Sorption Behavior of Triazole Fungicides in Indian Soils and Its Correlation with Soil Properties. **Journal of Agricultural and Food Chemistry**, v. 50, n. 22, p. 6434–6439, 1 out. 2002.

SJOBERG, Per.; POLITZER, Peter. Use of the electrostatic potential at the molecular surface to interpret and predict nucleophilic processes. **The Journal of Physical Chemistry**, v. 94, n. 10, p. 3959–3961, 1 maio 1990.

SMITH, Joshua A. *et al.* Oxidative stress, DNA damage, and the telomeric complex as therapeutic targets in acute neurodegeneration. **Neurochemistry International**, v. 62, n. 5, p. 764–775, abr. 2013.

SOTERO, Daiany Folador *et al.* Can Salvinia auriculata bioremediate the toxic effects of Fipronil 800wg on the tadpoles of Dendropsophus minutus? **Aquatic Toxicology**, v. 271, p. 106926, jun. 2024.

SPACKMAN, Mark A.; JAYATILAKA, Dylan. Hirshfeld surface analysis. **CrystEngComm**, v. 11, n. 1, p. 19–32, 2009.

SPACKMAN, Mark A.; MCKINNON, Joshua J. Fingerprinting intermolecular interactions in molecular crystals. **CrystEngComm**, v. 4, n. 66, p. 378–392, 2002.

SPACKMAN, Peter R. *et al. CrystalExplorer*: a program for Hirshfeld surface analysis, visualization and quantitative analysis of molecular crystals. **Journal of Applied Crystallography**, v. 54, n. 3, p. 1006–1011, 1 jun. 2021.

SPITZER, T.; KOPF, J.; NICKLESS, G. 1-(4-chlorophenoxy)-1-(1,2,4-triazol-1-yl)-3,3-dimethyl-butan-2-ol, C14H18O2N3Cl. **Crystal Structure Communications**, v. 11, p. 315–320, 1982.

STEPANENKO, A. A.; DMITRENKO, V. V. Pitfalls of the MTT assay: Direct and off-target effects of inhibitors can result in over/underestimation of cell viability. **Gene**, v. 574, n. 2, p. 193–203, dez. 2015.

STROBER, Warren. Trypan Blue Exclusion Test of Cell Viability. **Current Protocols in Immunology**, v. 111, n. 1, 2 nov. 2015.

SUN, Shengxin *et al.* Novel (Z)/(E)-1,2,4-triazole derivatives containing oxime ether moiety as potential ergosterol biosynthesis inhibitors: design, preparation, antifungal evaluation, and molecular docking. **Molecular Diversity**, v. 27, n. 1, p. 145–157, 15 fev. 2023.

TAMURA, Kei *et al.* Involvement of constitutive androstane receptor in liver hypertrophy and liver tumor development induced by triazole fungicides. **Food and Chemical Toxicology**, v. 78, p. 86–95, abr. 2015.

TANG, Tao *et al.* Determination of triazole fungicides in environmental water samples by high performance liquid chromatography with cloud point extraction using polyethylene glycol 600 monooleate. **Analytica Chimica Acta**, v. 680, n. 1–2, p. 26–31, nov. 2010.

TANG, Yutong *et al.* Toxicological risk assessment of triadimenol for human exposure, broiler health, and food safety. **Food and Chemical Toxicology**, v. 194, p. 115071, dez. 2024.

THE GIMP DEVELOPMENT TEAM. **GNU Image Manipulation Program (GIMP)**. Versão 2.10. [S. l.], 2025. Disponível em: https://www.gimp.org.

THOMPSON, George R.; WIEDERHOLD, Nathan P. Isavuconazole: A Comprehensive Review of Spectrum of Activity of a New Triazole. **Mycopathologia**, v. 170, n. 5, p. 291–313, 5 nov. 2010.

TICE, R. R. *et al.* Single cell gel/comet assay: Guidelines for *in vitro* and *in vivo* genetic toxicology testing. **Environmental and Molecular Mutagenesis**, v. 35, n. 3, p. 206–221, 6 jun. 2000.

TOFAN, Lucica *et al.* Multiple Assays on Non-Target Organisms to Determine the Risk of Acute Environmental Toxicity in Tebuconazole-Based Fungicides Widely Used in the Black Sea Coastal Area. **Toxics**, v. 11, n. 7, p. 597, 7 jul. 2023.

TYNDALL, Joel D. A. *et al.* Structural and functional elucidation of yeast lanosterol 14α-demethylase in complex with Agrochemical antifungals. **PLoS ONE**, v. 11, n. 12, 1 dez. 2016.

VENUGOPALA, Katharigatta N. *et al.* Crystallography, *in Silico* Studies, and *In Vitro* Antifungal Studies of 2,4,5 Trisubstituted 1,2,3-Triazole Analogues. **Antibiotics**, v. 9, n. 6, p. 350, 20 jun. 2020.

WALKER, Q. David; MAILMAN, Richard B. Triadimefon and Triadimenol: Effects on Monoamine Uptake and Release. **Toxicology and Applied Pharmacology**, v. 139, n. 2, p. 227–233, ago. 1996.

WANG, Fu-Cheng *et al.* A 1,2,3-Triazole Derivative of Quinazoline Exhibits Antitumor Activity by Tethering RNF168 to SQSTM1/P62. **Journal of Medicinal Chemistry**, v. 65, n. 22, p. 15028–15047, 24 nov. 2022.

WANG, Nan *et al.* Advances in Selective Bioactivity and Toxicity of Chiral Triazole Fungicides and Their Selective Behavior in Mammals. **Chirality**, v. 37, n. 11, 27 nov. 2025a.

WANG, Rui *et al.* Triazole fungicides disrupt embryonic stem cell differentiation: Potential modulatory role of the retinoic acid signaling pathway. **Ecotoxicology and Environmental Safety**, v. 283, 15 set. 2024.

WANG, Ruike *et al.* Combined toxicity assessment of a naturally occurring toxin and a triazole fungicide on different biological processes through toxicogenomic data mining with mixtures. **Pesticide Biochemistry and Physiology**, v. 193, p. 105440, jun. 2023.

WANG, Yanhua *et al.* Combined toxic effects of fludioxonil and triadimefon on embryonic development of zebrafish (Danio rerio). **Environmental Pollution**, v. 260, p. 114105, maio 2020.

WANG, Zikai *et al.* Effect of fungicides on soil respiration, microbial community, and enzyme activity: A global meta-analysis (1975–2024). **Ecotoxicology and Environmental Safety**, v. 289, p. 117433, jan. 2025b.

WEINHOLD, Frank; LANDIS, Clark R. NATURAL BOND ORBITALS AND EXTENSIONS OF LOCALIZED BONDING CONCEPTS. **Chem. Educ. Res. Pract.**, v. 2, n. 2, p. 91–104, 2001.

WEINHOLD, Frank; LANDIS, Clark R. **Discovering Chemistry with Natural Bond Orbitals**. *[S.l.]*: Wiley, 2012.

WEINSTEIN, Harel *et al.* Electrostatic Potentials as Descriptors of Molecular Reactivity: The Basis for Some Successful Predictions of Biological Activity. *In*: **Chemical Applications of Atomic and Molecular Electrostatic Potentials**. Boston, MA: Springer US, 1981. p. 309–334.

WISHART, David S. *et al.* HMDB 5.0: the Human Metabolome Database for 2022. **Nucleic Acids Research**, v. 50, n. D1, p. D622–D631, 7 jan. 2022.

WOOD, Peter A. *et al.* Evaluation of molecular crystal structures using Full Interaction Maps. **CrystEngComm**, v. 15, n. 1, p. 65–72, 2013.

WU, Shenggan *et al.* Synergistic potential of fenvalerate and triadimefon on endocrine disruption and oxidative stress during rare minnow embryo development. **Environmental Toxicology**, v. 33, n. 7, p. 759–769, 23 jul. 2018.

XU, Jiuyong *et al.* Comparative cytotoxic effects of five commonly used triazole alcohol fungicides on human cells of different tissue types. **Journal of Environmental Science and Health, Part B**, v. 55, n. 5, p. 438–446, 3 maio 2020.

YANG, Hongbin *et al.* admetSAR 2.0: web-service for prediction and optimization of chemical ADMET properties. **Bioinformatics**, v. 35, n. 6, p. 1067–1069, 15 mar. 2019.

ZANGER, Ulrich M.; RAIMUNDO, Sebastian; EICHELBAUM, Michel. Cytochrome P450 2D6: overview and update on pharmacology, genetics, biochemistry. **Naunyn-Schmiedeberg's Archives of Pharmacology**, v. 369, n. 1, p. 23–37, 1 jan. 2004.

ZARN, Jürg A.; BRÜSCHWEILER, Beat J.; SCHLATTER, Josef R. Azole fungicides affect mammalian steroidogenesis by inhibiting sterol 14 alpha-demethylase and aromatase. **Environmental Health Perspectives**, v. 111, n. 3, p. 255–261, mar. 2003.

ZHANG, Bo. Comprehensive review on the anti-bacterial activity of 1,2,3-triazole hybrids. **European Journal of Medicinal Chemistry**, v. 168, p. 357–372, abr. 2019.

ZHANG, Gang; MUSGRAVE, Charles B. Comparison of DFT Methods for Molecular Orbital Eigenvalue Calculations. **The Journal of Physical Chemistry A**, v. 111, n. 8, p. 1554–1561, 1 mar. 2007.

ZHANG, Hu *et al.* Insights into the effects of difenoconazole on the livers in male mice at the biochemical and transcriptomic levels. **Journal of Hazardous Materials**, v. 422, p. 126933, jan. 2022.

ZHANG, Jun; LU, Tian. Efficient evaluation of electrostatic potential with computerized optimized code. **Physical Chemistry Chemical Physics**, v. 23, n. 36, p. 20323–20328, 2021.

ZHANG, Wenjun *et al.* Comparison of triadimefon and its metabolite on acute toxicity and chronic effects during the early development of Rana nigromaculata tadpoles. **Ecotoxicology and Environmental Safety**, v. 156, p. 247–254, jul. 2018.

ZHANG, Wenjun *et al.* Effect of triadimefon and its metabolite on adult amphibians Xenopus laevis. **Chemosphere**, v. 243, p. 125288, mar. 2020.

ZHAO, Yan; SCHULTZ, Nathan E.; TRUHLAR, D. G. Exchange-correlation functional with broad accuracy for metallic and nonmetallic compounds, kinetics, and noncovalent interactions. **The Journal of Chemical Physics**, v. 123, n. 16, 22 out. 2005.

ZHAO, Yan; TRUHLAR, Donald G. The M06 suite of density functionals for main group thermochemistry, thermochemical kinetics, noncovalent interactions, excited states, and transition elements: two new functionals and systematic testing of four M06-class functionals and 12 other functionals. **Theoretical Chemistry Accounts**, v. 120, n. 1–3, p. 215–241, 12 maio 2008.

ZHOU, Dongxing *et al.* Study on the influential factors of Cd2+ on the earthworm *Eisenia fetida* in oxidative stress based on factor analysis approach. **Chemosphere**, v. 157, p. 181–189, ago. 2016.

ZHUO, Yonggan *et al.* Toxicological evaluation and metabolic profiling of earthworms (*Eisenia fetida*) after exposure to microplastics and acetochlor. **Environmental Research**, v. 276, p. 121546, jul. 2025.

ZOU, Pei-chen *et al.* Triazoles in the environment: An update on sample pretreatment and analysis methods. **Ecotoxicology and Environmental Safety**, v. 286, p. 117156, nov. 2024.

ZUBROD, Jochen P. *et al.* Fungicides: An Overlooked Pesticide Class? **Environmental Science & Technology**, v. 53, n. 7, p. 3347–3365, 2 abr. 2019.

ANEXO A – Artigo 01: Predição da toxicidade de fungicidas triazóis: uma perspectiva molecular sobre o triadimefon e o triadimenol

Results in Chemistry 25 (2026) 103268

Contents lists available at ScienceDirect

Results in Chemistry

journal homepage: www.sciencedirect.com/journal/results-in-chemistry

Predicting toxicity of triazole fungicide: A molecular-based insight into triadimefon and triadimenol

Áureo B. Souza [a], Ronaldo G. Freitas Junior [b], Ana L.M. Monteiro [b], Leonardo R. de Almeida [b], Lucas D. Dias [a], Lucas B. Ribeiro de Carvalho [c], Hamilton B. Napolitano [a,b], Leonardo L. Borges [b,c,*], Antônio S.N. Aguiar [a,b,*]

[a] Laboratório de Novos Materiais, Universidade Evangélica de Goiás, Anápolis, GO, Brazil
[b] Grupo de Química Teórica e Estrutural de Anápolis, Universidade Estadual de Goiás, Anápolis, GO, Brazil
[c] Escola de Ciências Médicas e da Vida, Pontifícia Universidade Católica de Goiás, Goiânia, GO, Brazil

ARTICLE INFO

Keywords:
Triazoles
Fungicides, DFT, supramolecular arrangement
Toxicity prediction

ABSTRACT

Background: Triazole fungicides, such as triadimefon (TF) and its stereoisomeric metabolite, triadimenol (TN), remain cornerstone agrochemicals. However, their stereochemistry may affect shape reactivity, intermolecular recognition, and ecotoxicity in different ways, with potential impacts on non-target species. **Objective**: This study employs computational methods to describe structural and electronic descriptors, quantify supramolecular interactions, and predict toxicological endpoints *in silico* for TF and its individual stereoisomer, TN. **Methods**: Density functional theory calculations were employed to optimize the molecular geometries and calculate reactivity descriptors at the M06-2×/6–311++G(d,p) level of theory. The intermolecular interactions were compared using Hirshfeld surface analysis, quantum theory of atoms in molecules, and natural bond orbital analysis. Chemical reactivity descriptors were calculated to assess reactive sites. Pharmacophore modeling was performed to verify the potential of the six isomers to interact with the lanosterol 14α-demethylase target. Toxicity was predicted using computational models available online. **Results**: Differences were found between the electronic properties and intermolecular interactions of TF and TN, due to the presence of –OH or –CO– functional groups. These variations influence the molecular electrostatic potential, reactivity descriptors, and interaction energies, affecting their biological behavior. The results of the pharmacophore modeling suggest that only the 1*R*-TF, 1*S*,2*R*-TN, and 1*S*,2*S*-TN isomers demonstrated potential for interaction with the lanosterol 14α-demethylase target. Toxicity predictions revealed that some triadimenol stereoisomers exhibit a greater potential for adverse effects on non-target organisms when compared to TF. **Conclusion**: The findings highlight the crucial role of stereochemistry in modulating the chemical behavior and toxicity of triazole fungicides. Additionally, the use of *in silico* methods proves effective in predicting the ecotoxicological profiles of such compounds and supports the development of safer and more sustainable agrochemical practices.

1. Introduction

In modern agriculture, pesticides are key tools that safeguard yield and quality by suppressing insect pests, plant diseases, and weeds [1]. However, due to their inherent bioactive nature designed to eliminate various species, these compounds are toxic [2]. Among the different classes, triazole fungicides stand out for their systemic efficacy, broad spectrum of action, and favorable physicochemical properties [3,4]. Since their introduction in the 1970s, triazole fungicides have become indispensable tools for managing fungal diseases worldwide. Owing to their broad-spectrum activity, high efficacy, rapid onset of action, long-lasting effects, and strong absorption and systemic translocation, these compounds are extensively employed in crops such as wheat, corn, fruits, vegetables, and ornamental plants to control rusts, powdery mildews, and to regulate plant growth [5–7].

Triazoles represent a significant class of heterocyclic compounds due to their broad spectrum of biological activities. Their core structure consists of a five-membered heterocycle containing three nitrogen atoms, which can occur in two distinct isomeric forms depending on the position of the nitrogen atoms: 1,2,3-triazoles and 1,2,4-triazoles [8].

* Corresponding authors at: Grupo de Química Teórica e Estrutural de Anápolis, Universidade Estadual de Goiás, Anápolis, GO, Brazil.
E-mail addresses: lucas.dias@unievangelica.edu.br (L.D. Dias), leonardoquimica@gmail.com (L.L. Borges), toninho.quimica@gmail.com (A.S.N. Aguiar).

https://doi.org/10.1016/j.rechem.2026.103268
Received 28 November 2025; Accepted 25 March 2026
Available online 31 March 2026

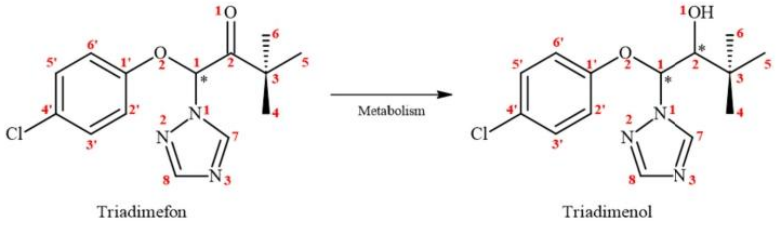

Fig. 1. Structural formulas of Triadimefon and its metabolite Triadimenol, with numbering schemes. The asterisk (*) indicates the chiral carbon present in their chemical structures.

Derivatives of 1,2,3-triazoles have demonstrated outstanding pharmacological properties, including potent antibacterial [9–12], anticancer [12,13], and antitumor [14,15] activities, making them valuable in medicinal chemistry. On the other hand, 1,2,4-triazole derivatives are extensively employed in agriculture as fungicidal agents [5–7], primarily due to their high efficacy and selectivity against a wide range of phytopathogenic *fungi*. 1,2,4-triazole fungicides present electronic stability and high affinity for lanosterol 14α-demethylase (CYP51), the target enzyme responsible for ergosterol biosynthesis. Their mechanism of action involves inhibition of this cytochrome P450 monooxygenase, which catalyzes the demethylation of lanosterol – a crucial step in the formation of fungal cell membranes [16].

Among them, triadimefon (TF), triadimenol (TN), diniconazole, hexaconazole, myclobutanil, and tebuconazole – exhibit chirality due to one or more stereocenters, influencing their biological activity and environmental behavior [17]. TF [1-(4-chlorophenoxy)-1-(1,2,4-triazol-1-yl)-3,3-dimethyl-butan-2-one] contains a single chiral center (*C_1) and exists as a pair of enantiomers *S*-(+) and *R*-(−) [18]. Its biotransformation leads to TN [1-(4-chlorophenoxy)-1-(1,2,4-triazol-1-yl)-3,3-dimethyl-butan-2-ol], its major metabolite in plants, soils, and animals (Fig. 1). While TF contains a single chiral center, TN possesses two, giving rise to four stereoisomers – (1*R*,2*S*), (1*S*,2*R*), (1*R*,2*R*), and (1*S*,2*S*) – which are organized into two diastereomeric pairs: TN-A and TN-B [19,20]. These structural variations significantly affect physicochemical and toxicological properties. Notably, the 1*S*,2*R* stereoisomer exhibits up to 1000-fold greater fungicidal activity than its counterparts, and the A diastereomer is markedly more toxic to mammals based on oral LD_{50} values in rats [21,22]. Such stereochemical asymmetry is essential for understanding the biological performance, toxicological profile, and environmental fate of these compounds.

Given the extensive agricultural use of TF and TN and the associated ecotoxicological concerns, this study elucidates their electronic and supramolecular characteristics through a comprehensive computational workflow. It was predicted that toxicological profiles using *in silico* models informed by intermolecular interaction patterns and reactivity descriptors, aiming to resolve stereoisomer-specific differences and anticipate potential impacts on non-target organisms. The findings are intended to inform safer and more rational use of these fungicides while supporting regulatory assessments that incorporate stereochemical considerations.

2. Computational procedures

2.1. Solid-state analysis

The crystallographic structures of TF and TN were obtained from the Cambridge Structural Database (CSD) [23], under the codes 1109431 [24] and 1108987 [25]. The selection considered the presence of functional groups associated with antifungal activity, such as triazoles [26]. The structural data of the compounds were obtained in crystallographic information file format and served as the basis for structural analyses, including geometry and supramolecular arrangement. Molecular representations, tables, and figures were constructed with Mercury (version 3.8) [27] and GIMP [28] software. Additionally, Hirshfeld surfaces (HS) in the d_{norm} and *shape index* configurations, as well as their respective 2D fingerprint plots, were obtained using the Crystal Explorer (version 21.5) [29], allowing a more detailed evaluation of the interactions. The HS was carried out using the normalized contact distance function (d_{norm}),

$$d_{\text{norm}} = \frac{d_i - r_i^{vdw}}{r_i^{vdw}} + \frac{d_e - r_e^{vdw}}{r_e^{vdw}}, \tag{1}$$

which identifies regions of molecular contact by considering the internal (d_i) and external (d_e) distances to the surface, normalized by the corresponding van der Waals radii (r^{vdw}). The shape index was employed to identify interactions involving π systems [30]. The compounds TF and TN feature a chiral center at C_1, while TN possesses an additional chiral center at C_2 (Fig. 1), resulting in four distinct stereoisomers for TN. For discussion purposes, the *R* and enantiomer B1 (1*R*,2*R*) configurations were chosen, respectively.

Quantum theory of atoms in molecules (QTAIM) [31,32] was employed to determine the exact nature of the observed intermolecular interactions. At the same time, natural bond orbital (NBO) [33,34] analysis was used to evaluate their respective stabilities. These calculations were performed using density functional theory (DFT) [35,36], as implemented in the Gaussian 16 [37] software package. Input geometries were constructed based on the experimentally observed structures and optimized using the highly parameterized exchange–correlation functional M06-2 × [38] in combination with the diffuse and polarized Pople-style split-valence triple-ζ basis set 6–311++G(d, p). Previous studies have demonstrated that this functional provides reliable descriptions of medium-range electronic correlation effects and non-covalent interactions and is among the best-performing options for modeling the thermodynamics of chemical processes [39]. Frequency calculations were also carried out to ensure that the molecular systems corresponded to true *minima* on the potential energy surface.

The topological parameters analyzed by QTAIM included the electron density [$\rho(\mathbf{r})$], the Laplacian of $\rho(\mathbf{r})$ ($\nabla^2\rho$), the electron kinetic energy density [$G(\mathbf{r})$], the electron potential energy density [$v(\mathbf{r})$], and the total energy density [$h(\mathbf{r})$] [40,41]. These parameters were collected by the Multiwfn 3.5 [42] program. For the NBO analysis, hyperconjugative interactions between donor (Lewis-type) and acceptor (non-Lewis-type) orbitals [43] were examined using the second-order perturbation theory formula,

$$E_{i\to j^*}^{(2)} = -n_\sigma \frac{\langle \sigma_i | \widehat{F} \sigma_{j^*} \rangle}{\varepsilon_{j^*} - \varepsilon_i} = -n_\sigma \frac{F_{ij}^2}{\varepsilon_{j^*} - \varepsilon_i}, \tag{1}$$

where $\langle \sigma_i | \widehat{F} \sigma_{j^*} \rangle$ (or F_{ij}^2) is the Fock matrix element between the *i* and *j* NBOs, ε_{σ^*} is the energy of the antibonding orbital σ^*, and ε_σ is the energy of the bonding orbital σ; n_σ is the population occupation of the σ donor orbital.

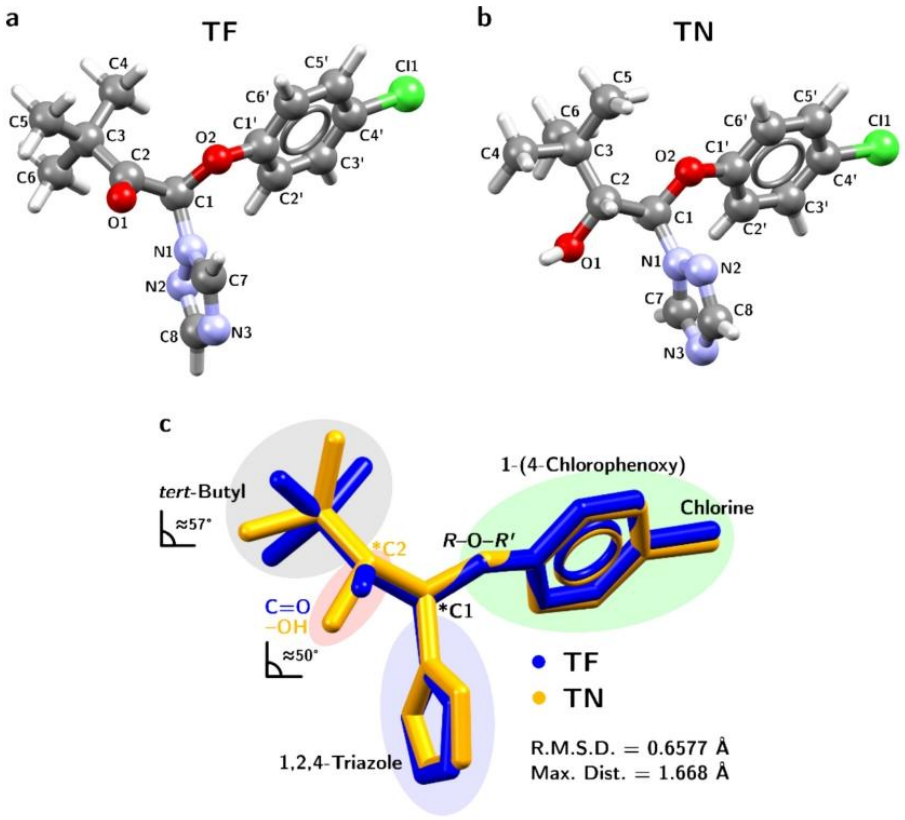

Fig. 2. Molecular structure of selected triazole fungicides, TF (**a**) and TN (**b**), and their numbering scheme for all non-hydrogen atoms. (**c**) Overlap of the compounds: TF (blue) and TN (orange), circles detach the chemical moieties in both molecules. RMSD of 0.6577 Å, and maximum distance of 1.668 Å. The superposition excludes hydrogen atoms and allows inversion to fit better. (For interpretation of the references to color in this figure legend, the reader is referred to the web version of this article.)

2.2. Molecular modeling study

The calculations were performed using the same level of theory. The TF and TN molecules were initially optimized following a conformational search based on a relaxed scan approach, aiming to identify the ground-state conformation. Subsequently, the energies of the frontier molecular orbitals [44] – the highest occupied molecular orbital (HOMO) and the lowest unoccupied molecular orbital (LUMO) – were used to calculate chemical reactivity descriptors, including chemical hardness [45,46],

$$\eta = \frac{1}{2}\left(\frac{\partial^2 E}{\partial N^2}\right)_{\upsilon} = \frac{I - A}{2}, \tag{2}$$

which measures the resistance to deformation of the electron cloud during chemical processes; chemical potential [46],

$$\mu = \left(\frac{\partial E}{\partial N}\right)_{\upsilon} = -\frac{I + A}{2} = -\chi, \tag{3}$$

which is related to charge transfer from a species with a higher chemical potential (μ_{large}) to one with lower chemical potential (μ_{small}); and the global electrophilicity index [47],

$$\omega = \frac{\mu^2}{2\eta}. \tag{4}$$

which measures energy stabilization when the system acquires an electronic charge from the environment. In Eqs. (2) and (3), E is the energy of the system, N is the number of particles, υ is the external potential, χ is the electronegativity, $I \approx -E_{HOMO}$ is the ionization potential, and $A \approx -E_{LUMO}$ is the electron affinity. The nucleophilic and electrophilic regions of the compound were evaluated using the molecular electrostatic potential (MEP) map [48,49], where the electrostatic potential, $V(\mathbf{r})$ [50], at point $\mathbf{r}$, is defined by

$$V(\mathbf{r}) = \sum_{\alpha} \frac{Z_\alpha}{|\mathbf{r}_\alpha - \mathbf{r}|} - \int \frac{\rho(\mathbf{r}')}{|\mathbf{r}' - \mathbf{r}|} d\mathbf{r}', \tag{5}$$

where Z_α is the charge of nuclei α at point $\mathbf{r}_\alpha$ and $\rho(\mathbf{r}')$ is the charge density at the point $\mathbf{r}'$ [48]. Furthermore, through the Fukui function [51,52], defined by the equation,

$$f^{0}(r) = \left[\frac{\partial \rho(\mathbf{r})}{\partial N}\right]_{\upsilon}^{0}, \tag{6}$$

it was possible to predict the local reactivity sites, so that the indices for the nucleophilic, electrophilic, and radical attacks were obtained.

2.3. Toxicity prediction and pharmacophore modeling

For the pharmacophore modeling of the different isomers of fungicides with lanosterol 14α-demethylase (CYP51 family) target ligands,

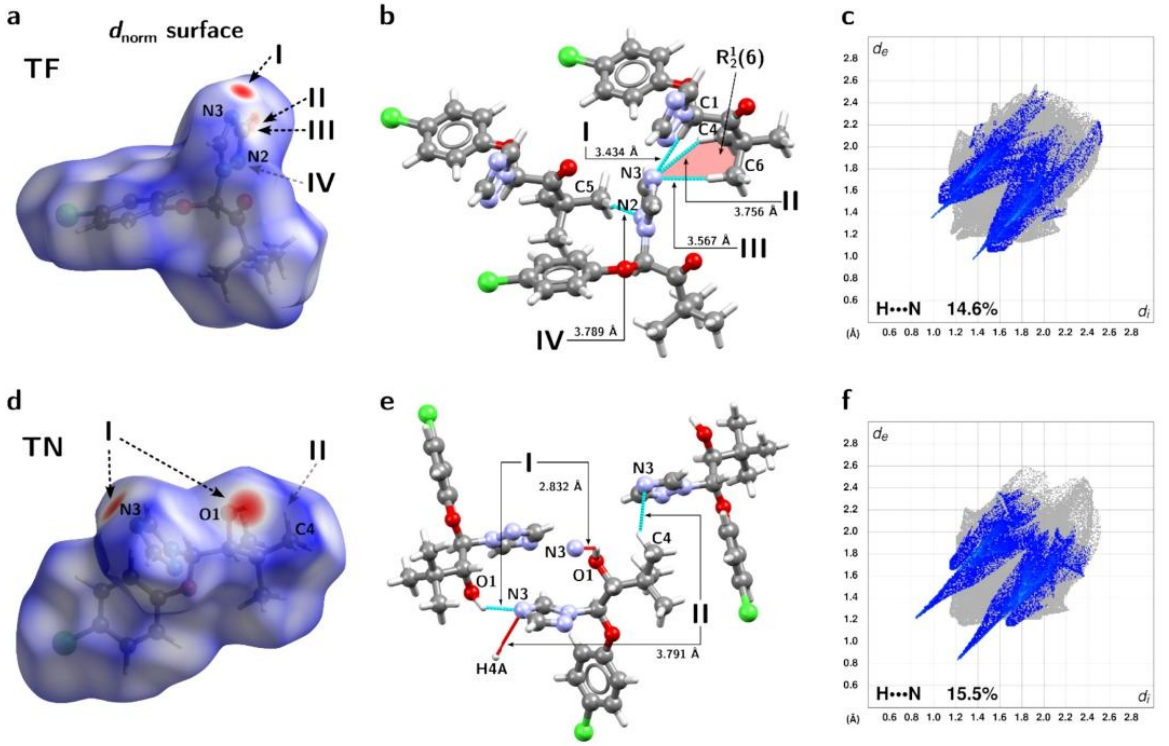

Fig. 3. HS with the d_{norm} property mapped and the detailed view of C–H···N and O—H···N interactions in the supramolecular arrangement of TF and TN. (a) d_{norm} surface mapped for TF. (b) Representation of C—H···N interactions I (C_1···N_3), II (C_4···N_3), III (C_6···N_3), and IV (C_5···N_2) with their donor-acceptor distances in TF. (c) The 2D *fingerprint* plot of the H···N, with 14.6% of the total contacts, was mapped for TF. (d) d_{norm} surface mapped for TN. (e) Representation of O—H···N interaction I (O_1···N_3), and C—H···N interaction II (C_4···N_3) with their donor-acceptor distances for TN. (f) The 2D *fingerprint* plot of the H···N with 15.5% of the total contacts was mapped for TN.

we employed LigandScout v4.5 [53] (https://docs.inteligand.com/ligandscout). LigandScout identified combinations of shared pharmacophoric features, including hydrogen-bond donors (HBDs), hydrogen-bond acceptors (HBAs), positively and negatively charged groups, hydrophobic (HyPho) regions, and aromatic rings (ARs) [53]. These unique pharmacophores were subsequently integrated into the alignment process to develop the shared feature pharmacophore (SFP) model. A literature review was conducted using the databases in Binding DB (https://www.bindingdb.org/rwd/bind/index.jsp) to identify compounds with lanosterol 14α-demethylase antagonist activity. A total of five compounds with the lowest inhibitory concentration (IC_{50}) values were included in a dataset used to calculate the pharmacophore models.

To assess the pharmaceutical viability, a pharmacokinetic study was carried out to measure parameters related to absorption, distribution, metabolism, and excretion (ADME). This study utilized the SwissADME online (http://www.swissadme.ch/) tool for analysis [54,55]. The following platform was used to predict the toxicity of chemical studies. ProTox-3.0 - Prediction of TOXicity of chemicals [56] (https://tox.charite.de/protox3/), which applies all the toxicity parameters to the most promising component that is likely to be the source of biological activity.

The assessment of potential toxic effects was conducted through computational predictions, with cardiac toxicity evaluated using the Pred-Herg server [57,58] (https://predherg.labmol.com.br/) and cutaneous toxicity assessed employing the Pred-Skin server [59,60] (https://predskin.labmol.com.br/). The environmental toxicity assessment was conducted using the ADMETSAR [61,62] server (https://lmmd.ecust.edu.cn/admetsar2/). The analyses included assessments of *Tetrahymena pyriformis* toxicity, honeybee toxicity, fish toxicity, and biodegradation.

3. Results and discussion

3.1. Solid-state analysis

The TN and TF compounds crystallize in the monoclinic systems $P2_1/c$ and $P2_1/n$ space groups (Fig. 2), respectively, with one independent molecule in the asymmetric unit ($Z' = 1$) and four in the unit cell ($Z = 4$) (see Fig. S1 a and b). Both structures have a chlorine atom in the *para*-position of aromatic ring 1 and a triazole attached to carbon 1, which is also connected to ring 1 *via* an ether moiety (R–O–R). The main difference lies in the presence of a hydroxyl (OH) at C_2 in TN, while TF has a carbonyl (C=O) and the second chiral center at C_2. Fig. 1a and b shows in detail the crystal structures and atomic numbering scheme through the illustration of the asymmetric unit. Overlayed compounds with root mean square deviation (RMSD) of 0.6577 Å and maximum distance of 1.668 Å, highlighting the angles formed between the *tert*-butyl groups of TF and TN in ≈57°, and at C_2 between the oxygen from hydroxyl (–OH) and carbonyl (C=O) in ≈50° (Fig. 1c).

The supramolecular analysis of TF and TN using the full interaction maps tool [63] revealed predominantly weak interactions such as C—H···N, C—H···O, C—H···Cl, C—H···π and π···π. Notably, O—H···N interactions were observed exclusively in TN, due to the presence of a hydroxyl group. The blue regions of the interaction maps highlight

Table 1
Geometries of the intermolecular interactions, distances are in angstrom (Å), and angles are in degrees (°), for TF and TN. Cg1 is the centroid of the phenyl ring, and Cg2 is the centroid of the triazole ring.

[(id)]Interaction	D···H (Å)	H···A (Å)	D···A (Å)	∠(D—H···A) (°)	Symmetry Codes
Triadimefon					
[(I)]C_1–H_1···N_3	1.080	2.354	3.434	178.80	$-\frac{1}{2}+x, \frac{3}{2}-y, \frac{1}{2}+z$
[(II)]C_4–H_{4C}···N_3	1.079	2.802	3.756	147.36	$\frac{1}{2}+x, \frac{3}{2}-y, \frac{1}{2}+z$
[(III)]C_6–H_{6A}···N_3	1.081	2.563	3.567	154.08	$-\frac{1}{2}+x, \frac{3}{2}-y, -\frac{1}{2}+z$
[(IV)]C_5–H_{5A}···N_2	1.080	2.710	3.789	176.40	$-\frac{1}{2}+x, \frac{3}{2}-y, \frac{1}{2}+z$
[(V)]C_5–H_5···O_1	1.081	2.810	3.602	130.09	$1-x, 1-y, 1-z$
[(VI)]C_6–H_6···O_2	1.079	2.823	3.903	179.06	$1-x, 1-y, 1-z$
[(VII)]C_4–H4A···Cg_1	1.080	2.855	3.912	166.15	$-1+x, y, z$
[(VIII)]C_6–H_{6C}···Cg_2	1.080	3.201	3.857	120.12	$1+x, y, z$
[(IX)]C_4–H_{4B}···Cl_1	1.080	3.275	3.672	102.96	$-x, 2-y, 1-z$
[(X)]C_5–H_{5C}···Cl_1	1.080	3.531	3.765	94.08	$1-x, 2-y, -z$
Triadimenol					
[(I)]O_1–H_{1A}···N_3	1.047	1.996	2.832	134.66	$-x, \frac{1}{2}+y, \frac{1}{2}-z$
[(II)]C_4–H_{4A}···N_3	1.155	2.819	3.791	141.42	$x, \frac{1}{2}-y, \frac{1}{2}+z$
[(III)]C_8–H_8···O_1	0.813	2.997	3.536	125.88	$-x, -\frac{1}{2}+y, \frac{1}{2}-z$
[(IV)]C_3–H_3···O_2	1.029	3.307	3.667	102.31	$\frac{2}{x}, 1+y, z$
[(V)]C_4–H_{4C}···Cg_1	0.991	3.121	4.104	172.03	$x, \frac{1}{2}-y, -\frac{1}{2}+z$
[(VI)]C_7–H_7···Cg_2	0.958	3.004	3.678	128.60	$-x, \frac{1}{2}+y, \frac{1}{2}-z$
[(VII)]C_5–H_{5A}···Cl_1	1.024	3.085	3.843	131.66	$1-x, 1-y, 1-z$
[(VIII)]C_6–H_{6C}···Cl_1	0.954	3.354	4.016	128.29	$1-x, 1-y, 1-z$

where donors are expected to be followed by CSD data, the red regions indicate likely acceptor positions, the orange regions indicate likely positions of hydrophobic groups, and the brown regions indicate likely positions of π···π interactions. The maps were created using carbonyl/oxygen, methyl/carbon, aromatic CH/carbon, and uncharged (NH) nitrogen probes. Illustrated in Fig. S1c-d, the intermolecular interaction maps of both compounds TF and TN, respectively, show two high-probability areas near the nitrogen atoms of the triazole ring, and two slightly lower probability regions near the oxygen of the carbonyl in TF. The hydroxyl group in TN donates a hydrogen bond in this structure, with a high-probability area close to it. Conversely, the C—H groups in the triazole and phenyl rings have the potential to interact with H-bond acceptors, as indicated by the red regions in the structure. Despite a subtle difference, it can play an important role, since the presence of such areas can perform interactions with other molecules, likely influencing the physical-chemical properties of the molecule, such as solubility, affinity with cell membranes, and interactions with biomolecules.

Depicting the interactions, we have applied the graph set analysis

Table 2
Percentage contribution of contacts present in theTriadimefon and Triadimenol crystal structures.

Molecule	H···H	H···N	H···O	H···C	H···Cl	C···C	Others
TF	41.2	14.6	11.8	15.4	12.8	0.6	3.6
TN	46.4	15.5	4.8	16.1	13.3	1.0	2.9

[64], to identify the interaction motifs in supramolecular arrangement, combining with the HS analysis [30] also used in this study through the d_{norm} surface of the compounds TF (volume = 372.04 Å^3; area = 330.42 Å^2) and TN (volume = 367.77 Å^3; area = 325.40 Å^2) as illustrated in Fig. 3a and c, representing both, acceptor and donor regions of interactions. The red color indicates closer contacts, while the blue color indicates outlying contacts. TN and TF compounds exhibit similar patterns of intermolecular interactions, and their respective geometry parameters are given in Table 1. The 2D *fingerprint* plots [65] of intermolecular interactions were mapped within the range of 0.8–2.6 Å view of d_e *vs* d_i for TF and TN compounds. The total contribution for each type of contact is described in Table 2.

Detaching the H···N contacts in the d_{norm} HS (Fig. 3a and d), they occur mainly through C—H···N type of interactions, in TF with N_2 as acceptor the C_5–H_{5A}···N_2 with donor acceptor distance (D···A = 3.789 Å), while N_3 alone as acceptor show three other interactions due to the arrangement where it is positioned surrounded by the methyl from *tert*-butyl group, than we observed the interaction C_1–H_1···N_3 (D···A = 3.434 Å), and also the bifurcated by C_4–H_{4C}···N_3 (D···A = 3.756 Å) and C_6–H_{6A}···N_3 (D···A = 3.567 Å) resulting in the formation of a $R_2^1(6)$ supramolecular motif, as detailed in Fig. 3b. Topological parameters from QTAIM [40] analysis indicate that electron density is depleted at the bond critical points (BCPs) of these interactions, with $\rho(r) < 0.1$ a.u. and $\nabla^2\rho > 0$, characterizing them as closed-shell interactions [41,66] with van der Waals nature [67,68] (See Table 3). Among these, C_1–H_1···N_3 exhibits the highest electron density at the internuclear region ($\rho(r) = 0.01268$ a.u.), representing the most stable intermolecular contact in TF, with a stabilization energy ($E^{(2)}_{i\to j^*}$) of 3.71 kcal/mol, as supported by the hyperconjugative interaction $\eta_1(N_3) \to \sigma^*(C_1$–$H_1)$ in the NBO analysis. The C_6–H_{6A}···N_3 interaction presents a relatively greater partially covalent character, as indicated by a $(|v|/G$ ratio of 0.9; however, the corresponding hyperconjugation $\eta_1(N_3) \to \sigma^*(C_6$–$H_{6A})$ contributes minimally to the supramolecular stabilization, with an $E^{(2)}_{i\to j^*}$ value of only 0.20 kcal/mol.

TN forms a bifurcated interaction on N_3 as acceptor from two molecules *via* the C_4–H_{4A}···N_3 (D···A = 3.791 Å) and an O—H···N interaction (Fig. 3d and e). The 2D fingerprint plot of H···N contacts is used to quantify the relative contribution of these types of interactions (C—H···N and O—H···N), with 14.6% of total contacts mapped for TN and 15.5% for TF 15.5% (Fig. 3c and f). However, the O—H···N interaction is only present in TN through the O_1–H_{1A}···N_3, which among all interactions and contacts for both compounds is the shortest donor-acceptor distance (D···A = 2.832 Å), occurring between the oxygen (O_1) from hydroxyl group towards the lone pair on nitrogen (N_3) in 1,2,4-triazole ring at position 4 (Fig. 3e). QTAIM analysis characterizes the O_1–H_{1A}···N_3 interaction with topological parameters of $\rho(\mathbf{r}) = 0.02195$ a.u., $\nabla^2\rho = 0.11416$ a.u., and $h(\mathbf{r}) = 0.00237$ a.u., suggesting a medium-intensity hydrogen bond [41]. The binding energy (*BE*), calculated by equation [69],

$$BE \approx -223,08\rho(r) + 0,7423, \quad (7)$$

is 8.4 kcal/mol [70], strongly contributing to the stabilization of TN's supramolecular arrangement. The observed hyperconjugation corroborates this $\eta_1(N_3) \to \sigma^*(O_1$–$H_{1A})$, with $E^{(2)}_{i\to j^*} = 10.47$ kcal/mol. In contrast, the C_4–H_{4A}···N_3 interaction is weaker, with topological descriptors of $\rho(\mathbf{r}) = 0.00527$ a.u., $\nabla^2\rho = 0.01651$ a.u., and $h(\mathbf{r}) = 0.00048$ a.u.,

Table 3
Topological parameters from QTAIM for the intermolecular interactions within the supramolecular arrangement of the Triadimefon and Triadimenol fungicides, obtained at the M06-2×/6–311++G(d,p) level of theory.

[(id)]Interaction	$\rho(r)^a$ (a.u.)	$\nabla^2\rho^b$ (a.u.)	$G(r)^c$ (a.u.)	$v(r)^d$ (a.u.)	$h(r)^e$ (a.u.)	$\frac{\lvert v\rvert}{G}$	Interaction Type
Triadimefon							
[(I)]C_1–H_1···N_3	0.01268	0.04872	0.01057	−0.00896	0.00161	0.8	van der Waals
[(II)]C_4–H_{4C}···N_3	0.00536	0.01783	0.00404	−0.00363	0.00041	0.9	van der Waals
[(III)]C_6–H_{6A}···N_3	0.00482	0.01480	0.00310	−0.00250	0.00060	0.8	van der Waals
[(IV)]C_5–H_{5A}···N_2	0.00555	0.01884	0.00406	−0.00340	0.00065	0.8	van der Waals
[(V)]$C_{5'}$–$H_{5'}$···O_1	0.00390	0.01614	0.00344	−0.00284	0.00060	0.8	van der Waals
[(VI)]$C_{6'}$–$H_{6'}$···O_2	0.00378	0.01546	0.00334	−0.00281	0.00053	0.8	van der Waals
[(IX)]C_4···Cl_1	0.00335	0.01399	0.00260	−0.00170	0.00090	0.7	van der Waals
[(X)]C_5–H_{5C}···Cl_1	****	****	****	****	****	****	****
Triadimenol							
[(I)]O_1–$H_{1A'}$···N_3	0.02195	0.11416	0.02617	−0.02379	0.00237	0.9	H-Bond
[(II)]C_4–H_{4A}···N_3	0.00527	0.01651	0.00365	−0.00317	0.00048	0.9	van der Waals
[(III)]$C_{9'}$–$H_{9'}$···O_1	0.00296	0.01424	0.00284	−0.00212	0.00072	0.7	van der Waals
[(IV)]$C_{3'}$–$H_{3'}$···O_2	****	****	****	****	****	****	****
[(VII)]C_5–H_{5A}···Cl_1	0.00195	0.00681	0.00129	−0.00087	0.00042	0.7	van der Waals
[(VIII)]C_6–H_{6C}···Cl_1	0.00437	0.01557	0.00311	−0.00232	0.00079	0.7	van der Waals

[a]Electron Density; [b]Laplacian of ρ; [c]Kinect Energy Density; [d]Potential Energy Density; [e]Total Energy Density

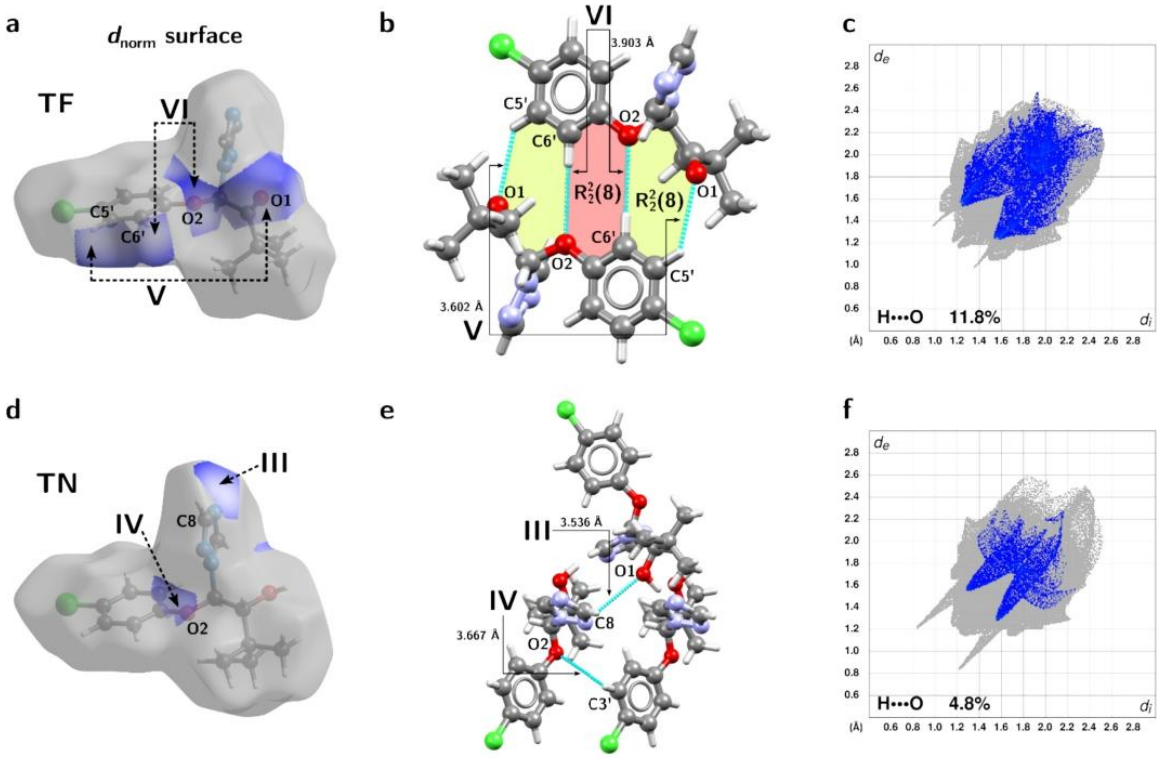

Fig. 4. HS with the d_{norm} property mapped and the detailed view of C—H···O interactions in the supramolecular arrangement of TF and TN. (a) d_{norm} surface mapped for TF. (b) Representation of interactions: V ($C_{5'}$···O_1) and VI ($C_{6'}$···O_2), with their donor-acceptor distances in TF forming a dimer with two parallel $\mathbf{R}_2^2(\mathbf{8})$ supramolecular motifs. (c) The 2D *fingerprint* plot of the H···O, with 11.8% of the total contacts, was mapped for TF. (d) d_{norm} surface mapped for TN. (e) Representation of interactions: III ($C_{9'}$···O_1) and IV ($C_{3'}$···O_2) with their donor-acceptor distances in TN. (f) The 2D *fingerprint* plot of the H···O, with 4.8% of the total contacts, was mapped for TN.

indicative of a van der Waals character. The corresponding hyperconjugation $\eta_1(N_3) \rightarrow \sigma^*(C_4–H_{4A})$ contributes minimally to stabilization, with an $E^{(2)}_{i\rightarrow j^*}$ value of only 0.32 kcal/mol. Alongside the chirality, this interaction is likely to play an essential role for TN in the biological

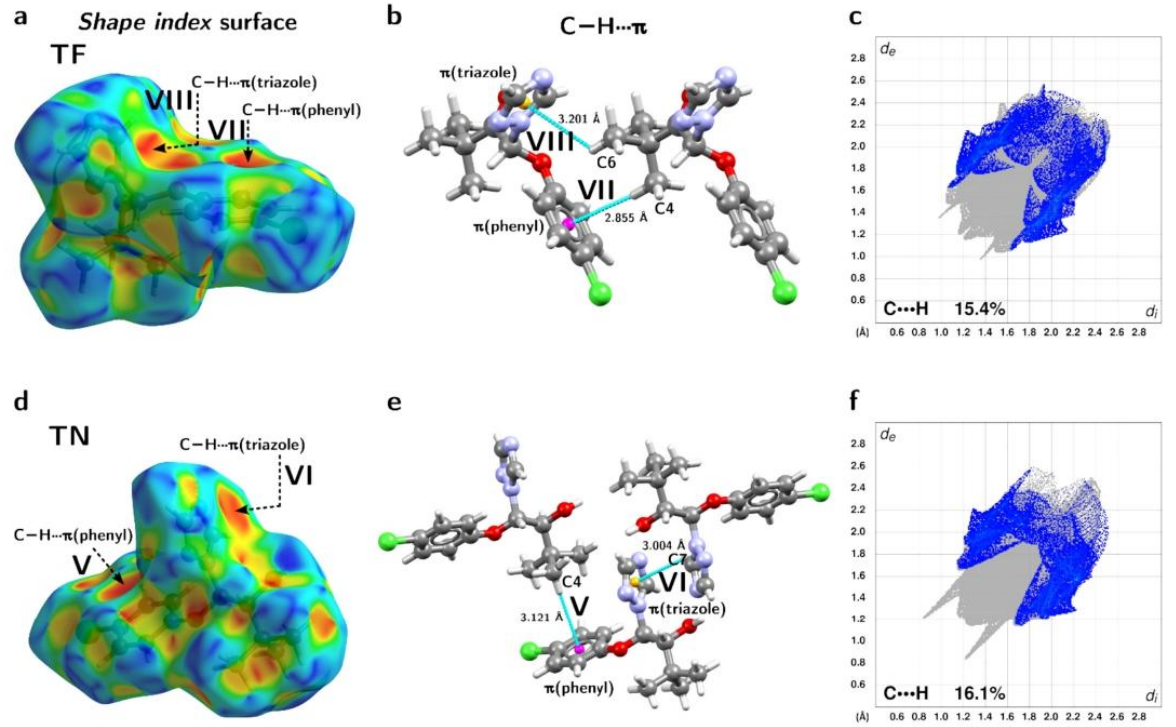

Fig. 5. HS with the *shape index* property mapped, highlighting the red concave regions where C–H···π interactions occur and the detailed view of these interactions in the supramolecular arrangement of TF and TN. (a) *shape index* surface mapped for TF. (b) Representation of C–H···π interactions VII [C_4–H_{4A}···π(phenyl)] and VIII [C_6–H_{6C}···π(triazole)], with their H···π(Cg) distances in TF. (c) The 2D *fingerprint* plot of the C···H with 15.4% of the total contacts was mapped for TF. (d) *shape index* surface mapped for TN. (e) Representation of interactions V [C_4–H_{4C}···π(phenyl)] and VI [C_7–H_7···π(triazole)] with their H···π(Cg) distances in TN. (f) The 2D *fingerprint* plot of the C···H with 16.1% of the total contacts was mapped for TN. (For interpretation of the references to color in this figure legend, the reader is referred to the web version of this article.)

environment, considering that it can result from TF by the enzymatic reduction of a carbonyl to an alcohol group in soils, plants, and fungi, forming this metabolite, which is also observed separately and with superior fungicidal activity than TF [71].

The C—H···O type of interactions was observed in both TF and TN, forming different patterns of arrangement, as illustrated in Fig. 4a. The d_{norm} surface of TF indicates the regions of H···O contacts located horizontally in the structure through the C—H groups in the phenyl ring towards the oxygens in carbonyl (O_1) and ether (O_2). Together, the interactions $C_{5'}$–$H_{5'}$···O_1 (3.602 Å) and $C_{6'}$–$H_{6'}$···O_2 (3.903 Å) form two parallel $R_2^2(8)$ supramolecular motifs resulting in a dimeric arrangement (see Fig. 4b), which corresponds to 11.8% of total contacts mapped for TF (Fig. 4c). The electron density at the bond critical points (BCPs) of these interactions is low, characterizing them as van der Waals interactions. Nevertheless, the $C_{6'}$–$H_{6'}$···O_2 interaction contributes more effectively to system stabilization, as indicated by the hyperconjugation $\eta_1(O_2) \rightarrow \sigma^*(C_{6'}–H_6)$, with an $E^{(2)}_{i\rightarrow j}$ value of 0.31 kcal/mol. In TN the d_{norm} surface also indicates the region of H···O contact, but on C—H group at C_8 from triazole ring towards the oxygen of carbonyl (O_1) to establish the interactions C_8–H_8···O_1 (3.536 Å) and $C_{3'}$–$H_{3'}$···O_2 (3.667 Å) (Fig. 4d and 4e), corresponding to only 4.8% of total contacts (Fig. 4f). In both cases, these are long-range interactions with donor-acceptor distances from 3.5 to 3.9 Å. None of these interactions produce hyperconjugations between donor and acceptor orbitals, meaning that they do not contribute to the stabilization of the supramolecular arrangement of TN.

Furthermore, the QTAIM topology showed the formation of a bond path (BP) only at C_8–H_8···O_1, whose parameters suggested a van der Waals character. However, distinct arrangements were observed through C—H···O interactions, reflecting a difference that is more than double in the percentage contribution of these contacts to TF in relation to TN. It is important to note that TF has oxygens only as H-bond acceptors, while TN has the hydroxyl group as a donor but is involved in an O—H···N interaction.

The occurrence of hydrophobic interactions involving systems such as methyl groups, phenyl rings, and triazole rings in both structures of TF and TN. These interactions are C—H···π and π···π-stacking, occurring between methyl (C—H) groups that act as donors and the π(phenyl) and π(triazole) systems as acceptors. To represent the π-electron system, measurements were taken using their respective centroids (Cg). The C—H···π interactions were identified through the HS mapped with the *shape index* property, which display red concave regions over the phenyl and triazole rings, and corresponding blue convex regions over the C—H atoms (see Fig. 5a and d). TF presents the shortest and the longest C—H···π interactions, with distances between H···π(Cg), C_4–H_{4A}···π(phenyl) with 2.855 Å, and C_6–H_{6C}···π(triazole) with 3.201 Å, respectively (Fig. 5b). It corresponds to 15.4% of total contacts, as illustrated in Fig. 5c. For this type of interaction in TN intermediate distances were observed, while the opposite is noted for C_4–H_{4C}···π(phenyl) with 3.121 Å – longer, and for C_7–H_7···π(triazole) with 3.004 Å – shorter (Fig. 5e), corresponding to 16.1% of total contacts (Fig. 5f). These percentage contributions suggest that such interactions occur with similar frequency in both structures, despite the differences between the π systems, which play a relevant role in the

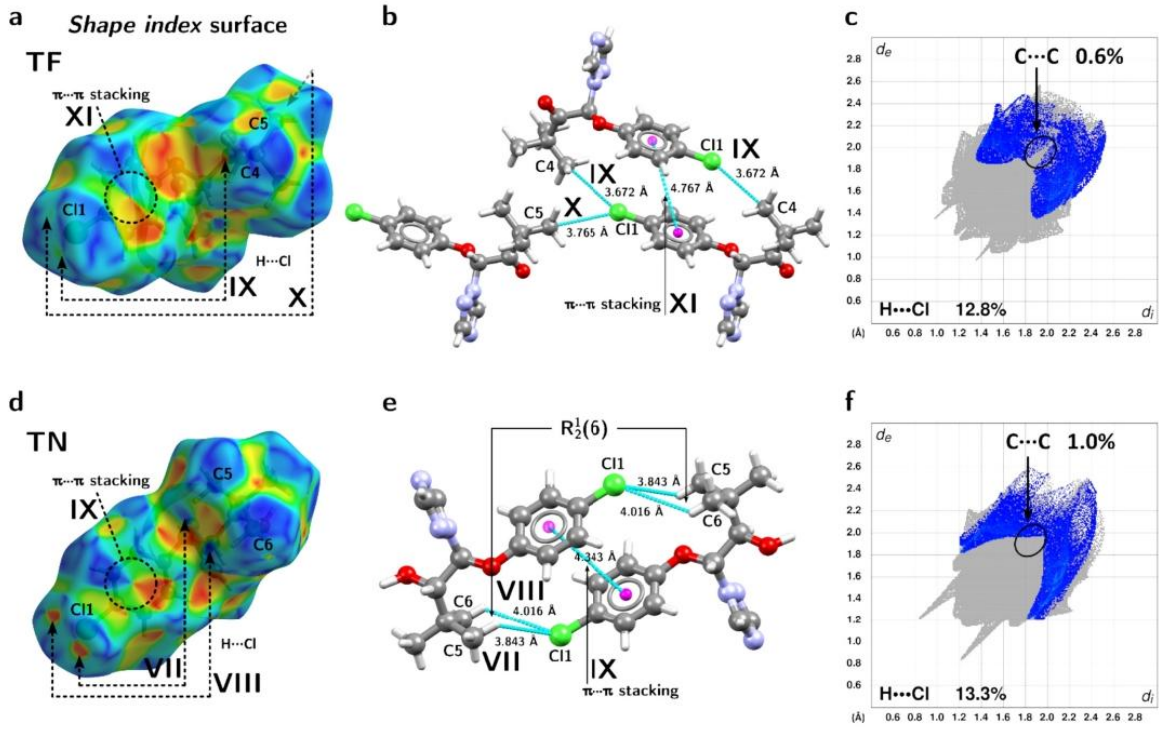

Fig. 6. HS with the *shape index* property mapped, highlighting the complementary patches (red and blue), where π···π interactions occur, also the blue convex and red concave patches for C—H···Cl interactions. A detailed view of C—H···Cl and π···π-stacking interactions in the supramolecular arrangement of TF and TN. (a) *shape index* surface mapped for TF. (b) Representation of C—H···Cl interactions: IX (C_4 ···Cl_1) and X (C_5···Cl_1), with their donor-acceptor distances in TF. Representation of π···π-stacking interaction XI, with the centroid distances (Cg-Cg) between phenyl rings. (c) The 2D *fingerprint* plot of the H···Cl with 12.8% and C···C with 0.6% of the total contacts was mapped for TF. (d) *shape index* surface mapped for TN. (e) Representation of the interactions VII (C_5···Cl_1) and VIII (C_6 ···Cl_1) with their donor-acceptor distances in TN. Representation of π···π-stacking interaction IX, with the centroid distances (Cg-Cg) between phenyl rings. (f) The 2D *fingerprint* plot of the H···Cl with 13.3% and C···C with 1.0% of the total contacts was mapped for TN. (For interpretation of the references to color in this figure legend, the reader is referred to the web version of this article.)

stability and organization of the crystal packing.

The π···π-stacking interactions were observed between centroids (Cg) from phenyl groups, it is highlighted in Fig. 6 and d through the shape index HS as two complementary triangular patches formed on the phenyl rings characteristic of π···π interactions [72], featuring a dimeric arrangement with centroid distances (Cg-Cg) of 4.767 Å in TF and 4.343 Å in TN (see Fig. 6b and e). The corresponding 2D *fingerprint* plot is characterized by the C···C contacts, centrally located in Fig. 6c and f, 0.6% in TF and 1.0% in TN of total contacts, respectively. These supramolecular assembly also include halogen-involved interactions, the weak C—H···Cl hydrogen bonds [73], in which the chlorine acts as an acceptor from the C—H from methyl group (CH_3) of the neighboring molecule, connecting two molecular units shorter in distance and angles in TF involving three molecules (Fig. 6b), includes the dimer with C_4–H_{4B}···Cl_1 (3.912 Å, 102.96°) and a side located C_5–H_{5C}···Cl_1 (3.765 Å, 94.08°), accounting 12.8% of total contacts (Fig. 6c). In the C_4–H_{4B}···Cl_1 interaction, no BP was detected connecting the Cl_1 atom to H_{4B}; instead, the BP connects Cl_1 to C_4 (see C_4···Cl_1 in Table 3). According to the topological parameters, this interaction exhibits van der Waals character. Similarly, for the C_5–H_{5C}···Cl_1 interaction, no BP was observed, indicating the absence of a direct interaction between these atoms. Whereas in TN, the assembly is also a dimer arrangement by bifurcated interactions in Cl_1, C_5–H_{5A}···Cl_1 (3.843 Å, 131.36°) and C_6–H_{6C}···Cl_1 (3.843 Å, 131.36°), forming two $R_2^1(6)$ supramolecular motifs (Fig. 6e), which sum to 13.3% of total contacts (Fig. 6f). The QTAIM parameters revealed that the electron density at the BCP for the C_5–H_{5A}···Cl_1 interaction is very low. In contrast, the electron density in the internuclear region of the C_6–H_{6C}···Cl_1 interaction is approximately 2.2 times higher. However, NBO analysis indicated a stronger hyperconjugation between the donor and acceptor orbitals [$\eta_3(Cl_1)$ → $\sigma^*(C_5–H_{5A})$] in the former, with an $E^{(2)}_{i\to j^*}$ value of 0.13 kcal/mol, compared to 0.07 kcal/mol in the latter, by the hyperconjugation $\sigma(C_6–H_{6C}) \to \sigma^*(C_4–Cl_1)$.

Halogen-involving interactions were also identified. In the TN structure, a C—H···Cl type interaction is observed, in which the chlorine atom acts as an acceptor towards a C—H group from a methyl group (CH_3) of a neighboring molecule, connecting two molecular units. This interaction occurs alongside a π···π interaction, characterized by a Cg···Cg distance of 4.343 Å, as illustrated in Fig. 6e. TF exhibits the same bonding pattern, with shorter distances for halogen-involving contacts and a longer distance for the π···π interaction (Fig. 6b).

3.2. Electronic structure analysis

The stereoisomers of each fungicidal were calculated and compared. The data indicated that the 1*S*-TF isomer exhibits slightly lower HOMO (E_H) and LUMO (E_L) energies (differences of 0.608 kcal/mol for E_H and 0.320 kcal/mol for E_L), suggesting a more pronounced oxidative character compared to the 1*R*-TF isomer (Fig. 7). The energy gap (ΔE_{H-L}) and chemical hardness (η) values suggest that the chemical reactivities

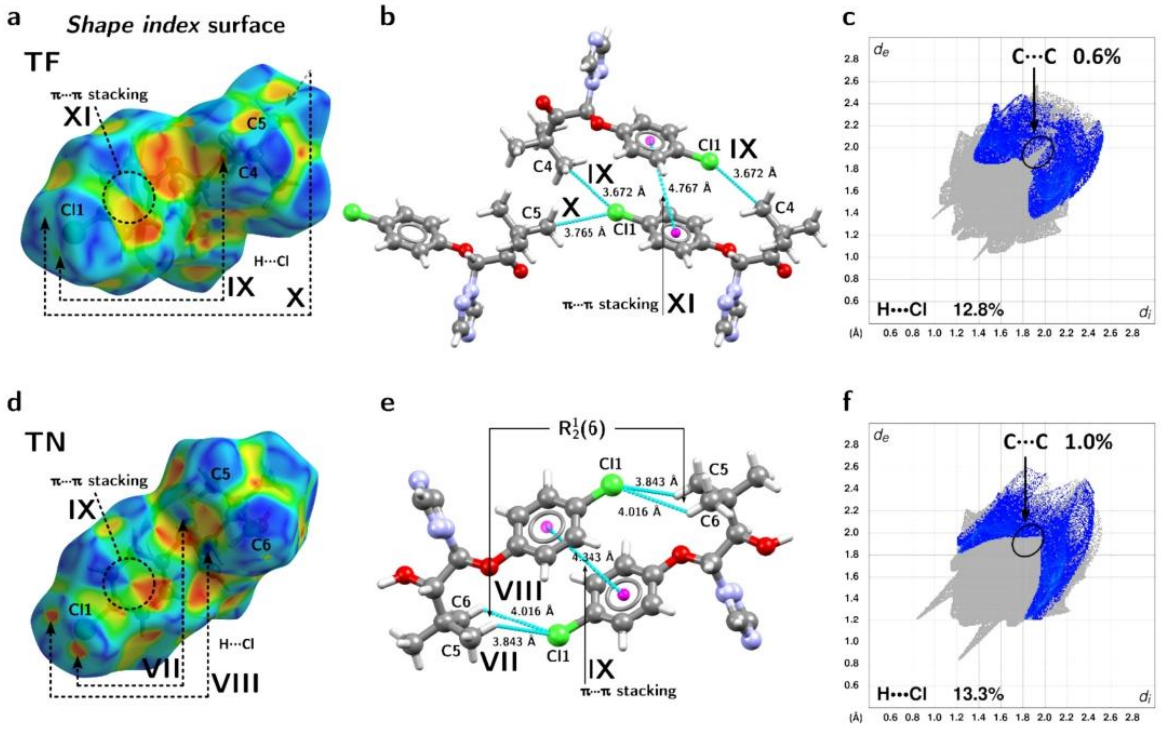

Fig. 6. HS with the *shape index* property mapped, highlighting the complementary patches (red and blue), where π···π interactions occur, also the blue convex and red concave patches for C—H···Cl interactions. A detailed view of C—H···Cl and π···π-stacking interactions in the supramolecular arrangement of TF and TN. (a) *shape index* surface mapped for TF. (b) Representation of C—H···Cl interactions: IX (C_4 ···Cl_1) and X (C_5···Cl_1), with their donor-acceptor distances in TF. Representation of π···π-stacking interaction XI, with the centroid distances (Cg-Cg) between phenyl rings. (c) The 2D *fingerprint* plot of the H···Cl with 12.8% and C···C with 0.6% of the total contacts was mapped for TF. (d) *shape index* surface mapped for TN. (e) Representation of the interactions VII (C_5···Cl_1) and VIII (C_6 ···Cl_1) with their donor-acceptor distances in TN. Representation of π···π-stacking interaction IX, with the centroid distances (Cg-Cg) between phenyl rings. (f) The 2D *fingerprint* plot of the H···Cl with 13.3% and C···C with 1.0% of the total contacts was mapped for TN. (For interpretation of the references to color in this figure legend, the reader is referred to the web version of this article.)

stability and organization of the crystal packing.

The π···π-stacking interactions were observed between centroids (Cg) from phenyl groups, it is highlighted in Fig. 6 and d through the shape index HS as two complementary triangular patches formed on the phenyl rings characteristic of π···π interactions [72], featuring a dimeric arrangement with centroid distances (Cg-Cg) of 4.767 Å in TF and 4.343 Å in TN (see Fig. 6b and e). The corresponding 2D *fingerprint* plot is characterized by the C···C contacts, centrally located in Fig. 6c and f, 0.6% in TF and 1.0% in TN of total contacts, respectively. These supramolecular assembly also include halogen-involved interactions, the weak C—H···Cl hydrogen bonds [73], in which the chlorine acts as an acceptor from the C—H from methyl group (CH_3) of the neighboring molecule, connecting two molecular units shorter in distance and angles in TF involving three molecules (Fig. 6b), includes the dimer with C_4–H_{4B}···Cl_1 (3.912 Å, 102.96°) and a side located C_5–H_{5C}···Cl_1 (3.765 Å, 94.08°), accounting 12.8% of total contacts (Fig. 6c). In the C_4–H_{4B}···Cl_1 interaction, no BP was detected connecting the Cl_1 atom to H_{4B}; instead, the BP connects Cl_1 to C_4 (see C_4···Cl_1 in Table 3). According to the topological parameters, this interaction exhibits van der Waals character. Similarly, for the C_5–H_{5C}···Cl_1 interaction, no BP was observed, indicating the absence of a direct interaction between these atoms. Whereas in TN, the assembly is also a dimer arrangement by bifurcated interactions in Cl_1, C_5–H_{5A}···Cl_1 (3.843 Å, 131.36°) and C_6–H_{6C}···Cl_1 (3.843 Å, 131.36°), forming two $R_2^1(6)$ supramolecular motifs (Fig. 6e), which sum to 13.3% of total contacts (Fig. 6f). The QTAIM parameters revealed that the electron density at the BCP for the C_5–H_{5A}···Cl_1 interaction is very low. In contrast, the electron density in the internuclear region of the C_6–H_{6C}···Cl_1 interaction is approximately 2.2 times higher. However, NBO analysis indicated a stronger hyperconjugation between the donor and acceptor orbitals [$\eta_3(Cl_1)$ → $\sigma^*(C_5$–$H_{5A})$] in the former, with an $E^{(2)}_{i\to j^*}$ value of 0.13 kcal/mol, compared to 0.07 kcal/mol in the latter, by the hyperconjugation $\sigma(C_6$–$H_{6C})$ → $\sigma^*(C_4$–$Cl_1)$.

Halogen-involving interactions were also identified. In the TN structure, a C—H···Cl type interaction is observed, in which the chlorine atom acts as an acceptor towards a C—H group from a methyl group (CH_3) of a neighboring molecule, connecting two molecular units. This interaction occurs alongside a π···π interaction, characterized by a Cg···Cg distance of 4.343 Å, as illustrated in Fig. 6e. TF exhibits the same bonding pattern, with shorter distances for halogen-involving contacts and a longer distance for the π···π interaction (Fig. 6b).

3.2. Electronic structure analysis

The stereoisomers of each fungicidal were calculated and compared. The data indicated that the 1*S*-TF isomer exhibits slightly lower HOMO (E_H) and LUMO (E_L) energies (differences of 0.608 kcal/mol for E_H and 0.320 kcal/mol for E_L), suggesting a more pronounced oxidative character compared to the 1*R*-TF isomer (Fig. 7). The energy gap (ΔE_{H-L}) and chemical hardness (η) values suggest that the chemical reactivities

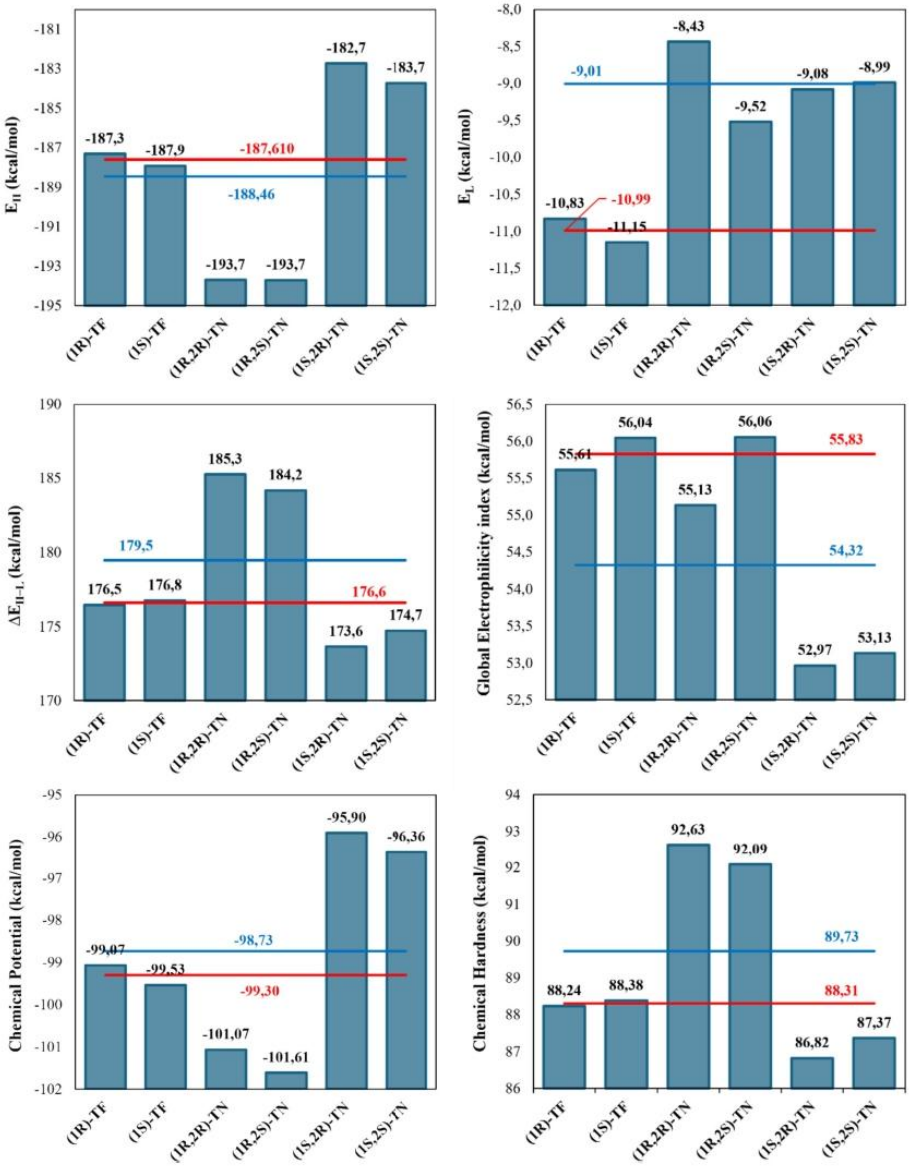

Fig. 7. escriptors of the stereoisomers of triadimefon and triadimenol, calculated at the M06-2×/6–311++G(d,p) level of theory. The columns represent each reactivity descriptor, while the red lines indicate the average values for triadimefon and the blue lines for triadimenol. (For interpretation of the references to color in this figure legend, the reader is referred to the web version of this article.)

of these two isomers are similar, although slightly higher for 1*S*-TF. For TN, the results allowed the stereoisomers to be grouped into two categories: Group A (1*R*,2*R*-TN and 1*R*,2*S*-TN) and Group B (1*S*,2*R*-TN and 1*S*,2*S*-TN). Group A isomers were found to be less reductive in redox processes, as indicated by their low E_H and ionization energy (*I*) values and higher chemical potentials (μ). Conversely, Group B isomers showed greater electron-donating capacity, suggesting a higher potential for interactions with biomolecules. This may translate into stronger adverse effects on fungi, as supported by *in vitro* activity against *Basidiomycete* fungi [74]. Moreover, the Group B isomers were found to be more chemically reactive, which may influence their persistence both in fungal organisms and in the environment. It is noteworthy that, in *in vitro* tests with *Aspergillus niger*, the 1*R*,2*S*-TN and 1*S*,2*R*-TN stereoisomers exhibited less prominent fungitoxic effects [75].

The electrophilicity index (ω) values of the stereoisomers ranged from 52 to 56 kcal/mol. According to the results reported by Domingo-Pérez [76,77], all these values classify the isomers as good electrophiles. The 1*R*-TF, 1*S*-TF, and Group A TN isomers exhibited similar ω values, with 1*S*-TF being the most electrophilic. The Group B TN isomers, in contrast, showed slightly lower electrophilicity. MEP maps of TF and TN stereoisomers are presented in Fig. 8 and show that the most electrophilic regions (dark blue) are located at the hydrogen atoms of carbons C_7 and C_8 of the triazole moiety, at the hydrogens of aromatic carbons, and in the acyclic regions of the molecules. Meanwhile, the triazolic N

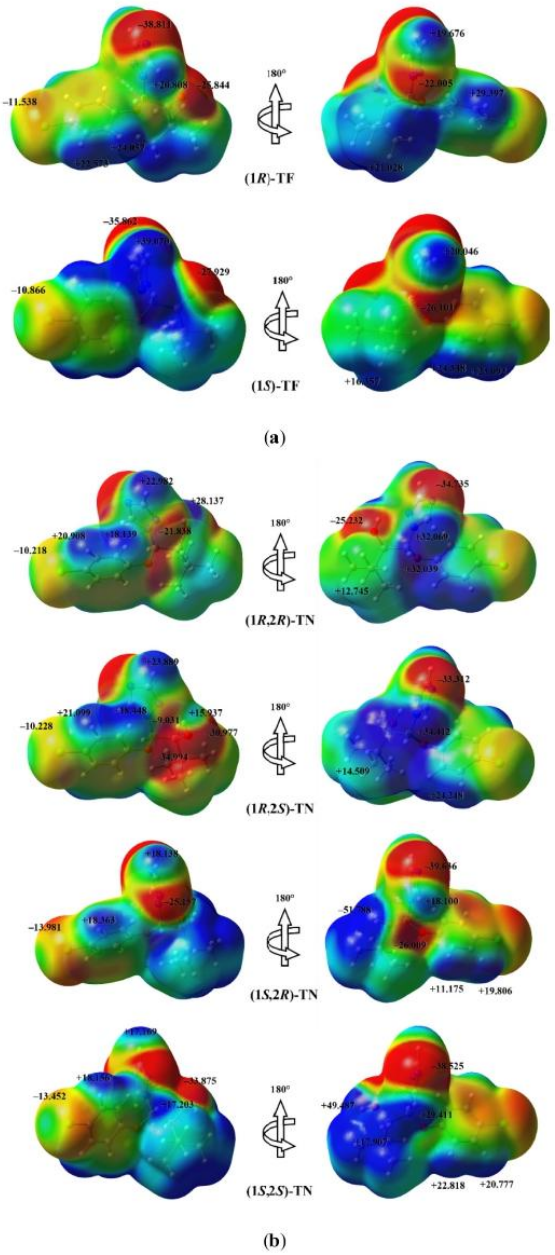

Fig. 8. Molecular electrostatic potential map at $\rho(\mathbf{r}) = 4.0 \times 10^{-4}$ electrons/Bohr [3] contour of the total SCF electron density, highlighting regions of electrophilic and nucleophilic character to (a) Triadimefon and (b) Triadimenol. Calculations were performed at the M06-2×/6–311++G(d,p) level of theory.

atoms and the O_1 oxygen atoms represent the main nucleophilic sites (in red) of the molecules. Overall, TF isomers tend to be more reactive than TN isomers (Fig. 7) and exhibit a more pronounced electrophilic character. These properties may help explain the lower environmental persistence of TF [78] and its less specific interactions with biological targets [79].

Moreover, the molecular polarity indices (MPI) of the fungicide stereoisomers exhibit distinct polarities, which may also account for their different biological effects. Overall, as shown in the graph in Fig. 9a, both compounds present similar polarity levels (10.65 kcal/mol for TF and 10.54 kcal/mol for TN). Individually, although 1R-TF and 1S-TF display comparable MPI values, the former stereoisomer shows a 6.54% higher polar surface area, as seen in the graph in Fig. 9b. For TN, an increase in MPI values was observed from Group A to Group B, corresponding to a proportional increase in the polar surface area of the isomers (Fig. 9b). The polar surface area of 1R,2R-TN is slightly smaller than that of benzene, comparatively. On average, the polar surface areas of TF stereoisomers and Group B TN isomers are approximately 17.7% and 24.2% higher, respectively, than the surface area of the benzene molecule.

Higher polar surface areas and molecular polarity indices (MPI) influence key physicochemical properties such as aqueous solubility, membrane permeability, and the affinity of molecules for lipophilic or hydrophilic biological compartments. As a result, the pharmacokinetic and toxicological behaviors of TF and TN—and of their stereoisomers—may vary in biological and environmental contexts. More polar stereoisomers tend to interact more readily with proteins, enzymes, and cellular membranes, potentially enhancing their biological effects [80]. In contrast, less polar stereoisomers may exhibit lower immediate bioavailability but greater environmental persistence, increasing the likelihood of bioaccumulation in non-target organisms. Molecular polarity also modulates the solubility of these fungicides in different media and their affinity for biological targets, contributing to the stabilization of intermolecular interactions and facilitating systemic distribution within fungal tissues as well as interactions with intracellular targets [81,82].

The reactivity descriptors obtained are essential for predicting the molecular behavior of these fungicides in biological systems. Scientific literature shows that the fungicidal efficacy of both compounds is highly dependent on the agricultural crop and the application method used. Studies conducted by Embrapa Trigo have shown that TN, when applied in seed treatment, provides efficient control of foliar diseases such as powdery mildew (*Blumeria graminis*) and leaf rust (*Puccinia triticina*) for up to 98 days after plant emergence. In addition, a significant increase in grain yield was observed, with productivity of 1815 kg/ha in plots treated with TN, compared to 1270 kg/ha in the untreated control [83].

On the other hand, TF has shown high efficacy when applied through the root system, particularly in the control of coffee rust (*Hemileia vastatrix*). Soil applications of TF have demonstrated significant systemic and protective effects, highlighting its suitability for perennial crops such as coffee. Thus, although both compounds exhibit consistent fungicidal properties, TN is more effective in seed treatment strategies, providing prolonged control of foliar phytopathogens. In contrast, TF is particularly effective in soil applications, making it more suitable for disease management in perennial crops. Therefore, the choice between these fungicides should take into account the application method, target crop, and the mechanisms of action most compatible with each agronomic context.

The Fukui index calculations revealed that the replacement of the carbonyl group (C═O) by a hydroxyl group (C—OH) between the compounds TF and TN induces significant changes in the electronic profile of their molecules. The C═O group is strongly electrophilic due to the high polarization of the carbonyl bond, in which the more electronegative oxygen atom attracts electron density, rendering the adjacent carbon (C_2) highly electron-deficient. As a result, this group withdraws electron density through both inductive and resonance effects, making the C_2 atom highly susceptible to nucleophilic attack (Fig. 10a). Furthermore, the electronic influence of the carbonyl group contributes to an increase in electron density over the $C_{4'}$ atom in TF, rendering it more prone to interactions with electrophiles.

Fig. 10 In contrast, the C—OH group, although also an electron-withdrawing group *via* the inductive effect, acts as an electron donor

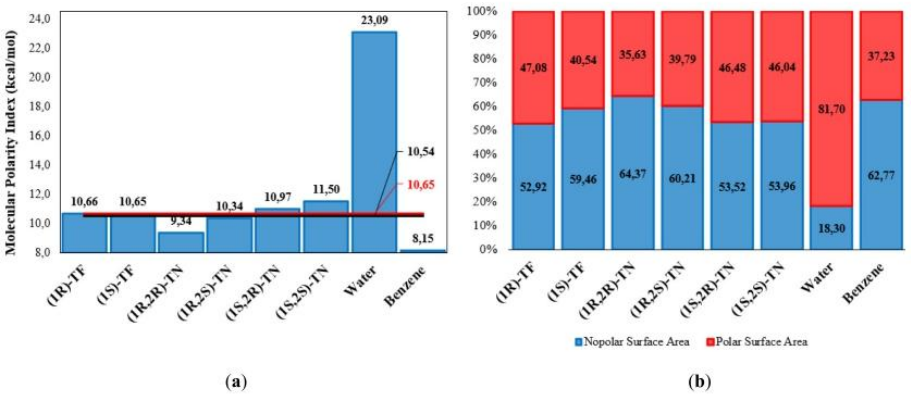

(a) (b)

Fig. 9. Variation in the polarity of Triadimefon and Triadimenol fungicides. (**a**) Molecular polarity index (MPI) values and (**b**) polar and nonpolar surface area contributions of these compounds, both compared to those of water and benzene.

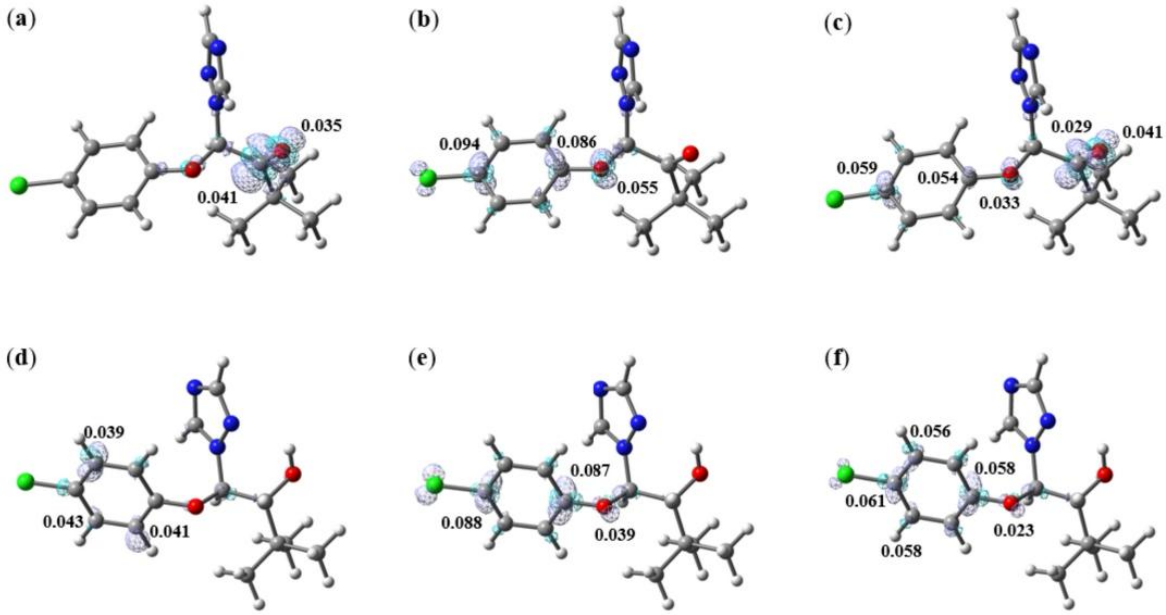

Fig. 10. Isosurfaces of Fukui function for nucleophilic attacks (a) and (d), electrophilic attacks (b) and (e), and radical attacks (c) and (f) for the fungicides Triadimefon (upper panel) and Triadimenol (lower panel).

through resonance, thereby reducing the electrophilic character of C_2 and making it less susceptible to nucleophilic attack. This shift promotes the aromatic ring as the preferred site for nucleophilic attack, with the $C_{5'}$ atom emerging as the primary center, followed by $C_{6'}$. Similar to TF, the C4′ atom in TN remains the leading site for electrophilic attack; however, the electronic effects induced by the C—OH group render it a less nucleophilic center.

3.3. Toxicity prediction and pharmacophore modeling

Pharmacophore analysis is an essential analysis for gaining insights into the molecular characteristics of lanosterol 14α-demethylase ligands, which are critical for effective drug design. Each pharmacophore model emphasizes key features such as hydrogen bond acceptors (HBAs), hydrogen-bond donors (HBDs), aromatic rings (ARs), and hydrophobic (HyPho) regions. These features are visually represented in Figs. 11, 12, and 13 as follows: the pharmacophore features are color-coded for hydrogen-bond acceptors (red), hydrogen-bond donors (green), hydrophobic (yellow), and aromatic rings (blue).

Of the six stereoisomers of TF and TN molecules, only three showed alignment with the five most potent lanosterol 14α-demethylase inhibitor ligands. The stereoisomers that exhibited the spatial characteristics were 1*R*-TF, 1*S*,2*R*-TN and 1*S*,2*S*-TN. The 1*R*-TF isomer shared two hydrogen bond acceptor groups and one aromatic ring (Fig. 11). The 1*S*,2*R*-TN stereoisomer exhibited one hydrogen bond acceptor group, one donor group, and one hydrophobic group (Fig. 12). The 1*S*,2*S*-TN stereoisomer also displayed three pharmacophoric groups, with two hydrogen bond acceptor groups and one hydrophobic group. It is possible that these three structures would have a greater potential for interaction with the target, which could explain part of their fungicidal

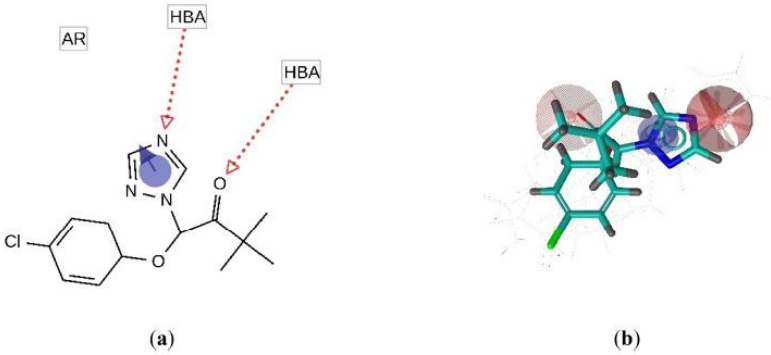

Fig. 11. Pharmacophore mapping analysis for 1*R*-TF for its potential interaction with the lanosterol 14α-demethylase. (**a**) Individual pharmacophores of 1*R*-TF. Hydrogen bond acceptors (HBA) and aromatic rings interactions (AR). (**b**) Three-dimensional model of shared feature pharmacophore between 1*R*-TF and the lanosterol 14α-demethylase ligands. The pharmacophore features are color-coded for hydrogen bond acceptors (red) and aromatic ring interactions (blue). The five compounds employed in this analysis were BDBM24656, BDBM25806, BDBM25807, BDBM25808, and BDBM25809 (color figure online). (For interpretation of the references to color in this figure legend, the reader is referred to the web version of this article.)

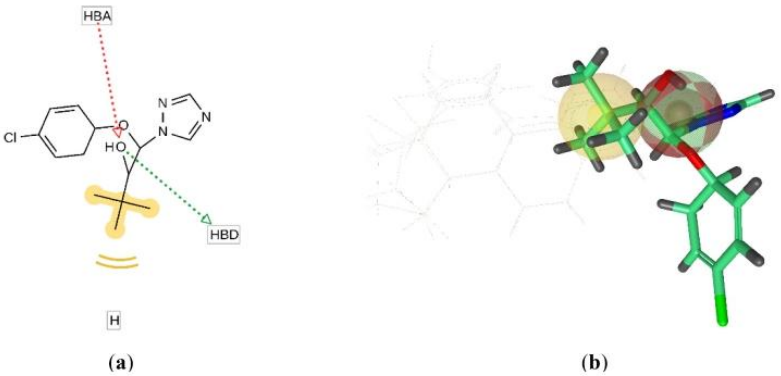

Fig. 12. Pharmacophore mapping analysis for 1*S*,2*R*-TN for its potential interaction with the lanosterol 14α-demethylase. (**a**) Individual pharmacophores of 1*S*,2*R*-TN. Hydrogen bond acceptors (HBA) and aromatic rings interactions (AR). (**b**) Three-dimensional model of shared feature pharmacophore between 1*S*,2*R*-TN and the lanosterol 14α-demethylase ligands. The pharmacophore features are color-coded for hydrogen bond acceptors (red) and aromatic ring interactions (blue). The five compounds employed in this analysis were BDBM24656, BDBM25806, BDBM25807, BDBM25808, and BDBM25809 (color figure online). (For interpretation of the references to color in this figure legend, the reader is referred to the web version of this article.)

effects.

The pharmacophore modeling study of triadimenol (TN) and triadimefon (TF) isomers provides crucial insights into the stereoselective interaction of these fungicides with the lanosterol 14α-demethylase target [84]. The finding that only three out of six isomers – 1*R*-TF, 1*S*,2*R*-TN, and 1*S*,2*S*-TN – align with the most potent inhibitor ligands allows us to propose a definitive structure-activity relationship (SAR) and hypothesize their binding mode at the molecular level.

The development of effective antifungal agents is fraught with a unique and critical challenge: achieving selectivity. Unlike bacterial pathogens, fungi are eukaryotic organisms, sharing fundamental cellular machinery with their plant and animal hosts. This similarity means that a compound designed to inhibit a vital fungal process can easily disrupt equivalent pathways in the host, leading to detrimental toxic effects. In an agricultural context, this toxicity extends to the environment and human health through pesticide residues on food and ecosystem contamination [85]. Therefore, the pursuit of selectivity is not merely a desirable goal but a fundamental requirement for sustainable agrochemistry. It is within this framework that the pharmacophore alignment of specific isomers, such as 1*R*-TF, 1*S*,2*R*-TN and 1*S*,2*S*-TN, emerges as a powerful tool for designing safer and more targeted fungicides.

Both antifungals showed high gastrointestinal absorption and blood-brain barrier permeability in the toxicokinetic prediction analyses. Furthermore, the studies indicate that both compounds could inhibit the cytochrome P450 2C19 (CYP2C19) enzyme. This suggests potential for drug-drug interactions with medications metabolized by CYP2C19. Some drugs that are substrates of this enzyme include Omeprazole, Citalopram, Voriconazole, and Diazepam. Consequently, the presence of these two antifungals could lead to increased bioavailability and a higher risk of toxicity for these substances [86].

In the toxicity analysis, the two compounds exhibited similar adverse effects, including hepatotoxicity, neurotoxicity, blood-brain barrier disruption, ecotoxicity, and aromatase inhibition. However, the LD_{50} values for TF and TN were 363 mg/kg and 3250 mg/kg, respectively. This result suggests that TN is more toxic. The presence of a hydroxyl group instead of a carbonyl group in the TN molecule appears to influence this compound's toxicity primarily in a quantitative manner. Some studies have shown that triazole fungicides can cause liver toxicity [87], neurotoxicity [88], reproductive toxicity [89], and carcinogenic effects [90] in both *in vivo* and *in vitro* mouse models. This evidence suggests that the *in silico* analyses were suitable for predicting these effects in this

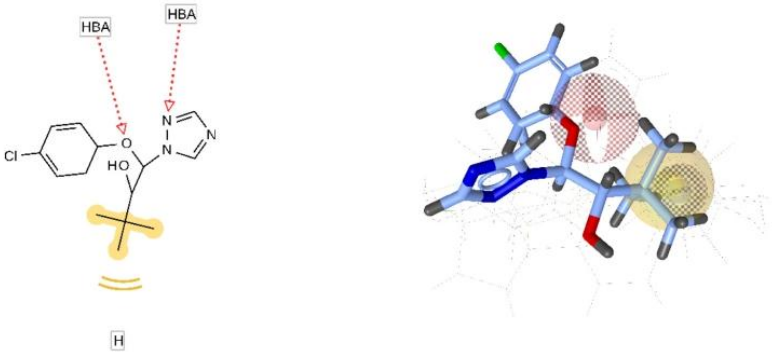

(a) (b)

Fig. 13. Pharmacophore mapping analysis for 1*S*,2*S*-TN for its potential interaction with the lanosterol 14α-demethylase. (**a**) Individual pharmacophores of 1*S*,2*S*-TN. Hydrogen bond acceptors (HBA) and aromatic rings interactions (AR). (**b**) Three-dimensional model of shared feature pharmacophore between 1*S*,2*S*-TN and the lanosterol 14α-demethylase ligands. The pharmacophore features are color-coded for hydrogen bond acceptors (red) and aromatic ring interactions (blue). The five compounds employed in this analysis were BDBM24656, BDBM25806, BDBM25807, BDBM25808, and BDBM25809 (color figure online). (For interpretation of the references to color in this figure legend, the reader is referred to the web version of this article.)

kind of compound.

It was shown that TN causes significant changes in hematological parameters, and induces higher hepatotoxic and nephrotoxic effects in broilers, and the residues in the edible tissues could also bring problems to human health [91]. The analysis on the Pred-Herg server suggests that the two antifungals could present a moderate potential for heart block according to the multiclass prediction model. Regarding the prediction of cutaneous toxicity, TF showed potential for sensitizing dendritic cells and inducing the production of pro-inflammatory cytokines. The TN compound exhibited the same property, in addition to potential covalent interaction with skin proteins and increased proliferation of specific antigens in T cells. This suggests that contact with these compounds has the potential to cause toxicity when in contact with the skin. Through the ADMETSAR server, it was possible to corroborate the hypothesis of ecotoxicity previously indicated by PROTOX 3.0. The predictive analyses indicated high toxicity in fish, high toxicity in *Tetrahymena pyriformis*, low toxicity in bees, and non-biodegradability. Studies have shown that TF acts as a fungicide in crops by converting into TN [92], which has greater fungicidal activity than TF itself [93]. Therefore, improper or excessive use of TF or TN can lead to excessive residues in the environment and agricultural raw materials, exposing organisms to TN and adversely affecting human and animal health.

The structural and electronic differences, as well as the distinct supramolecular arrangements observed for TF and TN, provided a consistent rationale for the divergent toxicological profiles of these compounds, highlighting the value of integrated theoretical approaches in predicting toxicity. Differences in their solid-state intermolecular interaction patterns can decisively influence toxicodynamic behavior. The relatively weaker and more dissociable supramolecular structure of TF, due to the presence of nonclassical hydrogen bonds (C—H···O), can facilitate greater molecular mobility, faster dissolution, and reduced environmental persistence—factors that may reduce its overall bioaccumulation and toxicity. In contrast, the more robust and stable crystal lattice of TN, due to the presence of classical hydrogen bonds (O–H···N), can significantly modulate physicochemical properties such as solubility, release kinetics, and transport through biological membranes, while promoting stronger and more selective interactions with biomolecular targets. These characteristics are likely to result in greater environmental retention and more pronounced ecotoxicological impacts. Furthermore, the electronic redistribution associated with the replacement of the carbonyl group (C═O) in TF by a hydroxyl group (C—OH) in TN modifies the molecular reactivity landscape—altering the nucleophilic and electrophilic centers and, consequently, the compounds' potential for biochemical interaction. Molecular polarity further refines this differentiation, such that the greater polarity of TF correlates with increased aqueous solubility and bioavailability, while the lower polarity of TN may increase its partitioning into lipophilic compartments, thus intensifying its toxicological potential.

4. Conclusion

This study presents a comprehensive theoretical analysis of TF and its stereoisomeric metabolite, TN, combining solid-state characteristics, molecular modeling, and *in silico* toxicity prediction tools. It was shown that replacing the carbonyl group in TF by the hydroxyl group in TN, together with stereochemical configuration, systematically shifts molecular electrostatic potential and reactivity indices, and remodels noncovalent recognition (*e.g.*, stronger H-bond and π-contacts in selected TN stereoisomers as evidenced by Hirshfeld/QTAIM/NBO metrics) These variations are closely related to their differential behavior in biological systems and may explain the asymmetric toxicological effects observed experimentally.

The data further suggests that specific stereoisomers of triadimenol may pose greater ecotoxicological risks to non-target organisms. Taken together, these findings reinforce the importance of considering stereochemistry in environmental risk assessments of fungicides and support the application of computational approaches as efficient tools in predictive toxicology. Future work could integrate these predictions with experimental ecotoxicity assays to validate theoretical models and guide more sustainable pesticide use.

CRediT authorship contribution statement

Áureo B. Souza: Writing – review & editing, Writing – original draft, Visualization, Investigation. **Ronaldo G. Freitas Junior:** Writing – review & editing, Writing – original draft, Investigation. **Ana L.M. Monteiro:** Writing – review & editing, Writing – original draft, Investigation. **Leonardo R. de Almeida:** Writing – review & editing, Writing – original draft, Visualization, Methodology, Investigation, Formal analysis. **Lucas D. Dias:** Writing – review & editing, Writing – original draft, Visualization, Formal analysis. **Lucas B. Ribeiro de Carvalho:** Writing – original draft, Visualization, Investigation. **Hamilton B. Napolitano:** Writing – review & editing, Visualization, Formal analysis. **Leonardo L. Borges:** Writing – review & editing, Writing – original draft,

Visualization, Validation, Methodology, Investigation, Formal analysis, Data curation, Conceptualization. **Antônio S.N. Aguiar:** Writing – review & editing, Writing – original draft, Visualization, Validation, Supervision, Project administration, Methodology, Investigation, Formal analysis, Data curation, Conceptualization.

Declaration of competing interest

The authors declare that they have no known competing financial interests or personal relationships that could have appeared to influence the work reported in this paper.

Acknowledgments

This work was supported by Fundação de Amparo à Pesquisa do Estado de Goiás (FAPEG) and Innovation, Development and Sustainability: Strengthening the University and the Productive Sector in the State of Goiás Agreement for research, development and innovation – PD&I 07/2020, notice 21/2024 – Public Call for Aid 2024 (Process: 202510267000600), notice 12/2023 CAPES/FAPEG – Research and Development Network of the Central-West Region, FAPEG/SES No. 18/2025 research support – Technological Innovations for Vector Control of Arboviruses, FAPEG notice 12/2025 – Support for Extension Projects of Institutions of Higher Education of the State of Goiás, Coordination for the Improvement of Higher Education Personnel (CAPES), and National Council for Scientific and Technological Development – CNPq (Productivity Grant/303307/2025-0; Inova Talentos Project (IEL/CNPq/Laboratório Teuto; Universal Call CNPq/MCTI No. 44/2024; Process: 404074/2025-1).

Appendix A. Supplementary data

Supplementary data to this article can be found online at https://doi.org/10.1016/j.rechem.2026.103268.

Data availability

Data will be made available on request.

References

[1] M. Aliste, G. Pérez-Lucas, I. Garrido, J. Fenoll, S. Navarro, Risk assessment of 1,2,4-Triazole-typed fungicides for groundwater pollution using leaching potential indices, Water Air Soil Pollut. 232 (2021) 469.
[2] D.L. Roman, D.I. Voiculescu, M. Filip, V. Ostafe, A. Isvoran, Effects of triazole fungicides on soil microbiota and on the activities of enzymes found in soil: a review, Agriculture (Switzerland) 11 (2021), https://doi.org/10.3390/agriculture11090893.
[3] C.J.R. Klittich, Fungicide Mobility and the Influence of Physical Properties, 2014, pp. 95–109, https://doi.org/10.1021/bk-2014-1171.ch005.
[4] N. Singh, Sorption behavior of triazole fungicides in indian soils and its correlation with soil properties, J. Agric. Food Chem. 50 (2002) 6434–6439.
[5] V. Nagappan, S. Deresinski, Posaconazole: A Broad-Spectrum triazole antifungal agent, Clin. Infect. Dis. 45 (2007) 1610–1617.
[6] C. Li, et al., Toxicity, bioactivity of triazole fungicide metconazole and its effect on mycotoxin production by fusarium verticillioides: new perspective from an enantiomeric level, Sci. Total Environ. 828 (2022) 154432.
[7] G.R. Thompson, N.P. Wiederhold, Isavuconazole: a comprehensive review of spectrum of activity of a new triazole, Mycopathologia 170 (2010) 291–313.
[8] B. Zhang, Comprehensive review on the anti-bacterial activity of 1,2,3-triazole hybrids, Eur. J. Med. Chem. 168 (2019) 357–372.
[9] A. Ramírez-Villalva, et al., Synthesis and antifungal activity of novel oxazolidin-2-one-linked 1,2,3-triazole derivatives, Medchemcomm 8 (2017) 2258–2262.
[10] K.N. Venugopala, et al., Crystallography, in silico studies, and in vitro antifungal studies of 2,4,5 trisubstituted 1,2,3-Triazole analogues, Antibiotics 9 (2020) 350.
[11] N. Marepu, S. Yeturu, M. Pal, 1,2,3-Triazole fused with pyridine/pyrimidine as new template for antimicrobial agents: Regioselective synthesis and identification of potent n-heteroarenes, Bioorg. Med. Chem. Lett. 28 (2018) 3302–3306.
[12] K. Ratnakar Reddy, et al., Synthesis of novel 1,2,3-triazole/isoxazole functionalized 2H-Chromene derivatives and their cytotoxic activity, Bioorg. Med. Chem. Lett. 24 (2014) 1661–1663.
[13] A. Németh-Rieder, et al., Synthesis and in vitro anticancer evaluation of flavone—1,2,3-Triazole hybrids, Molecules 28 (2023) 626.
[14] F.-C. Wang, et al., A 1,2,3-Triazole derivative of quinazoline exhibits antitumor activity by tethering RNF168 to SQSTM1/P62, J. Med. Chem. 65 (2022) 15028–15047.
[15] P. Deng, et al., Synthesis and antitumor activity of erlotinib derivatives linked with 1,2,3-Triazole, Front. Pharmacol. 12 (2022).
[16] B.C. Monk, et al., Fungal lanosterol 14α-demethylase: a target for next-generation antifungal design, Biochim. Biophy. Acta Proteins Proteomics 1868 (2020) 140206.
[17] N.C.P. Albuquerque, D.B. Carrão, M.D. Habenschus, A.R.M. de Oliveira, Metabolism studies of chiral pesticides: a critical review, J. Pharm. Biomed. Anal. 147 (2018) 89–109.
[18] N. Kurihara, et al., Pesticides report 37: chirality in synthetic agrochemicals: bioactivity and safety consideration (technical report), Pure Appl. Chem. 69 (1997) 2007–2026.
[19] Y. Li, et al., Chiral fungicide triadimefon and triadimenol: Stereoselective transformation in greenhouse crops and soil, and toxicity to daphnia magna, J. Hazard. Mater. 265 (2014) 115–123.
[20] J.F. Kenneke, C.S. Mazur, S.E. Ritger, T.J. Sack, Mechanistic investigation of the noncytochrome P450-mediated metabolism of triadimefon to triadimenol in hepatic microsomes, Chem. Res. Toxicol. 21 (2008) 1997–2004.
[21] J.F. Kenneke, et al., Integration of metabolomics and in vitro metabolism assays for investigating the stereoselective transformation of triadimefon in rainbow trout, Chirality 22 (2010) 183–192.
[22] R.S. Burden, et al., Comparative activity of the enantiomers of triadimenol and paclobutrazol as inhibitors of fungal growth and plant sterol and gibberellin biosynthesis, Pestic. Sci. 21 (1987) 253–267.
[23] Cambridge Crystallographic Data Centre, Inc, CCDC- The Cambridge Crystallographic Data Centre. Cambridge Structural Database (CSD). https://www.ccdc.cam.ac.uk/, 2023.
[24] I.W. Nowell, P.E. Walker, N.H. Anderson, Structure of 1-(4-chlorophenoxy)-3,3-dimethyl-1-(1,2,4-triazol-1-yl)-2-butanone, Acta Crystallogr. B 38 (1982) 1857–1859.
[25] T. Spitzer, J. Kopf, G. Nickless, 1-(4-chlorophenoxy)-1-(1,2,4-triazol-1-yl)-3,3-dimethyl-butan-2-ol C<sub>14<sub>H<sub>18<sub>O<sub>2<sub>N<sub>3<sub>cl, Cryst. Struct. Commun. 11 (1982) 315–320.
[26] T. Huang, et al., A comprehensive review of 1,2,4-triazole fungicide toxicity in zebrafish (danio rerio): a mitochondrial and metabolic perspective, Sci. Total Environ. 809 (2022) 151177.
[27] C.F. Macrae, et al., Mercury 4.0 : from visualization to analysis, design and prediction, J. Appl. Crystallogr. 53 (2020) 226–235.
[28] The GIMP Development Team, GNU image manipulation program (GIMP), Preprint at, 2025.
[29] P.R. Spackman, et al., CrystalExplorer: a program for hirshfeld surface analysis, visualization and quantitative analysis of molecular crystals, J. Appl. Crystallogr. 54 (2021) 1006–1011.
[30] M.A. Spackman, D. Jayatilaka, Hirshfeld surface analysis, CrystEngComm 11 (2009) 19–32.
[31] R.F.W. Bader, Atoms in molecules, Acc. Chem. Res. 18 (1985) 9–15.
[32] R.F.W. Bader, Atoms in Molecules - a Quantum Theory, Clarendon Press Publication, Ontario, 1994.
[33] F. Weinhold, C.R. Landis, Discovering Chemistry with Natural Bond Orbitals, John Wiley & Sons, Inc, USA, 2012.
[34] F. Weinhold, C.R. Landis, Natural bond orbitals and extensions of localized bonding concepts, Chem. Educ. Res. Pract. 2 (2001) 91–104.
[35] P. Hohenberg, W. Kohn, Inhomogeneous electron gas, Phys. Rev. 136 (1964) B864.
[36] W. Kohn, L.J. Sham, Self-consistent equations including exchange and correlation effects, Phys. Rev. 140 (1965) A1133–A1138.
[37] M.J. Frisch, et al., Gaussian 16, Revision C.01, Preprint at, 2016.
[38] Y. Zhao, D.G. Truhlar, The m06 suite of density functionals for main group thermochemistry, thermochemical kinetics, noncovalent interactions, excited states, and transition elements: two new functionals and systematic testing of four m06-class functionals and 12 other functionals, Theor. Chem. Accounts 120 (2008) 215–241.
[39] Y. Zhao, N.E. Schultz, D.G. Truhlar, Exchange-correlation functional with broad accuracy for metallic and nonmetallic compounds, kinetics, and noncovalent interactions, J. Chem. Phys. 123 (2005).
[40] R.F.W. Bader, T.T. Nguyen-Dang, Y. Tal, A topological theory of molecular structure, Rep. Prog. Phys. 44 (1981) 893.
[41] R.F.W. Bader, H. Essén, The characterization of atomic interactions, J. Chem. Phys. 80 (1983) 1943–1960.
[42] T. Lu, F. Chen, Multiwfn: a multifunctional wavefunction analyzer, J. Comput. Chem. 33 (2012) 580–592.
[43] I.V. Alabugin, K.M. Gilmore, P.W. Peterson, Hyperconjugation, Wiley Interdiscip Rev Comput Mol Sci 1 (2011) 109–141.
[44] G. Zhang, C.B. Musgrave, Comparison of DFT methods for molecular orbital eigenvalue calculations, J. Phys. Chem. A 111 (2007) 1554–1561.
[45] R.G. Pearson, Chemical hardness and density functional theory, J. Chem. Sci. 117 (2005) 369–377.
[46] R.G. Pearson, The electronic chemical potential and chemical hardness, J. Mol. Struct. (THEOCHEM) 255 (1992) 261–270.
[47] R.G. Parr, L.V. Szentpály, S. Liu, Electrophilicity index, J. Am. Chem. Soc. 121 (1999) 1922–1924.
[48] H. Weinstein, R. Osman, J.P. Green, S. Topiol, Electrostatic potentials as descriptors of molecular reactivity: The basis for some successful predictions of biological activity, in: Chemical Applications of Atomic and Molecular Electrostatic

Potentials 309–334, Springer US, Boston, MA, 1981, https://doi.org/10.1007/978-1-4757-9634-6_14.
[49] P. Sjoberg, P. Politzer, Use of the electrostatic potential at the molecular surface to interpret and predict nucleophilic processes, J. Phys. Chem. 94 (1990) 3959–3961.
[50] J. Zhang, T. Lu, Efficient evaluation of electrostatic potential with computerized optimized code, Phys. Chem. Chem. Phys. 23 (2021) 20323–20328.
[51] K. Fukui, Role of frontier orbitals in chemical reactions, Science 1979 (218) (1982) 747–754.
[52] Y. Li, J.N.S. Evans, The Fukui function: a key concept linking frontier molecular orbital theory and the hard-soft-Acid-Base principle, J. Am. Chem. Soc. 117 (1995) 7756–7759.
[53] T. Langer, G. Wolber, Pharmacophore definition and 3D searches, Drug Discov. Today Technol. 1 (2004) 203–207.
[54] A. Daina, O. Michielin, V. Zoete, SwissADME: a free web tool to evaluate pharmacokinetics, drug-likeness and medicinal chemistry friendliness of small molecules, Sci. Rep. 7 (2017) 42717.
[55] E.M. Salah, et al., Chemical composition and antifungal activity of teucrium leucocladum boiss. Essential oils growing in Egypt using two different techniques. Futur, J. Pharm. Sci. 10 (2024) 51.
[56] P. Banerjee, E. Kemmler, M. Dunkel, R. Preissner, ProTox 3.0: a webserver for the prediction of toxicity of chemicals, Nucleic Acids Res. 52 (2024) W513–W520.
[57] I.H. Sanches, R.C. Braga, V.M. Alves, C.H. Andrade, Enhancing hERG risk assessment with interpretable classificatory and regression models, Chem. Res. Toxicol. 37 (2024) 910–922.
[58] R.C. Braga, et al., Pred-hERG: a novel web-accessible computational tool for predicting cardiac toxicity, Mol Inform 34 (2015) 698–701.
[59] J.V.B. Borba, et al., Pred-skin: a web portal for accurate prediction of human skin sensitizers, Chem. Res. Toxicol. 34 (2021) 258–267.
[60] V.M. Alves, et al., A perspective and a new integrated computational strategy for skin sensitization assessment, ACS Sustain. Chem. Eng. 6 (2018) 2845–2859.
[61] H. Yang, et al., AdmetSAR 2.0: web-service for prediction and optimization of chemical ADMET properties, Bioinformatics 35 (2019) 1067–1069.
[62] F. Cheng, et al., AdmetSAR: a comprehensive source and free tool for assessment of chemical ADMET properties, J. Chem. Inf. Model. 52 (2012) 3099–3105.
[63] P.A. Wood, et al., Evaluation of molecular crystal structures using full interaction maps, CrystEngComm 15 (2013) 65–72.
[64] J. Bernstein, R.E. Davis, L. Shimoni, N.-L. Chang, Patterns in hydrogen bonding: functionality and graph set analysis in crystals, Angew. Chem. Int. Ed. Eng. 34 (1995) 1555–1573.
[65] M.A. Spackman, J.J. McKinnon, Fingerprinting intermolecular interactions in molecular crystals, CrystEngComm 4 (2002) 378–392.
[66] C.F. Matta, R.F.W. Bader, Atoms-in-molecules study of the genetically encoded amino acids. III. Bond and atomic properties and their correlations with experiment including mutation-induced changes in protein stability and genetic coding, Proteins Struct. Funct. Genet. 52 (2003) 360–399.
[67] W. Nakanishi, S. Hayashi, K. Narahara, Atoms-in-molecules dual parameter analysis of weak to strong interactions: behaviors of electronic energy densities versus laplacian of electron densities at bond critical points, J. Phys. Chem. A 112 (2008) 13593–13599.
[68] W. Nakanishi, S. Hayashi, K. Narahara, Polar coordinate representation of hb(rc) versus $(\hbar^2/8m)\nabla^2\rho b(rc)$ at BCP in AIM analysis: classification and evaluation of weak to strong interactions, J. Phys. Chem. A 113 (2009) 10050–10057.
[69] S. Emamian, T. Lu, H. Kruse, H. Emamian, Exploring nature and predicting strength of hydrogen bonds: a correlation analysis between atoms-in-molecules descriptors, binding energies, and energy components of symmetry-adapted perturbation theory, J. Comput. Chem. 40 (2019) 2868–2881.
[70] G. Gilli, P. Gilli, The Nature of the Hydrogen Bond: Outline of a Comprehensive Hydrogen Bond Theory vol. 23, Oxford University Press, 2009.
[71] J. Li, et al., Tissue distribution and metabolism of triadimefon and triadimenol enantiomers in chinese lizards (eremias argus), Ecotoxicol. Environ. Saf. 142 (2017) 284–292.
[72] J.J. McKinnon, M.A. Spackman, A.S. Mitchell, Novel tools for visualizing and exploring intermolecular interactions in molecular crystals, Acta Crystallogr. Sect. B: Struct. Sci. 60 (2004).
[73] P. Panini, E. Boel, L. Van Meervelt, G. Van den Mooter, Solvatomorphism in Miconazole: The Role of Weak C—H···Cl Hydrogen Bonds and C—Cl···Cl—C Halogen Interactions in Similarities and Differences in the Crystal Packing, Cryst. Growth Des. 22 (2022) 2703–2724.
[74] A.H.B. Deas, D.R. Clifford, Reductive and oxidative metabolism of triazolylmethanes by two basidiomycete fungi, Pestic. Biochem. Physiol. 22 (1984) 276–284.
[75] A.H.B. Deas, D.R. Clifford, Metabolism of the 1,2,4-triazolylmethane fungicides, triadimefon, triadimenol, and diclobutrazol, by aspergillus Niger (van tiegh.), Pestic. Biochem. Physiol. 17 (1982) 120–133.
[76] L.R. Domingo, M.J. Aurell, P. Pérez, R. Contreras, Quantitative characterization of the global electrophilicity power of common diene/dienophile pairs in Diels–Alder reactions, Tetrahedron 58 (2002) 4417–4423.
[77] P. Pérez, L.R. Domingo, M.J. Aurell, R. Contreras, Quantitative characterization of the global electrophilicity pattern of some reagents involved in 1,3-dipolar cycloaddition reactions, Tetrahedron 59 (2003) 3117–3125.
[78] L. Hou, et al., Triadimefon in aquatic environments: occurrence, fate, toxicity, and ecological risk, Environ. Sci. Eur. 34 (2022) 12.
[79] Y. Li, et al., Chiral fungicide triadimefon and triadimenol: Stereoselective transformation in greenhouse crops and soil, and toxicity to daphnia magna, J. Hazard. Mater. 265 (2014) 115–123.
[80] P.P. Madeira, L.A. Ferreira, V.N. Uversky, B.Y. Zaslavsky, Polarity of Aqueous Solutions. Liquids 4 (2024) 107–116.
[81] D.L. Roman, M.A. Matica, A. Ciorsac, B.V. Boros, A. Isvoran, The effects of the fungicide myclobutanil on soil enzyme activity, Agriculture 13 (2023) 1956.
[82] Q.D. Walker, R.B. Mailman, Triadimefon and triadimenol: effects on monoamine uptake and release, Toxicol. Appl. Pharmacol. 139 (1996) 227–233.
[83] E.C. Picinini, J.M.C. Fernandes, Efeito do tratamento de sementes com fungicida sobre o controle de doenças na parte aérea do trigo, Fitopatol. Bras. 28 (2003) 515–520.
[84] B.C. Monk, et al., Architecture of a single membrane spanning cytochrome p450 suggests constraints that orient the catalytic domain relative to a bilayer, Proc. Natl. Acad. Sci. 111 (2014) 3865–3870.
[85] N. Wang, Y. Liu, J. Li, L. Xu, X. Liang, Advances in selective bioactivity and toxicity of chiral triazole fungicides and their selective behavior in mammals, Chirality 37 (2025).
[86] C. Dücker, J. Brockmöller, How precise is quantitative prediction of pharmacokinetic effects due to drug-drug interactions and genotype from in vitro data? A comprehensive analysis on the example CYP2D6 and CYP2C19 substrates, Pharmacol. Ther. 217 (2021) 107629.
[87] H. Zhang, et al., Insights into the effects of difenoconazole on the livers in male mice at the biochemical and transcriptomic levels, J. Hazard. Mater. 422 (2022) 126933.
[88] F. Direnzo, M. Broccia, E. Giavini, E. Menegola, Citral, an inhibitor of retinoic acid synthesis, attenuates the frequency and severity of branchial arch abnormalities induced by triazole-derivative fluconazole in rat embryos cultured in vitro, Reprod. Toxicol. 24 (2007) 326–332.
[89] E. Menegola, M.L. Broccia, F. Di Renzo, V. Massa, E. Giavini, Study on the common teratogenic pathway elicited by the fungicides triazole-derivatives, Toxicol. in Vitro 19 (2005) 737–748.
[90] K. Tamura, et al., Involvement of constitutive androstane receptor in liver hypertrophy and liver tumor development induced by triazole fungicides, Food Chem. Toxicol. 78 (2015) 86–95.
[91] Y. Tang, et al., Toxicological risk assessment of triadimenol for human exposure, broiler health, and food safety, Food Chem. Toxicol. 194 (2024) 115071.
[92] L. Hongwei, et al., Translocation and enrichment behavior of triadimefon and its metabolite triadimenol in rubber trees, Chin. J. Pesti. Sci. 25 (2023) 444–452.
[93] H. Liang, et al., Stereoselective transformation of triadimefon to metabolite triadimenol in wheat and soil under field conditions, J. Hazard. Mater. 260 (2013) 929–936.

ANEXO B – Artigo 02: Dano no DNA induzido pelos fungicidas triadimefon, triadimenol e sua mistura em linfócitos humanos: citogenotoxicidade e análise computacional das vias metabólicas

Drug and Chemical Toxicology

Taylor & Francis
Taylor & Francis Group

ISSN: 0148-0545 (Print) 1525-6014 (Online) Journal homepage: www.tandfonline.com/journals/idct20

DNA damage induced by fungicides triadimefon, triadimenol, and their mixture in human lymphocytes: cytogenotoxicity and computational analysis of metabolic pathways

Amanda Silva Fernandes, Áureo Barbosa de Souza, Marcelino Benvindo de Souza, Luciane Madureira Almeida, Octavio Luiz Franco, Elisa Flávia Luiz Cardoso Bailão, Leonardo Luiz Borges & Antônio Sérgio Nakao de Aguiar

To cite this article: Amanda Silva Fernandes, Áureo Barbosa de Souza, Marcelino Benvindo de Souza, Luciane Madureira Almeida, Octavio Luiz Franco, Elisa Flávia Luiz Cardoso Bailão, Leonardo Luiz Borges & Antônio Sérgio Nakao de Aguiar (09 Feb 2026): DNA damage induced by fungicides triadimefon, triadimenol, and their mixture in human lymphocytes: cytogenotoxicity and computational analysis of metabolic pathways, Drug and Chemical Toxicology, DOI: 10.1080/01480545.2026.2626753

To link to this article: https://doi.org/10.1080/01480545.2026.2626753

DRUG AND CHEMICAL TOXICOLOGY
https://doi.org/10.1080/01480545.2026.2626753

Taylor & Francis
Taylor & Francis Group

RESEARCH ARTICLE

DNA damage induced by fungicides triadimefon, triadimenol, and their mixture in human lymphocytes: cytogenotoxicity and computational analysis of metabolic pathways

Amanda Silva Fernandes[a], Áureo Barbosa de Souza[b], Marcelino Benvindo de Souza[c], Luciane Madureira Almeida[c], Octavio Luiz Franco[d,e], Elisa Flávia Luiz Cardoso Bailão[c], Leonardo Luiz Borges[a,f] and Antônio Sérgio Nakao de Aguiar[b]

[a]School of Medical and Life Sciences, Pontifical Catholic University of Goiás, Goiânia, GO, Brazil; [b]Laboratory of New Materials, Evangelical University of Goiás, Anápolis, GO, Brazil; [c]Biotechnology Laboratory, Central Campus, State University of Goiás, Anápolis, Goiás, Brazil; [d]S-Inova Biotech, Graduate Program in Biotechnology, Dom Bosco Catholic University, Campo Grande, Mato Grosso do Sul, Brazil; [e]Proteomic and Biochemical Analysis Center, Graduate Program in Genomic Sciences and Biotechnology, Catholic University of Brasília, Brasília, Federal District, Brazil; [f]Laboratory for Research, Development & Innovation of Biodiversity Products, State University of Goiás, Anápolis, Goiás, Brazil

ABSTRACT

Triadimefon (TF) and triadimenol (TN) are triazole fungicides widely used to prevent fungal infections in cereals, fruits, and other economically important crops. Their harmful effects on non-target organisms have been reported. This study investigated the cytogenotoxic effects of TF and TN, isolated and combined, at environmentally relevant concentrations (TF: 0.006, 0.012, and 0.024 mg/mL; TN: 1.5, 3.0, and 6.0 mg/mL; and 0.012 mg/mL TF + 3.0 mg/mL TN) on human lymphocytes using the trypan blue exclusion test and the comet assay. Additionally, *in silico* tools, BioTransformer and DIGEP-Pred, were employed to elucidate metabolic pathways more effectively for detoxifying these xenobiotics and to evaluate their putative effects on gene transcription, respectively. Exposure to TF and TN, either alone or in combination, did not affect lymphocyte viability at the tested concentrations. However, both compounds induced an increase in the percentage of DNA strand breaks after treatment. The *in silico* predictions suggested that the interaction with the cytochrome P450 isoforms (CYP1A2, CYP2A6, CYP2C9, and CYP2D6) differed for each compound analyzed. Gene expression prediction indicated that TF and TN may up-regulate genes involved with hormonal alterations, Alzheimer's disease risk, and cancer progression (SF1, SPON1, ADGRF5, and RORB). While they may down-regulate a gene involved with changes in heart rhythm and neurotoxicity (HCN1). In conclusion, our findings reinforced that the triazole fungicides TF and TN, while effective in agriculture, may pose risks to genomic stability in humans, highlighting the importance of biomonitoring studies in exposed populations.

ARTICLE HISTORY
Received 21 November 2025
Revised 14 January 2026
Accepted 30 January 2026

KEYWORDS
Triazole fungicides; DNA damage; genotoxicity; cytochrome P450; gene transcription regulation

Introduction

Pesticides are widely used in modern agriculture to protect crops from pests, fungi, and diseases (Boros, Roman, and Isvoran 2024). Fungicides, a primary class of pesticides, play a crucial role in controlling fungal infections that compromise crop productivity (Zubrod et al., 2019). Among these, triazoles constitute a primary class due to their broad-spectrum activity and systemic properties, which inhibit ergosterol biosynthesis and prevent the formation of fungal cell membranes (Dong et al., 2023). Despite their effectiveness, triazoles have been linked to adverse effects on non-target organisms, raising concerns about their toxicological safety and potential long-term environmental consequences (Boros, Roman, and Isvoran 2024; Tofan et al., 2023; Zarn, Brüschweiler, and Schlatter 2003).

Triadimefon (TF) is a triazole fungicide primarily used to control rust and powdery mildew (Han et al., 2024). Conversely, several adverse effects on non-target organisms have been reported to this compound, including neurotoxicity, hepatotoxicity, cardiovascular toxicity, oxidative stress, and teratogenic effects (Zarn, Brüschweiler, and Schlatter 2003). TF has been shown to provoke developmental alterations in aquatic organisms, including malformations of amphibian branchial arches and impaired embryogenesis in zebrafish (Hou et al., 2022).

Triadimenol (TN), the primary metabolite of TF, is widely used as a fungicide to control fungal infections in crops (Zhang et al., 2018). Similar to TF, TN has been associated with genotoxic effects, including micronucleus formation and chromosomal aberrations in various cell types (Rasgele 2025), as well as oxidative stress in tadpoles (Zhang et al., 2018). Furthermore, TN induced developmental, endocrine, and reproductive toxicity in mammals (Zarn, Brüschweiler, and Schlatter 2003).

CONTACT Leonardo Luiz Borges leonardo.borges@ueg.br School of Medical and Life Sciences, Pontifical Catholic University of Goiás, Goiânia 74605-010, GO, Brazil; Laboratory for Research, Development and Innovation of Biodiversity Products, State University of Goiás, Central Campus, Anápolis 75132-903, GO, Brazil.
Supplemental data for this article can be accessed online at https://doi.org/10.1080/01480545.2026.2626753.

Although TF and TN are not generally marketed as a combined fungicide, their close chemical and metabolic similarity suggests that co-exposure is possible (Garrison, Avants, and Jones 2011; Hou et al., 2022). The high stability, low biodegradability, and easy transport of TF and TN contribute to their differential persistence in soils and water. Consequently, this persistence increases the occurrence of sequential or simultaneous exposure, underscoring the necessity for further investigation into the potential synergistic or additive genotoxic effects that may result from such co-exposures (Hou et al., 2022; Zhang et al., 2018). Given the established classification of TF and TN as possible human carcinogens (Hou et al., 2022) and their association with diverse toxicological outcomes, it is relevant to investigate their potential to induce DNA damage in human cells. Human exposure to these compounds may occur through occupational handling or dietary intake of residues (Pedroso et al., 2022). It has been reported that occupational exposure to pesticides can lead to genotoxic effects, including sister chromatid exchanges, micronucleus formation, chromosomal aberrations, DNA adducts, and strand breaks. These effects have the potential to impair the nervous, respiratory, reproductive, and immune systems, which can, in turn, increase the risk of cancer (Ahmad et al., 2024; Pedroso et al., 2022).

Although several studies have described the cytotoxicity and genotoxicity of TF and TN on aquatic organisms and mammalian models, little is known about their effects on human cells. Furthermore, no study has yet evaluated the combined impact of TF and TN on human lymphocytes. Human peripheral blood lymphocytes are relevant peripheral cell types that reflect systemic exposure and genomic stability (Antoniou et al., 2023). The use of lymphocytes as a model provides an appropriate correlation between *in vitro* findings and real-world human exposure, thereby supporting the extrapolation to potential occupational and dietary risks (Lebailly et al., 2015). In light of the environmental persistence and potential co-occurrence of TF and TN, a comprehensive assessment that incorporates both individual and combined exposures is required.

The comet assay is a rapid, simple, and sensitive method that can detect DNA strand breaks (*i.e.,* single-and double-strand breaks, alkali-labile sites, and DNA-protein crosslinks) in individual cells. This assay has been extensively used to evaluate the genotoxic effects induced by chemical agents in various cell types and experimental conditions (Calderón-Segura et al., 2012; Ramos et al., 2021; Sasikala et al., 2023). Moreover, it is commonly employed in human biomonitoring studies as a biomarker of exposure to genotoxic agents (Ladeira et al., 2024; Ramos et al., 2021). Moreover, predicting the metabolic features induced by TF and TN provides a powerful approach for elucidating some possible mechanisms of toxic action. By investigating how these compounds disrupt essential biochemical pathways, we can identify early biomarkers of adverse effects, predict chronic toxicity, and establish the basis for improved risk assessment (Hasselgren and Myatt 2018; Loiodice, Nogueira da Costa, and Atienzar 2019).

In this way, this work aimed to investigate the cytogenotoxicity of TF and TN, isolated and combined, at environmentally relevant concentrations, on human lymphocytes. Moreover, *in silico* tools were utilized to elucidate metabolic pathways more effectively to detoxify these xenobiotics and to evaluate their putative effects on gene transcription. In short, this work linked the *in vitro* and *in silico* toxicology investigation of TF and TN to real-world exposure, enabling science-based policy while supporting the development of lower-risk alternatives.

Material and methods

Chemicals

TF ($C_{14}H_{16}ClN_3O_2$) and TN ($C_{14}H_{18}ClN_3O_2$) were acquired from Sigma-Aldrich®. The chemical agent doxorubicin hydrochloride (DXR) was obtained from Glenmark Pharmaceutical Ltda (São Paulo, Brazil). The reagents used in the culture of human lymphocytes and Comet assay, including Triton X-100 and a stock lysate solution (distilled H_2O, NaCl, EDTA, TRIS, NaOH, and sodium lauryl sarcosinate), were purchased from Neon Comercial Ltda (São Paulo, Brazil). Phosphate-buffered saline (PBS, pH 7.4), 0.4% trypan blue solution, RPMI medium with L-glutamine, sodium bicarbonate, neutralizing buffer solution (Tris-HCl), standard melting agarose, and low-melting agarose were purchased from Sigma Aldrich Brasil Ltda (São Paulo, Brazil). Ficoll-Paque Plus was acquired from GE Healthcare (Sweden and the UK). Sodium salt of penicillin G and streptomycin sulfate were purchased from Life Technologies (São Paulo, Brazil). Fetal bovine serum was obtained from Laborclin (Campinas, Brazil). Phytohemagglutinin was purchased from Cultilab (Campinas, Brazil), and Diamond Nucleic Acid was procured from Promega (Madison, WI).

Blood samples and culture of human lymphocytes

Peripheral blood samples were obtained from healthy volunteers ($n=4$), aged between 18 and 30 years, with no history of smoking, alcohol consumption, or chronic illnesses. All procedures were approved by the Research Ethics Committee of Universidade Estadual de Goiás (CAAE No. 66860023.1.0000.8113) and conducted in accordance with national ethical guidelines. Written informed consent was obtained from all participants before sample collection. Lymphocyte cultures were prepared according to the method proposed by Fernandes et al. (2024). A total of 20 mL of venous blood was collected into sterile heparinized tubes and diluted with an equal volume of RPMI 1640 medium. The mixture was centrifuged at 120 × g for 4 min at 18 °C. After discarding the plasma, the buffy coat layer was isolated and carefully layered onto Ficoll-Paque plus for density gradient separation. The sample was then centrifuged at 200 × g for 10 min at 18 °C to isolate the human lymphocytes. The resulting cell pellet was resuspended in RPMI 1640 medium supplemented with 10% fetal bovine serum, 0.5% phytohemagglutinin (mitogen stimulator), and 0.2% antibiotic solution containing penicillin and streptomycin (1:1). The lymphocyte suspension was then transferred to a 25 cm^2 culture flask and incubated at 37 °C for 24 h in a biological oxygen demand (BOD) incubator to promote cell proliferation and growth.

Cytotoxicity assessment on human lymphocytes

Cell viability was evaluated using the trypan blue (0.4%) dye exclusion method. Initially, the concentration of viable lymphocytes was determined using a hemocytometer. Subsequently, cells were plated in 12-well (4×10^5 cells/well) culture plates and exposed to different concentrations of TF (0.006, 0.012, and 0.024 mg/mL) or TN (1.5, 3.0, and 6.0 mg/mL) and a combined treatment of TF (0.012 mg/mL) and TN (3.0 mg/mL). All treatment solutions were prepared using 0.1% dimethyl sulfoxide (DMSO). The concentrations of the treatments were based on previous studies of these compounds in other cell lines, considering environmentally relevant concentrations (Rasgele 2025; Tang et al., 2010). Control groups included sterile distilled water (negative control), 0.1% DMSO (diluent control), and 0.050 mg/mL doxorubicin (DXR) diluted in sterile water (positive control). All treatments were performed in triplicate. After a three-hour incubation at 37 °C, viable cells were manually quantified using a hemocytometer (Strober 2015).

Genotoxicity assessment (comet assay)

The genotoxic potential of TF and TN was determined using the alkaline version of the Comet assay, following the protocol established by Tice et al. (2000) with modifications. A lymphocyte cell suspension was introduced into the 12-well plate (4×10^5 cells/well), and cells then incubated at 37 °C for three hours with varying concentrations of TF (0.006, 0.012, and 0.024 mg/mL) or TN (1.5, 3.0, and 6.0 mg/mL) and a combined treatment of TF (0.012 mg/mL) + TN (3.0 mg/mL) diluted in DMSO 0.1%. The negative (sterile distilled water), positive (0.050 mg/mL, DXR), and diluent (DMSO 0.1%) controls were incorporated into the experiments. After incubation, 80 µL of the treated lymphocytes were mixed with 120 µL low-melting-point agarose (1%) and layered on agarose-coated slides. The slides were then incubated in a Triton X-100-based lysis buffer for 24 h at 4 °C to facilitate DNA unfolding. Subsequently, electrophoresis was carried out under alkaline conditions (300 mM NaOH, 25 V/cm, 30 min, 4 °C) to facilitate the visualization of DNA strand breaks. Following electrophoresis, slides were neutralized using 0.4 M Tris-HCl buffer (pH 7.5), stained with Diamond™ Nucleic Acid Dye (1:10,000 dilution in PBS), and analyzed under a fluorescence microscope (Axioplan-Imaging, Carl Zeiss, 10× objective). DNA damage parameters (% tail DNA, Tail Length, and Olive Tail Moment) was quantified using CometScore™ (v1.5), with 100 cells analyzed per concentration.

In silico metabolism prediction

For the prediction analysis of metabolites generated through the cytochrome P450 system, the Biotransformer server was used, a robust metabolite prediction tool that leverages both machine learning and knowledge-based techniques, including CypReact and CyProduct, to forecast potential metabolites derived from metabolically sensitive bonds in the human body and gut (Djoumbou-Feunang et al., 2019; Wishart et al., 2022). The canonical SMILE structures of TF and TN were used to predict metabolite products in BioTransformer 3.0 (Djoumbou-Feunang et al., 2019). Bioactivity prediction regarding gene expression was performed using DIGEP-Pred (Drug-Induced Gene Expression Profiles Prediction) tools (Lagunin et al., 2013). For both methods, Pa and Pi estimate the probability that the compound is active or inactive, respectively, for each type of activity based on the activity database. The activities presenting Pa > Pi were selected for the analysis. Besides, DIGEP-Pred results were added to the IAP values (Invariant Accuracy of Prediction), which is the average accuracy of prediction that is obtained for the whole PASS training set in a leave-one-out cross-validation procedure.

Statistical analysis

Statistical analyses were performed using one-way ANOVA followed by Tukey's *post hoc* test (GraphPad Prism v8). For the cytotoxicity assay, mean values were converted to percentages before analysis. In the Comet assay, DNA damage was evaluated based on the % of DNA in the comet tail across all treatment and control groups. Furthermore, a Principal Component Analysis (PCA) was conducted to explore the relationships between the comet assay parameters and the different concentrations. The criterion for significance was set at $p<0.05$.

Results

Cytotoxicity assessment on human lymphocytes

None of the examined concentrations of TF (0.006, 0.012, and 0.024 mg/mL) or TN (1.5, 3.0, and 6.0 mg/mL) significantly affected lymphocyte viability in comparison to the negative control (Figure 1). Similarly, the combined treatment of TF (0.012 mg/mL) + TN (3.0 mg/mL) did not significantly affect viability, indicating that no interactive effect between TF and TN occurred (Figure 1). The positive control, DXR (0.050 mg/mL), induced a significant decrease in lymphocyte viability compared to the negative control.

Genotoxicity assessment (comet assay)

In the assessment of genotoxicity, lymphocytes exposed to different concentrations of TF (0.006, 0.012, and 0.024 mg/ml), TN (1.5, 3.0, and 6.0 mg/ml) or the combined treatment of TF (0.012 mg/ml) and TN (3.0 mg/ml) induced significant alterations in % DNA damage compared to negative control (Figures 2 and 3). However, no interactive effect was observed in the mixture of TF and TN. Thus, these findings indicate that TF, TN, and their mixture exert genotoxic effects on human lymphocytes. To complement the visualization of the data, a PCA was performed. The first two principal components explained 96.60% (PC1 89.32% and PC2 7.28%) of the total variance among the parameters and concentrations (Figure 4). It can be observed that concentrations such as TF2, TF3, TN2, and TN3 are located farther from the center, indicating a trend of increased DNA damage at these concentrations. Moreover, the comet assay parameters were positively correlated with each other and associated with the treated

groups. The TF2+TN2 mixture suggests a modest additive effect, in which the combined exposure to the fungicides enhances DNA damage without surpassing that observed at the highest individual concentrations.

In silico predictions

Metabolite prediction utilizes biotransformation dictionaries based on preliminary predictions of likely biotransformation classes, which also describe the substances' metabolomics profiles. Figure 5 presents the chemical structures of these two compounds and their predicted metabolite products. The predicted metabolites for both compounds showed similarities in metabolic pathways (some pathways involved the same cytochrome) and in the compounds formed through the action of the cytochrome P450 superfamily. The cytochromes involved were CYP1A2, CYP2A6, CYP2C9, and CYP2D6 for TF, and CYP1A2 and CYP2A6 for TN. The compounds resulting from these phase I reactions are more polar, which aims to facilitate the renal excretion of these xenobiotics. Some cytochromes can cause drug interactions, increasing the risk of exposure to these compounds for individuals using medications or other molecules metabolized by the same cytochromes.

The gene expression regulation analyses obtained from the DIGEP 2.0 server indicated up-regulation of the steroidogenic factor 1 (SF1; IAP = 0.948), spondin 1 (SPON1; IAP = 0.788), adhesion G protein-coupled receptor F5 (ADGRF5; IAP = 0.862), and RAR-related orphan receptor B (RORB; IAP = 0.774) genes in the presence of TF or TN. The hyperpolarization-activated cyclic nucleotide-gated potassium channel 1 (HCN1; IAP = 0.796) gene is putatively down-regulated in the presence of these compounds. The IAP (Invariant Accuracy of Prediction) values were the same for both compounds due to their high structural similarity. The effects on gene expression appear to occur with the same intensity, which is associated with the significant structural similarity between the two molecules.

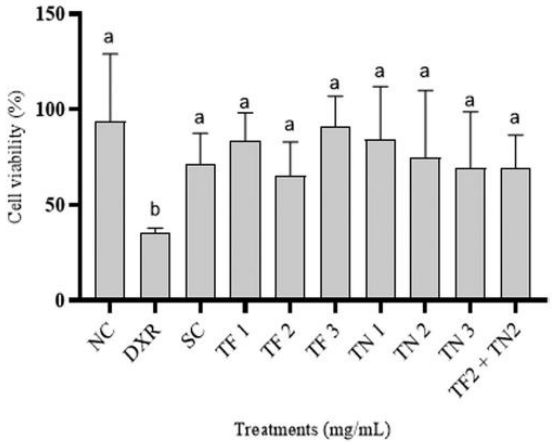

Figure 1. Cytotoxicity of triadimefon (TF), triadimenol (TN), and their mixture on human lymphocytes. Treatments included TF (0.006; 0.012; 0.024 mg/ml), TN (1.5; 3.0; 6.0 mg/ml), TF+TN (0.012 + 3.0 mg/ml), positive control (DXR 0.050 mg/ml), solvent control (DMSO 0.1%), and negative control (water). The cells were incubated for three hours, and the trypan blue exclusion test determined the viability. All results are means ± standard deviation from three independent experiments. Bars with different letters indicate statistically significant differences among treatments ($p < 0.05$). Bars with the same letter do not differ significantly. ANOVA followed by tukey's test.

Discussion

Despite their effectiveness in controlling fungal pathogens in various crops, particularly cereals and fruits (Rasgele 2025), the human toxicological profiles of TF and TN, as well as

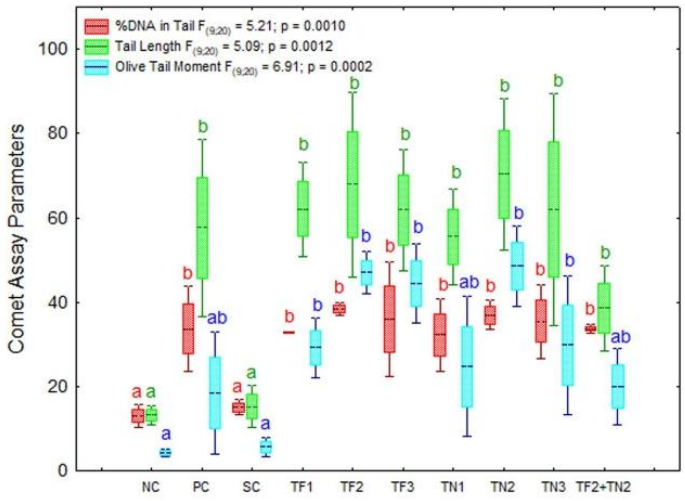

Figure 2. Genotoxicity of triadimefon (TF), triadimenol (TN), and their mixture on human lymphocytes. Assessment of genotoxicity after exposure to TF (0.006, 0.012, 0.024 mg/ml), TN (1.5, 3.0, 6.0 mg/ml), and TF+TN (0.012 + 3.0 mg/ml). Controls: PC (positive, 0.050 mg/ml), SC DMSO 0.1% (solvent), and NC sterile water (negative). The percentage of DNA in tail, tail length and olive moment were quantified using the CometScore software. All results are means ± standard deviations from three independent experiments. Bars with different letters indicate statistically significant differences among treatments ($p < 0.05$), whereas bars with the same letter do not differ significantly. ANOVA followed by tukey's test.

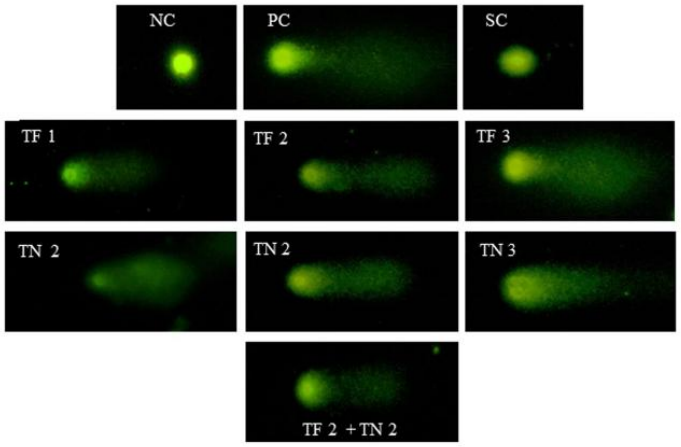

Figure 3. Representative photomicrographs of DNA damage induced by triadimefon (TF), triadimenol (TN), and their mixture on human lymphocytes. The genotoxicity evaluation of different concentrations of TF (0.006, 0.012, 0.024 mg/ml), TN (1.5, 3.0, 6.0 mg/ml), and TF + TN (0.012 + 3.0 mg/ml) was evaluated using the comet assay technique after 3h incubation on human lymphocytes. The cells were stained with Diamond™ nucleic acid dye and the images were acquired using a fluorescence microscope (Axioplan-ImagingVR, 10x objective). Controls: PC (positive, 0.050 mg/ml), SC DMSO 0.1% (solvent), and NC sterile water (negative).

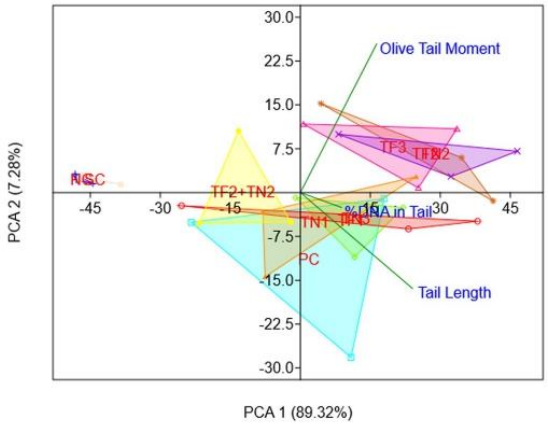

Figure 4. Principal component analysis performed using the concentrations and parameters from the comet assay. Controls: PC (positive, 0.050 mg/ml), SC) DMSO 0.1% (solvent), and NC) sterile water (negative); TF1, 2, and 3 (0.006, 0.012, and 0.024 mg/mL, respectively); TN1, 2, and 3 (1.5, 3.0, and 6.0 mg/mL); and TF2 + TN2 (0.012 + 3.0 mg/mL) represents the mixture. Data from three independent experiments were used.

those of their mixture, remain poorly characterized. This knowledge gap is critical, as interactions between active ingredients in mixtures can lead to synergistic, additive, or antagonistic effects, potentially altering their genotoxicity compared to individual compounds (Barbieri et al., 2022).

In the cytotoxicity assessment, exposure to all tested concentrations of TF, TN, and their mixture did not significantly reduce the number of viable cells compared to the negative control. It was demonstrated that TF and TN exerted variable effects on cell viability depending on the cell line (Xu et al., 2020). Specifically, these triazoles promoted viability on HeLa and A549 cells, showed no significant impact on HCT116 cells, and inhibited viability in K562 cells in a concentration-dependent manner. These differences were attributed to variations in receptor subtype affinities among cell types. Despite this, studies involving triazole-based mixtures in other cellular models have demonstrated that co-exposure may still modulate cytotoxic mechanisms, including the induction of apoptosis and reduced proliferation rates (Koleničová et al., 2020). In the present study, however, the absence of interactive effects suggests that co-exposure to TF and TN at environmentally relevant concentrations does not potentiate cytotoxicity on human lymphocytes.

The trypan blue exclusion assay was used to assess cytotoxicity because it directly evaluates cell membrane integrity, allowing reliable discrimination between viable and non-viable cells (Strober 2015). In this study, this method was suitable to confirm the absence of cytotoxicity in human lymphocytes exposed to TF and TN, ensuring that the DNA damage observed in the comet assay was not a secondary consequence of cell death (Collins 2004). Nevertheless, trypan blue has limitations, including low sensitivity to early apoptotic events and sublethal metabolic alterations, as well as potential operator-dependent variability (Fotakis and Timbrell, 2006; Sabotic et al., 2024).

In this context, alternative assays such as the MTT assay are widely used due to their high sensitivity and reproducibility and are considered well-established standards for cytotoxicity evaluation, as they primarily reflect mitochondrial metabolic activity rather than direct cell viability (Ghasemi et al., 2021; Sabotic et al., 2024). However, MTT reduction depends on cellular metabolic activity and mitochondrial function, which may be altered by metabolic or oxidative stress independently of cell death (Stepanenko and Dmitrenko, 2015). Since triazole fungicides are known to induce oxidative stress and metabolic disturbances without necessarily compromising membrane integrity (Jiang et al., 2017; Xu et al., 2020), MTT-based measurements may lead to an overestimation of cytotoxicity under such conditions (Stepanenko and Dmitrenko, 2015).

In the comet assay, both TF and TN induced significant DNA damage in human lymphocytes, indicating their

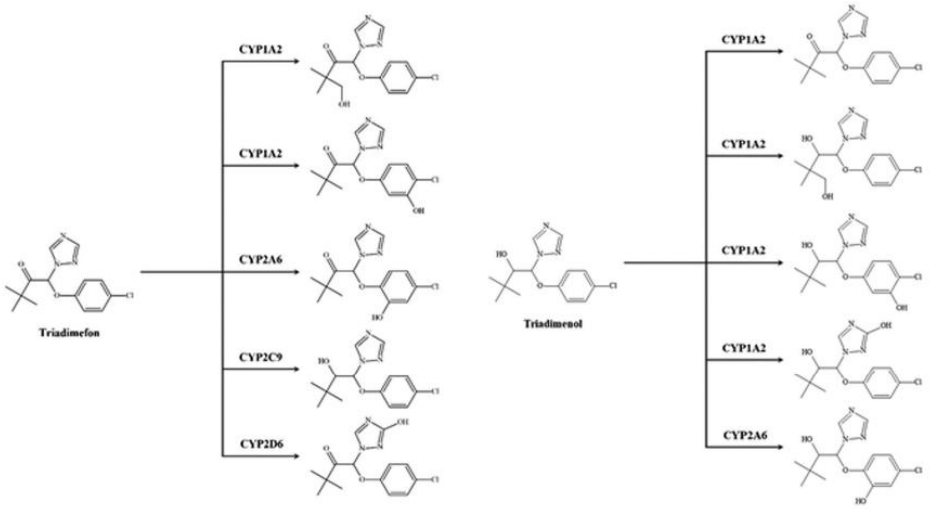

Figure 5. The metabolism profile and chemical structures of triadimefon (TF), triadimenol (TN), and their predicted metabolites were analyzed using BioTransformer 3.0.

genotoxic potential even at low, environmentally relevant concentrations (Tang et al., 2010). Previous studies using the comet assay have consistently demonstrated the genotoxicity of triazole fungicides in various biological models. For instance, significant DNA damage was reported in lymphocytes of agricultural workers exposed to penconazole (Ferri et al., 2019), bovine lymphocytes exposed to epoxiconazole (Koleničová et al., 2020), and rat glioma F98 cells exposed to bromuconazole (Rjiba-Touati et al., 2023). In aquatic organisms, difenoconazole also induced genotoxic effects in *Pethia conchonius* at environmentally relevant levels (Ray et al., 2025).

Exposure to the TF and TN mixture also significantly increased DNA damage, although this effect was not additive compared to the individual compounds, but probably synergistic. Supporting this observation, previous studies have shown that exposure to triazole fungicides, either alone or in combination with other compounds, can alter multiple biomarkers. The interactive effects of TF and citrinin in zebrafish embryos affected oxidative stress, apoptosis, and endocrine biomarkers (Wang et al., 2023). Similarly, mixtures of triazole-based fungicides have been shown to increase DNA fragmentation in the soil organism *Eisenia fetida* (Campani et al., 2025). These findings highlight the importance of evaluating mixture toxicity under realistic environmental exposure scenarios, as multiple agrochemicals frequently co-occur in the environment (Reffstrup, Larsen, and Meyer 2010).

TF and TN have also been associated with the overproduction of reactive oxygen species (ROS), which contributes to the oxidative stress observed in non-target organisms (Jiang et al., 2017; Rasgele 2025; Xu et al., 2020). Excess ROS is a significant cause of cellular damage, leading to lipid peroxidation, protein oxidation, and oxidative DNA damage. These processes disrupt cellular homeostasis and compromise cell function (Hazuková et al., 2024; Smith et al., 2013). DNA, an essential biomolecule responsible for maintaining genomic stability, is particularly susceptible to oxidative stress, which can promote chromosomal instability (Hazuková et al. 2024). ROS produced during pesticide exposure may cause single- and double-strand DNA breaks, as well as modifications in purines, pyrimidines, and deoxyribose moieties (Aguilar-Bañuelos et al., 2025; Calderón-Segura et al., 2012; Dikilitas et al., 2015). The comet assay, widely employed for detecting such damage at the single-cell level, is especially useful for quantifying DNA strand breaks and oxidative lesions (Collins 2004; Olive and Banáth 2006).

Triazole fungicides such as TF and TN act by inhibiting ergosterol biosynthesis, an essential constituent of fungal cell membranes, through the inhibition of lanosterol-14α-demethylase (CYP51) (Chen et al., 2022; Rasgele 2025). In mammals, azoles have been shown to interact with cytochrome P450 (CYP) hepatic enzymes, as also predicted in this study. Exposure to chemicals that can interfere with hepatic metabolism should be investigated, as changes in the metabolic sphere can also increase the potential for drug interactions, in addition to the risk of intoxication with antifungals. Interactions with CYP enzymes may impair steroidogenesis (Petricca et al., 2023), alter the metabolism of several drugs, and reduce the bioactivation of prodrugs.

Cytochrome P450 2D6 (CYP2D6), an enzyme of great historical significance in pharmacogenetics, is responsible for metabolizing a wide range of drugs used in clinical practice, including analgesics (*e.g.*, codeine, oxycodone), antiarrhythmics (*e.g.*, flecainide), antidepressants, antipsychotics (*e.g.*, risperidone), and antiemetics (*e.g.*, ondansetron) (Zanger, Raimundo, and Eichelbaum 2004). Clopidogrel, a prodrug requiring hepatic metabolism by cytochrome CYP2C19 (and also CYP3A4, CYP1A4, and CYP2B6), may have its antiplatelet efficacy reduced if bioactivation is impaired by azole interference with these isoenzymes (Bouziana and Tziomalos 2015). Additionally, CYP1A2 inhibition, also predicted for these fungicides, could further affect metabolic pathways involving xenobiotics. CYP2A6, which metabolizes about 3% of drugs and several procarcinogens (*e.g.*, nitrosamines, aflatoxin B1), also plays a significant role in nicotine metabolism and in the biotransformation of retinoic acid and steroids (Di et al., 2009). Thus, competitive inhibition of CYP2A6 by TF and TN may lead to elevated plasma concentrations of co-administered substances,

potentially increasing their toxicity. It is crucial to emphasize that the primary goal of this metabolism prediction was not to provide a definitive metabolic map, but rather to leverage these insights to amplify the discussion on the potential range of toxic effects and interactions of TF and TN. However, further studies are necessary to determine whether TF and TN exhibit different toxicological behavior in the presence of a metabolic activation system. This is important because peripheral blood lymphocytes have low CYP450 activity, and the experiments were performed without the S9 fraction. This limitation indicates that the present results primarily reflect the effects of the parent compounds rather than metabolite-mediated responses.

In addition, analyzing the potential to influence gene expression helps to understand some toxic manifestations of agricultural compounds, such as TF and TN. Prediction of induced gene expression profiles with DIGEP-Pred indicated that TF and TN could up-regulate the genes SF1, SPON1, ADGRF5, and RORB. The SF1 gene is associated with a steroidogenic effect, responsible for producing steroid hormones. Therefore, the up-regulation of this gene, as suggested by the DIGEP 2.0 analysis, indicates potential hormonal alterations, including obesity (Rouabhi et al., 2021). SPON1 encodes an extracellular matrix protein with a role in nerve growth and repair. This gene has been shown to be associated with Alzheimer's disease risk (Reynolds et al., 2010). The RORB gene encodes the ROR-beta protein, a nuclear receptor that regulates gene expression and contributes to maintaining the circadian rhythm. Variations in this gene can lead to symptoms such as epilepsy and neurodevelopmental changes. Furthermore, this gene is also associated with Alzheimer's disease risk. ADGRF5 is essential for maintaining the proper function of numerous processes, such as airway function, immune response, metabolism, vascularization, and cancer progression (Jacenik, Karagiannidis, and Beswick 2023).

Prediction of repressed gene expression profiles with DIGEP-Pred indicated that TF and TN could down-regulate the gene HCN1. This gene encodes a hyperpolarization-activated cyclic nucleotide-gated channel protein essential for regulating neuronal excitability and contributing to pacemaker currents in the heart. Therefore, its putative down-regulation by antifungal agents could cause changes in heart rhythm, in addition to potential neurotoxicity (Li et al., 2025).

Conclusion

In conclusion, our integrated *in vitro* and *in silico* approach provides compelling evidence on the toxicological risks associated with triadimefon (TF) and triadimenol (TN). While these triazole fungicides did not compromise lymphocyte viability at environmentally relevant concentrations, they significantly induced DNA strand breaks, as demonstrated by the comet assay, both individually and in combination. This indicates a clear genotoxic hazard to human cells, independent of cytotoxic effects.

The computational analysis further suggested potential mechanisms underlying these risks. The prediction of distinct metabolic interactions with key cytochrome P450 isoforms (CYP1A2, CYP2A6, CYP2C9, and CYP2D6) indicates a significant potential for TF and TN to interfere with the metabolism of drugs and endogenous substances, which could lead to adverse drug interactions and altered xenobiotic processing. Moreover, the predicted modulation of gene expression—specifically the up-regulation of SF1, SPON1, ADGRF5, and RORB and the down-regulation of HCN1—points to potential long-term consequences, including endocrine disruption, neurotoxicity, and an increased risk for chronic diseases, such as Alzheimer's.

Together, these findings reinforce the growing body of evidence that triazole-based agrochemicals, while agriculturally effective, can compromise genomic integrity in non-target organisms, including humans. They may disrupt metabolic pathways, interfere with drug metabolism, and contribute to the onset of chronic diseases. Their environmental persistence and potential for bioaccumulation underscore the need for careful risk assessment, particularly among populations subject to chronic occupational or dietary exposure.

Acknowledgements

We would like to thank FAPEG and FUNDECT for their financial support through the HidroCerrado research network and the research network on Desenvolvimento de Bioinsumos e Bioeconomia com foco na pecuária.

Disclosure statement

No potential conflict of interest was reported by the author(s).

Funding

We thank the Fundação de Amparo à Pesquisa do Estado de Goiás (FAPEG) for funding through projects 21/2024. LMA acknowledges the grant of the Research Productivity Fellowship – PQ, process no. 305180/2025-8 and the Fundação de Apoio ao Desenvolvimento do Ensino, Ciência e Tecnologia do Estado de Mato Grosso do Sul (Fundect-MS) for funding through projects 20/2023, process no. 202410267000982.

Data availability statement

Data sharing will be made available upon request.

References

Aguilar-Bañuelos, J. A., Bernal-Hernández, Y. Y., Medina-Díaz, I. M., Ruiz-Arias, M. A., Herrera-Moreno, J. F., Barrón-Vivanco, B. S., González-Arias, C. A., Agraz-Cibrián, J. M., Zambrano-Zaragoza, J. F., Verdín-Betancourt, F. A., Ruiz, N. P., Flores-Alfaro, E., & Rojas-García, A. E. (2025). Environmental exposure to pesticides is associated with oxidative stress, oxidative DNA damage, and elevated Interleukin-8 in a child population. *Environmental Toxicology and Pharmacology*, *114*, 104656. https://doi.org/10.1016/j.etap.2025.104656

Ahmad, M. F., Ahmad, F. A., Alsayegh, A. A., Zeyaullah, M., AlShahrani, A. M., Muzammil, K., Saati, A. A., Wahab, S., Elbendary, E. Y., Kambal, N., Abdelrahman, M. H., & Hussain, S. (2024). Pesticides impacts on human health and the environment with their mechanisms of action and possible countermeasures. *Heliyon*, *10*(7), e29128. https://doi.org/10.1016/j.heliyon.2024.e29128

Antoniou, E., Rooseboom, M., Kocabas, N. A., North, C. M., & Zeegers, M. P. (2023). Micronuclei in human peripheral blood & bone marrow as genotoxicity markers: A systematic review and meta-analysis. *Mutation Research. Genetic Toxicology and Environmental Mutagenesis*, *891*, 503689. https://doi.org/10.1016/J.MRGENTOX.2023.503689

Barbieri, G. F., Young, B. G., Dayan, F. E., Streibig, J. C., Takano, H. K., Merotto, A., Jr., & Avila, L. A. (2022). Herbicide mixtures: Interactions and modeling. *Advances in Weed Science*, *40*(spe1), e020220051. https://doi.org/10.51694/AdvWeedSci/2022;40:seventy-five011

Boros, B. V., Roman, D.-L., & Isvoran, A. (2024). Evaluation of the aquatic toxicity of several triazole fungicides. *Metabolites*, *14*(4), 197. https://doi.org/10.3390/metabo14040197

Bouziana, S. D., & Tziomalos, K. (2015). Clinical relevance of clopidogrel-proton pump inhibitors interaction. *World Journal of Gastrointestinal Pharmacology and Therapeutics*, *6*(2), 17–21. https://doi.org/10.4292/WJGPT.V6.I2.17

Calderón-Segura, M. E., Gómez-Arroyo, S., Villalobos-Pietrini, R., Martínez-Valenzuela, C., Carbajal-López, Y., Calderón-Ezquerro, M. C., Cortés-Eslava, J., García-Martínez, R., Flores-Ramírez, D., Rodríguez-Romero, M. I., Méndez-Pérez, P., & Bañuelos-Ruíz, E. (2012). Evaluation of genotoxic and cytotoxic effects in human peripheral blood lymphocytes exposed in vitro to neonicotinoid insecticides news. *Journal of Toxicology*, *2012*, 612647–612611. https://doi.org/10.1155/2012/612647

Campani, T., Caliani, I., Di Noi, A., & Casini, S. (2025). Toxicity of four commercial fungicides, alone and in combination, on the earthworm Eisenia Fetida: A field experiment. *Toxics*, *13*(3), 209. https://doi.org/10.3390/toxics13030209

Chen, W., Wei, L., Hou, R., Zhao, Y., Zhao, Y., & Liu, F. (2022). Sterol demethylation inhibitor fungicide resistance in Colletotrichum Siamense from chili is caused by mutations in CYP51A and CYP51B. *Phytopathology Research*, *4*(1), 1–16. https://doi.org/10.1186/s42483-022-00146-w

Collins, A. R. (2004). The comet assay for DNA damage and repair: principles, applications, and limitations. *Molecular Biotechnology*, *26*(3), 249–261. https://doi.org/10.1385/MB:26:3:249

Di, Y. M., Chow, V. D.-W., Yang, L.-P., & Zhou, S.-F. (2009). Structure, function, regulation and polymorphism of human cytochrome P450 2A6. *Current Drug Metabolism*, *10*(7), 754–780. https://doi.org/10.2174/138920009789895507

Dikilitas, M., Kocyigit, A., Bilinc, H., Taskin, A., & Karakas, S. (2015). Evaluation of genotoxicity of environmentally friendly pesticides on higher cells using the single cell gel electrophoresis (SCGE) assay. *Fresenius Environmental Bulletin*, *24*, 39–47.

Djoumbou-Feunang, Y., Fiamoncini, J., Gil-de-la-Fuente, A., Greiner, R., Manach, C., & Wishart, D. S. (2019). BioTransformer: A comprehensive computational tool for small molecule metabolism prediction and metabolite identification. *Journal of Cheminformatics*, *11*(1), 2. https://doi.org/10.1186/S13321-018-0324-5

Dong, Z., Cui, K., Liang, J., Guan, S., Fang, L., Ding, R., Wang, J., Li, T., Zhao, S., & Wang, Z. (2023). The widespread presence of triazole fungicides in greenhouse soils in Shandong Province, China: A systematic study on human health and ecological risk assessments. *Environmental Pollution (Barking, Essex: 1987)*, *328*, 121637. https://doi.org/10.1016/j.envpol.2023.121637

Fernandes, A. S., Bisneto, A. V. d M., Silva, L. S., Bailão, E. F. L. C., Cardoso, C. G., Carneiro, C. C., Santos, S. C., & Chen-Chen, L. (2024). Tellimagrandin-I and Camptothin a Exhibit chemopreventive effects in *Salmonella enterica* Serovar Typhimurium strains and human lymphocytes. *Journal of Toxicology and Environmental Health. Part A*, *87*(5), 185–198. https://doi.org/10.1080/15287394.2023.2290641

Ferri, G. M., Cavone, D., Dambrosio, M., Intranuovo, G., Schiavulli, N., Birtolo, F., Vilardi, V., Delfino, M. C., Macinagrossa, L., Corrado, V., & Vimercati, L. (2019). Lymphocytes DNA damages and exposure to chlorpyrifos, deltamethrin, penconazole, copper oxicloride. *Biomarkers: biochemical Indicators of Exposure, Response, and Susceptibility to Chemicals*, *24*(2), 186–198. https://doi.org/10.1080/1354750X.2018.1539766

Fotakis, G., & Timbrell, J. A. (2006). In vitro cytotoxicity assays: comparison of LDH, neutral red, MTT and protein assay in hepatoma cell lines following exposure to cadmium chloride. *Toxicology Letters*, *160*(2), 171–177. https://doi.org/10.1016/j.toxlet.2005.07.001

Garrison, A. W., Avants, J. K., & Jones, W. J. (2011). Microbial transformation of triadimefon to triadimenol in soils: Selective production rates of triadimenol stereoisomers affect exposure and risk. *Environmental Science & Technology*, *45*(6), 2186–2193. https://doi.org/10.1021/ES103430S

Ghasemi, M., Turnbull, T., Sebastian, S., & Kempson, I. (2021). The MTT assay: Utility, limitations, pitfalls, and interpretation in bulk and single-cell analysis. *International Journal of Molecular Sciences*, *22*(23), 12827. https://doi.org/10.3390/ijms222312827

Han, L., Jiang, Z., Zhang, X., & Wu, X. (2024). Dissipation and residue of Triadimefon in *Rosa roxburghii*. *Food Additives & Contaminants. Part A, Chemistry, Analysis, Control, Exposure & Risk Assessment*, *41*(8), 914–922. https://doi.org/10.1080/19440049.2024.2357351

Hasselgren, C., & Myatt, G. J. (2018). Computational toxicology and drug discovery. *Methods in Molecular Biology (Clifton, N.J.)*, *1800*, 233–244. https://doi.org/10.1007/978-1-4939-7899-1_11

Hazuková, R., Zadák, Z., Pleskot, M., Zdráhal, P., Pumprla, M., & Táborský, M. (2024). Oxidative DNA damage and arterial hypertension in light of current ESC guidelines. *International Journal of Molecular Sciences*, *25*(23), 12557. https://doi.org/10.3390/ijms252312557

Hou, L., Jin, X., Liu, N., Luo, Y., Yan, Z., Chen, M., Liu, Y., Xie, H., Giesy, J. P., Wu, F., & Xu, J. (2022). Triadimefon in aquatic environments: Occurrence, fate, toxicity, and ecological risk. *Environmental Sciences Europe*, *34*(1), 12. https://doi.org/10.1186/s12302-022-00590-7

Jacenik, D., Karagiannidis, I., & Beswick, E. J. (2023). Th2 cells inhibit growth of colon and pancreas cancers by promoting anti-tumorigenic responses from macrophages and eosinophils. *British Journal of Cancer*, *128*(2), 387–397. https://doi.org/10.1038/s41416-022-02056-2

Jiang, J., Hu, G., Zhang, C., Zhao, X., Wang, Q., & Chen, L. (2017). Toxicological analysis of triadimefon on endocrine disruption and oxidative stress during rare minnow (*Gobiocypris rarus*) larvae development. *Environmental Science and Pollution Research International*, *24*(34), 26681–26691. https://doi.org/10.1007/s11356-017-0317-3

Koleničová, S., Holeková, B., Galdíková, M., Schwarzbacherová, V., & Drážovská, M. (2020). Genotoxicity testing of bovine lymphocytes exposed to epoxiconazole using alkaline and neutral comet assay. *Caryologia*, *73*, 99–109. https://doi.org/10.13128/caryologia-984.

Ladeira, C., Møller, P., Giovannelli, L., Gajski, G., Haveric, A., Bankoglu, E. E., Azqueta, A., Gerić, M., Stopper, H., Cabêda, J., Tonin, F. S., & Collins, A. (2024). The Comet Assay as a tool in human biomonitoring studies of environmental and occupational exposure to chemicals—A systematic scoping review. *Toxics*, *12*(4), 270. https://doi.org/10.3390/toxics12040270

Lagunin, A., Ivanov, S., Rudik, A., Filimonov, D., & Poroikov, V. (2013). DIGEP-Pred: Web service for in silico prediction of drug-induced gene expression profiles based on structural formula. *Bioinformatics (Oxford, England)*, *29*(16), 2062–2063. https://doi.org/10.1093/BIOINFORMATICS/BTT322

Lebailly, P., Mirey, G., Herin, F., Lecluse, Y., Salles, B., & Boutet-Robinet, E. (2015). DNA damage in B and T lymphocytes of farmers during one pesticide spraying season. *International Archives of Occupational and Environmental Health*, *88*(7), 963–972. https://doi.org/10.1007/S00420-015-1024-3

Li, N., Webb, A., Kennelly, J., Sharma, R., Whitson, B. A., Mohler, P. J., Hummel, J. D., Zhao, J., & Fedorov, V. V. (2025). Heart rate mystery unveiled: Sex differences in human Sinoatrial node genes and female Tachycardia. *Circulation. Arrhythmia and Electrophysiology*, *18*(5), e013534. https://doi.org/10.1161/CIRCEP.124.013534

Loiodice, S., Nogueira da Costa, A., & Atienzar, F. (2019). Current trends in in silico, in vitro toxicology, and safety biomarkers in early drug development. *Drug and Chemical Toxicology*, *42*(2), 113–121. https://doi.org/10.1080/01480545.2017.1400044

Olive, P. L., & Banáth, J. P. (2006). The comet assay: A method to measure DNA damage in individual cells. *Nature Protocols*, *1*(1), 23–29. https://doi.org/10.1038/nprot.2006.5

Pedroso, T. M. A., Benvindo-Souza, M., Nascimento, F. d A., Woch, J., Reis, F. G. d., & Silva, D. d M. (2022). Cancer and occupational exposure to pesticides: A bibliometric study of the past 10 years. *Environmental Science and Pollution Research International*, *29*(12), 17464–17475. https://doi.org/10.1007/s11356-021-17031-2

Petricca, S., Carnicelli, V., Luzi, C., Cinque, B., Celenza, G., & Iorio, R. (2023). Oxidative stress, cytotoxic and inflammatory effects of azoles combinatorial mixtures in sertoli TM4 cells. *Antioxidants (Basel, Switzerland)*, *12*(6), 1142. https://doi.org/10.3390/antiox12061142

Ramos, J. S. A., Pedroso, T. M. A., Godoy, F. R., Batista, R. E., Almeida, F. B. d., Francelin, C., Ribeiro, F. L., Parise, M. R., Silva, D., & de, M. (2021). Multi-biomarker responses to pesticides in an agricultural population from Central Brazil. *The Science of the Total Environment*, *754*, 141893. https://doi.org/10.1016/j.scitotenv.2020.141893

Rasgele, P. G. (2025). Comparative assessment of short- and long-term effects of triadimenol fungicide on danio rerio erythrocytes using the micronucleus and erythrocyte nuclear abnormality assays. *Toxics*, *13*(3), 199. https://doi.org/10.3390/toxics13030199

Ray, A., Dutta, D., Sarkar, A., & Bahadur, M. (2025). Evaluation of toxic effects of a triazole fungicide, difenoconazole in a freshwater fish model. *Ecotoxicology (London, England)*, *34*(8), 1368–1383. https://doi.org/10.1007/s10646-025-02926-4

Reffstrup, T. K., Larsen, J. C., & Meyer, O. (2010). Risk assessment of mixtures of pesticides. Current approaches and future strategies. *Regulatory Toxicology and Pharmacology: RTP*, *56*(2), 174–192. https://doi.org/10.1016/j.yrtph.2009.09.013

Reynolds, C. A., Hong, M.-G., Eriksson, U. K., Blennow, K., Johansson, B., Malmberg, B., Berg, S., Gatz, M., Pedersen, N. L., Bennet, A. M., & Prince, J. A. (2010). Sequence variation in SORL1 and dementia risk in Swedes. *Neurogenetics*, *11*(1), 139–142. https://doi.org/10.1007/S10048-009-0210-4

Rjiba-Touati, K., Ayed-Boussema, I., Hamdi, H., & Abid, S. (2023). Genotoxic damage and apoptosis in rat glioma (F98) cell line following exposure to bromuconazole. *Neurotoxicology*, *94*, 108–116. https://doi.org/10.1016/j.neuro.2022.11.006

Rouabhi, M., Guo, D.-F., Morgan, D. A., Zhu, Z., López, M., Zingman, L., Grobe, J. L., & Rahmouni, K. (2021). BBSome ablation in SF1 neurons causes obesity without comorbidities. *Molecular Metabolism*, *48*, 101211. https://doi.org/10.1016/j.molmet.2021.101211

Sabotič, J., Bayram, E., Ezra, D., Gaudêncio, S. P., Haznedaroğlu, B. Z., Janež, N., Ktari, L., Luganini, A., Mandalakis, M., Safarik, I., Simes, D., Strode, E., Toruńska-Sitarz, A., Varamogianni-Mamatsi, D., Varese, G. C., & Vasquez, M. I. (2024). A guide to the use of bioassays in exploration of natural resources. *Biotechnology Advances*, *71*, 108307. https://doi.org/10.1016/j.biotechadv.2024.108307

Sasikala, S., Jenifer, M. M., Velavan, K., Sakthivel, M., Sivasamy, R., & Anton, E. R. F. (2023). Predicting the relationship between pesticide genotoxicity and breast cancer risk in South Indian women in in vitro and in vivo experiments. *Scientific Reports*, *13*(1), 9712. https://doi.org/10.1038/s41598-023-35552-3

Smith, J. A., Park, S., Krause, J. S., & Banik, N. L. (2013). Oxidative stress, DNA damage, and the telomeric complex as therapeutic targets in acute neurodegeneration. *Neurochemistry International*, *62*(5), 764–775. https://doi.org/10.1016/j.neuint.2013.02.013

Stepanenko, A. A., & Dmitrenko, V. V. (2015). Pitfalls of the MTT assay: Direct and off-target effects of inhibitors can result in over/underestimation of cell viability. *Gene*, *574*(2), 193–203. https://doi.org/10.1016/j.gene.2015.08.009

Strober, W. (2015). Trypan blue exclusion test of cell viability. *Current Protocols in Immunology*, *111*(1), A3.B.1–A3.B.3. https://doi.org/10.1002/0471142735.ima03bs111

Tang, T., Qian, K., Shi, T., Wang, F., Li, J., & Cao, Y. (2010). Determination of triazole fungicides in environmental water samples by high performance liquid chromatography with cloud point extraction using polyethylene Glycol 600 monooleate. *Analytica Chimica Acta*, *680*(1–2), 26–31. https://doi.org/10.1016/j.aca.2010.09.034

Tice, R. R., Agurell, E., Anderson, D., Burlinson, B., Hartmann, A., Kobayashi, H., Miyamae, Y., Rojas, E., Ryu, J. C., & Sasaki, Y. (2000). Single cell gel/comet assay: Guidelines for in vitro and in vivo genetic toxicology testing. *Environmental and Molecular Mutagenesis*, *35*(3), 206–221. https://doi.org/10.1002/(SICI)1098-2280(2000)35:3≤206::AID-EM8≥3.0.CO;2-J

Tofan, L., Niță, V., Nenciu, M., Coatu, V., Lazăr, L., Damir, N., Vasile, D., Popoviciu, D. R., Brotea, A.-G., Curtean-Bănăduc, A. M., Avramescu, S., & Aonofriesei, F. (2023). Multiple assays on non-target organisms to determine the risk of acute environmental toxicity in tebuconazole-based fungicides widely used in the Black Sea Coastal Area. *Toxics*, *11*(7), 597. https://doi.org/10.3390/toxics11070597

Wang, R., Liu, N., Huang, N., Shu, F., Lou, Y., Zhang, S., Zhu, H., & Chen, C. (2023). Combined toxicity assessment of a naturally occurring toxin and a triazole fungicide on different biological processes through toxicogenomic data mining with mixtures. *Pesticide Biochemistry and Physiology*, *193*, 105440. https://doi.org/10.1016/j.pestbp.2023.105440

Wishart, D. S., Guo, A., Oler, E., Wang, F., Anjum, A., Peters, H., Dizon, R., Sayeeda, Z., Tian, S., Lee, B. L., Berjanskii, M., Mah, R., Yamamoto, M., Jovel, J., Torres-Calzada, C., Hiebert-Giesbrecht, M., Lui, V. W., Varshavi, D., Varshavi, D., … Gautam, V. (2022). HMDB 5.0: The Human Metabolome Database for 2022. *Nucleic Acids Research*, *50*(D1), D622–D631. https://doi.org/10.1093/NAR/GKAB1062

Xu, J., Xiong, H., Zhang, X., Muhayimana, S., Liu, X., Xue, Y., & Huang, Q. (2020). Comparative cytotoxic effects of five commonly used triazole alcohol fungicides on human cells of different tissue types. *Journal of Environmental Science and Health. Part. B, Pesticides, Food Contaminants, and Agricultural Wastes*, *55*(5), 438–446. https://doi.org/10.1080/03601234.2019.1709377

Zanger, U. M., Raimundo, S., & Eichelbaum, M. (2004). Cytochrome P450 2D6: Overview and update on pharmacology, genetics, biochemistry. *Naunyn-Schmiedeberg's Archives of Pharmacology*, *369*(1), 23–37. https://doi.org/10.1007/S00210-003-0832-2

Zarn, J. A., Brüschweiler, B. J., & Schlatter, J. R. (2003). Azole fungicides affect mammalian steroidogenesis by inhibiting sterol 14α-demethylase and aromatase. *Environmental Health Perspectives*, *111*(3), 255–261. https://doi.org/10.1289/ehp.5785

Zhang, W., Lu, Y., Huang, L., Cheng, C., Di, S., Chen, L., Zhou, Z., & Diao, J. (2018). Comparison of triadimefon and its metabolite on acute toxicity and chronic effects during the early development of Rana Nigromaculata Tadpoles. *Ecotoxicology and Environmental Safety*, *156*, 247–254. https://doi.org/10.1016/j.ecoenv.2018.03.009

Zubrod, J. P., Bundschuh, M., Arts, G., Brühl, C. A., Imfeld, G., Knäbel, A., Payraudeau, S., Rasmussen, J. J., Rohr, J., Scharmüller, A., Smalling, K., Stehle, S., Schulz, R., & Schäfer, R. B. (2019). Fungicides: An overlooked pesticide class? *Environmental Science & Technology*, *53*(7), 3347–3365. https://doi.org/10.1021/acs.est.8b04392

ANEXO C – Artigo 03: Efeito genotóxico, mutagênico e na biomassa de *eisenia fetida* expostas ao fungicida triadimefon e triadimenol

Environmental Toxicology and Pharmacology 124 (2026) 105018

Contents lists available at ScienceDirect

Environmental Toxicology and Pharmacology

journal homepage: www.elsevier.com/locate/etap

Genotoxic, mutagenic, and biomass effects on *Eisenia fetida* exposed to the fungicides triadimefon and triadimenol

Marcelino Benvindo-Souza [a,b,1], Áureo Barbosa de Souza [c,2], Amanda Silva Fernandes [e,3], Elisa Flávia Luiz Cardoso Bailão [a,4], Luciane Madureira de Almeida [a,5], Leonardo Luiz Borges [d,e,*,6], Antônio Sérgio Nakao de Aguiar [c,7]

[a] Biotechnology Laboratory, Central Campus, State University of Goiás, Anápolis, Goiás, Brazil
[b] Graduate Program in Conservation of Cerrado Natural Resources, Instituto Federal Goiano, Urutaí, Goiás, Brazil
[c] Laboratory of New Materials, Evangelical University of Goiás, Anápolis, GO, Brazil
[d] Laboratory for Research, Development & Innovation of Biodiversity Products, State University of Goiás, Anápolis, Goiás, Brazil
[e] School of Medical and Life Sciences, Pontifical Catholic University of Goiás, Goiânia, GO, Brazil

ARTICLE INFO

Keywords:
Micronuclei
Comet assay
Triazole
Pesticides
Earthworms

ABSTRACT

Triadimefon and triadimenol are broad-spectrum fungicides widely used in agriculture. This study assessed their genotoxic and biomass effects on *Eisenia fetida* earthworms exposed for 7, 14 and 21 days to concentrations of triadimefon (0.006, 0.12, 0.24 mg/kg), triadimenol (1.5, 3, 6 mg/kg), and their mixture (0.012 + 3.0 mg/kg). At 14 and 21 days, weight loss exceeded 20%, reaching over 40% at the highest concentrations of both triazoles. Genotoxic effects were detected at 6 mg/kg triadimefon and 0.024 mg/kg triadimenol, individually and in mixture, particularly after 14 and 21 days. A slight mutagenic increase was observed only at the highest triadimefon concentration. Exposure to the fungicides promoted significant biomass reduction from day 14 onward. These results reinforce the need for monitoring triazoles' environmental impact, as even at relevant concentrations, they can induce genotoxic damage in soil organisms.

1. Introduction

Pesticides are widely used in commercial agriculture and have contributed significantly to increasing agricultural productivity by controlling pests and diseases, thereby ensuring food security for a constantly growing global population (Lammertyn et al., 2024). However, their excessive or improper use can lead to the accumulation of residues in the environment and compromise soil quality, biodiversity, and human health. Among these compounds, triazole pesticides constitute a class of systemic fungicides containing the 1,2,4-triazole molecule (Liu et al., 2014). Due to their broad spectrum and versatility, triazoles are widely used as fungicides or medicinal agents and represent the second largest group of fungicides worldwide (Tang et al., 2024).

Introduced to the market in the mid-1970s by researchers from companies such as Ciba-Geigy®, a Swiss agrochemical and pharmaceutical firm, triazole compounds are absorbed by plants and distributed throughout their structure, providing long-lasting protection (Nasonov and Yakuba, 2024; Sun et al., 2023). They exhibit systemic effects and are a popular class of agricultural pesticides used to control various fungal diseases in crops of global economic importance (Kong et al., 2020).

These compounds primarily act as inhibitors of ergosterol biosynthesis, a steroid precursor to vitamin D2 and a key component of fungal

* Corresponding author at: Laboratory for Research, Development & Innovation of Biodiversity Products, State University of Goiás, Anápolis, Goiás, Brazil.
E-mail address: leonardo.borges@ueg.br (L.L. Borges).
[1] https://orcid.org/0000-0001-9008-6087
[2] https://orcid.org/0009-0006-5146-9417
[3] https://orcid.org/0000-0002-5436-5799
[4] https://orcid.org/0000-0001-6737-7548
[5] https://orcid.org/0000-0003-1764-1480
[6] https://orcid.org/0000-0003-2183-3944)
[7] https://orcid.org/0000-0001-9410-9194

https://doi.org/10.1016/j.etap.2026.105018
Received 18 January 2026; Received in revised form 6 March 2026; Accepted 7 April 2026
Available online 9 April 2026

cell membranes. The mechanism of action of these compounds centers on the inhibition of the enzyme lanosterol 14α-demethylase (CYP51), a cytochrome P450 monooxygenase crucial in the ergosterol synthesis pathway from lanosterol. Given their extensive application, it is essential to understand in detail their chemical properties, which directly influence their environmental behavior, transport, persistence, biological activity, and ecotoxicological potential (Malik et al., 2024).

Despite their effectiveness, several studies have reported that triadimefon and triadimenol can exert adverse effects on wildlife and humans. In anuran amphibians, triadimefon and triadimenol affected swimming, endocrine disruption, and hepatic alterations (Zhang et al., 2020), as well as disruption of hormonal pathways involved in metamorphosis (Zhang et al., 2018). In Chinese lizards (*Eremias argus*), the biotransformation of triadimefon metabolites in adipose tissue showed low degradation capacity (Li et al., 2017). In *Daphnia magna*, it was observed that at triadimefon concentrations above 0.1 mg/L, both the number of individuals and the intrinsic population growth rate showed a decreasing trend with increasing exposure concentration (Hou et al., 2023). Hou et al. (2022), reviewing triadimefon and triadimenol, observed that these triazoles can cause neurotoxicity, hepatotoxicity, and cardiovascular toxicity in mammals and fish, suggesting that the same effects could occur in humans. Furthermore, both compounds are classified as possible human carcinogens (Li et al., 2017). According to their specificities, triadimefon is a lipophilic conazole fungicide that is systemic and broad-spectrum, with eradicant and protective action against various plant pathogens, especially powdery mildew, loose smut, and rusts in cereals and other crops (Crowell et al., 2011; Li et al., 2011a). Triadimefon does not persist for long periods in soil, with half-lives ranging from 5 to 39 days depending on soil type (Hou et al., 2022). Triadimenol, on the other hand, is a metabolite of triadimefon and constitutes the most widely used triazole fungicide (Hou et al., 2022; Tang et al., 2024), with a half-life exceeding 70 days (Aliste et al., 2021).

Among the wide variety of soil pollutants, agrochemicals exert the major impact on soil biota, underscoring the need for effective soil-quality monitoring through the utilization of sensitive bioindicators (Mishra et al., 2022), making the monitoring of soil quality through bioindicators essential. Earthworms are widely recognized as global bioindicators and are fundamental models for assessing soil pollution and environmental quality (Zhou et al., 2016). Species such as *Eisenia fetida*, used in this study, have been extensively employed as standard test organisms for pesticide risk assessment (Rico et al., 2016). Studies have shown that earthworms exposed to triazoles exhibit significant histopathological alterations, which can seriously affect motor function (Gao et al., 2013). Furthermore, chronic exposure to triadimenol at environmentally relevant concentrations (3, 30, and 300 μg/L) adversely affected various toxicity parameters, including growth, brood size, and locomotor behavior of worms (How et al., 2018). Despite the observed harmful effects, studies investigating the genotoxic and mutagenic effects of fungicides using genetic biomarkers, such as the comet assay and the micronucleus test, remain scarce.

One of its primary metabolites, both in the environment and in living organisms, is triadimenol (Liu et al., 2014; Zhang et al., 2020; Zhuo et al., 2025). Triadimefon possesses one chiral center, while its transformation via reduction leads to the formation of triadimenol, which features two chiral centers, resulting in four distinct stereoisomers (1 R, 2S; 1S,2 R; 1 R,2 R; and 1S,2S). These are grouped into two enantiomeric pairs known as triadimenol-A and triadimenol-B (Garrison et al., 2011; Li et al., 2011b). The conversion of triadimefon to triadimenol can significantly alter the properties and toxicity of the original compound. Studies have demonstrated, for example, differences in acute toxicity between triadimefon and triadimenol in aquatic organisms (Hou et al., 2022; Zhang et al., 2018).

Thus, this study aimed to investigate the toxicological effects of triadimefon and triadimenol on the earthworms of the species *Eisenia fetida*. Therefore, the biomass parameters of the earthworms, genotoxicity, and mutagenicity in organisms exposed for 7, 14, and 21 days. The central hypothesis of the study is that exposure to low concentrations of triadimefon, triadimenol, and their mixture may increase the frequency of DNA damage and also induce changes in earthworm biomass. To our knowledge, this is the first study to jointly assess genotoxicity in *Eisenia fetida* earthworms for triadimenol and triadimefon and to propose a model for the physical and chemical properties of these compounds.

2. Materials and methods

2.1. Exposure of earthworms to triadimefon and triadimenol

In this study, the selected concentrations were based on previous work with zebrafish (Qiao et al., 2020) and earthworms (Gao et al., 2013; Martyniuk and Goc Rasgele, 2025). The applied doses were adjusted to 0.006, 0.012, and 0.024 mg/kg of soil for triadimefon and 1.5, 3, and 6 mg/kg for triadimenol. The mixture concentration (triadimefon 0.012 mg/kg + triadimenol 3.0 mg/kg) was also tested. The triazole stock solutions were prepared using dimethyl sulfoxide (DMSO, analytical grade) as the solvent. The soil used was Acric Red Latosol, collected from an intact native forest area in the Brazilian Cerrado biome, with no documented history of pesticide use. Soil preparation followed the guidelines of the Organisation for Economic Co-operation and Development (OECD, 1984), as well as Jovana et al. (2014) and Xue et al. (2023).

The earthworms used in the assays were adults of the species *Eisenia fetida* (with a visible clitellum; average weight of 1.02 g), purchased from a commercial breeder located in Anápolis, Goiás, Brazil. Before the start of the experiment, the organisms were acclimated for 24 h in an incubator at 26 °C, under a 16:8 h light-dark photoperiod. After acclimation, they were rinsed with deionized water, transferred to moistened filter paper for purging of intestinal contents, rinsed again with distilled water, carefully dried on clean filter paper, and weighed in groups of ten individuals on an analytical balance before beginning the exposure. The animals remained exposed for 7, 14, and 21 days, maintaining the same conditions as during acclimation. For each concentration, including the control, 10 individuals were used in triplicate. The animals were fed 5 g of cattle manure once a week (Jovana et al., 2014), provided by the commercial annelid breeder.

2.2. Coelomocyte collection

After exposure, each worm was rinsed in running water to remove soil residues and detritus and weighed as described by Silva et al. (2023). This biomass was measured for each group of 10 earthworms. Subsequently, the individuals were subjected to a previously prepared extrusion buffer (Cooper et al., 1991) at a ratio of 200 μL per organism for three minutes. The extruded coelomic fluid containing cells was centrifuged at 7200 rpm for 3 min, and the supernatant was discarded. The resulting cellular sample was washed in PBS, and the obtained cell suspension was used to assess DNA damage via the comet assay and the micronucleus test.

2.3. Comet assay

The comet assay was used to evaluate the genotoxicity of exposure to the triazoles, following a protocol modified from Singh (2005), Shao et al. (2019), and Benvindo-Souza et al. (2025). Microscope slides were pre-coated with 1.5% standard agarose. Subsequently, 20 μL of the coelomocyte suspension was mixed with 120 μL of 0.5% low-melting-point agarose and spread over the pre-coated slides. A coverslip was placed over the sample and removed after the agarose solidified. The slides were then immersed in a freshly prepared lysis solution for one hour. After this period, they were transferred to a horizontal electrophoresis chamber and incubated in alkaline buffer for 30 min. Electrophoresis was performed in the dark for 20 min, at 25 V

and 300 mA. Upon completion, the slides were neutralized three times in 0.4 M Tris buffer (pH 7.5) for 5 min each, rinsed in distilled water, and fixed in absolute ethanol. After drying, the DNA was stained with 100 µL of the fluorescent dye Diamond™ (10%). Comet observation was performed using a fluorescence microscope (Axio Imager® A2, Carl Zeiss AG, Germany), equipped with a 510–560 nm excitation filter, a 590 nm emission filter, and a 20 × objective. A single examiner conducted all analyses. DNA damage was quantified using TriTek CometScore 2.2 software, based on 100 nucleoids per sample. The following parameters were evaluated: tail DNA percentage (%DNA), tail length (TL), and Olive tail moment (OTM). It is worth highlighting that we did not perform the discrimination of coelomocytes/amebocytes in the coelomic fluid before the DNA analyses.

2.4. Micronucleus test

The micronucleus frequency was analyzed as an indicator of genotoxicity in earthworms exposed to triazoles. After coelomocyte extraction, approximately 10 µL of coelomic fluid was deposited onto microscope slides (two slides per individual) for the micronucleus test. Each slide was prepared by smearing the coelomic fluid. After air-drying at room temperature, the slides were fixed in absolute methanol for 10 min and stained using a rapid Panoptic staining kit. A total of 2000 cells (amebocytes) were analyzed under an optical microscope with an immersion objective (100 ×) by a single researcher. Micronucleus frequency was expressed as: Micronucleus Frequency (%) = Number of micronucleated cells / Number of cells counted (2000) x 100.

2.5. Statistical analysis

For biomass, the weight values refer to each exposed group (10 earthworms). They are presented in absolute and relative frequency. Subsequently, we conducted a Kruskal-Wallis analysis, followed by Dunn's test, considering only the exposure days. In general, whenever possible, the data were presented as mean ± standard deviation. Normality and homogeneity of variances were assessed using the Shapiro-Wilk and Levene tests, respectively. Since genotoxicity and mutagenicity biomarkers did not follow a normal distribution, the Kruskal-Wallis test was used, followed by Dunn's post hoc test. The same tests were applied to biomass data. A Principal Component Analysis (PCA) was used to integrate biomarkers of genotoxicity and mutagenicity in response to triazoles. All statistical analyses were performed using Statistica 7, Past 4, and Jamovi 2.5.6 software, adopting a significance level of $p < 0.05$ for all comparisons.

3. Results and discussion

3.1. Earthworm biomass

Four deaths were observed for triadimefon and one death for triadimenol over 21 days of exposure. In the control group, no mortality occurred at any exposure time. Overall, greater weight loss was observed in the fungicide-treated groups (Fig. 1A and B). At 14 and 21 days, weight loss exceeded 20%, reaching more than 40% at the highest concentrations of both triazoles (Fig. 1B). Regardless of the concentrations of the triazoles tested, the initial average biomass of the

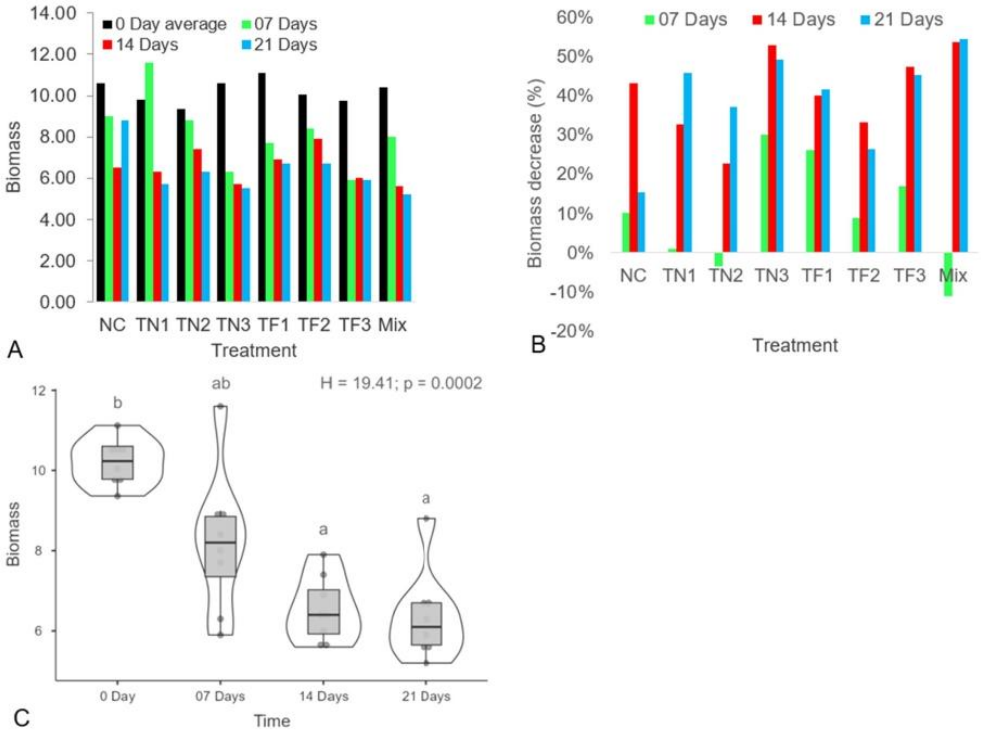

Fig. 1. Biomass values (g) of *Eisenia fetida* during the exposure period to triazoles (triadimefon and triadimenol). A) biomass as a function of concentrations; B) biomass loss as a percentage; C) biomass independent of concentrations (Triadimenol and Triadimefon). A and B) data are presented as relative frequency. C) mean data of the absolute frequency from Fig. 1A, disregarding the concentrations. Different letters compared to the control indicate a statistically significant difference; same letters or absence of letters indicate no significant difference. Kruskal-Wallis followed by Dunn's post hoc test. NC: Negative control; Triadimenol: TN1 (1.5 mg/kg); TN2 (3 mg/kg) and TN3 (6 mg/kg); Triadimefon: TF1 (0.06 mg/kg); TF2 (0.012 mg/kg) and TF3 (0.024 mg/kg); Mix: TN2 (3 mg/kg) + TF2 (0.012 mg/kg).

earthworms was 10.21 ± 0.58 g, progressively decreasing to 8.21 ± 1.76 g at 7 days, 6.54 ± 0.82 g at 14 days, and 6.35 ± 1.13 g at 21 days of exposure. These results indicate a significant reduction in biomass starting from the 14th day compared to the initial value, with the weight loss trend persisting until the end of the experiment (Fig. 1C).

The observed weight loss suggests a possible sublethal effect of triadimenol and triadimefon, likely associated with increased energy expenditure on detoxification processes and metabolic stress (Rico et al., 2016; Zhuo et al., 2025). Furthermore, the reduction in biomass may reflect alterations in feeding behavior and/or nutrient assimilation efficiency, factors frequently reported as adverse physiological responses in organisms exposed to chemical contaminants (Pelosi et al., 2014; Bart et al.,2017). Thus, even in the absence of high mortality, the results indicate that triadimefon and triadimenol can compromise the physiological condition and ecological performance of earthworms over time. Decreased body weight has been recognized as a sensitive sublethal endpoint in earthworm ecotoxicology, often reflecting early physiological stress before lethal effects become evident (Pelosi et al., 2014). Consistent with these findings, reductions in body weight and reproductive performance have been observed in *Eisenia fetida* exposed to pesticides at concentrations that did not result in significant mortality, indicating that physiological impairment may precede lethal effects (Yasmin and D'Souza, 2007). Similar reductions in biomass have been reported for triazole fungicides such as tebuconazole, where weight loss and biochemical alterations were detected at sublethal concentrations (Rico et al., 2016). Likewise, exposure to tebuconazole and epoxiconazole has been shown to reduce earthworm biomass, highlighting the sensitivity of growth-related endpoints to fungicidal stress (Bart et al., 2017).

3.2. Cytogenetic biomarkers

Triadimefon and triadimenol were tested for their comet assay and *micronucleus test* effects in earthworms of the species *Eisenia fetida* (Fig. 2).

3.2.1. Genotoxicity

The effects of the fungicides were assessed at each exposure time. Overall, the highest concentrations of both triadimefon and triadimenol showed significant differences in at least one parameter of the comet assay when compared to the negative control (Fig. 3). It is essential to highlight that, at 21 days, at least one of the highest concentrations exhibited a significant effect. Additionally, the parameters %Tail DNA and Olive Tail Moment indicated greater genotoxicity at the 14- and 21-day time points. Finally, in the micronucleus test, a slight difference was observed only at the highest concentration of triadimefon compared to the control (Fig. 4).

Genetic biomarkers such as the comet assay and micronucleus test are globally recognized for assessing the genotoxicity and mutagenicity of pesticides in animals. In the present study, these biomarkers were applied to quantify DNA damage in *Eisenia fetida* exposed to triadimenol and triadimefon. In the comet assay, both triadimenol and triadimefon induced genotoxic damage in earthworms, but to different extents. The higher concentrations of triadimefon proved more toxic in inducing DNA breaks than triadimenol. Regarding the mixture (Mix), the effect was similar to the higher doses, suggesting that combined exposure neither attenuated nor strongly potentiated the effect (additive or synergistic), but maintained high levels of genotoxic damage. These effects were more evident starting from the 7th day of exposure and persisted until 21 days, indicating that the repair mechanisms were insufficient to reverse the induced damage, particularly considering the observed mutagenicity for triadimefon. It is also worth noting that triadimefon metabolism is faster, but elimination is slower (Li et al., 2017); this likely may be related to the greater genotoxic damage observed at later time points, although damage was also present at high concentrations at the 7-day exposure.

For the micronucleus test, genotoxicity was observed only for triadimefon at the highest concentration after 21 days of exposure. A previous study evaluating doses of 1200 and 1071 mg/kg of triadimefon in male and female mice did not show a significant increase (Kevekordes et al., 1996). For triadimenol, an experiment with zebrafish (*Danio rerio*) exposed to concentrations of 1.5, 3, and 6 mg/L observed an increase in micronucleus frequency in acute (up to 72 h) and chronic (up to 20 days) exposures (Martyniuk and Goc Rasgele, 2025), as well as mortality at concentrations of 3 and 6 mg/L over 30 days. In the present study, triadimenol did not significantly increase micronucleus frequency, perhaps due to the inherent biology of annelids compared to fish.

The genotoxic effects of other triazole fungicides have been investigated in different animals, including humans. For example, Prosaro® (tebuconazole/prothioconazole), tested at concentrations of 1.5, 3, 7.5, 15, and 30 μg mL^{-1} for 24 and 48 h, or two hours using micronucleus and comet assays in bovine lymphocyte cultures, did not show an increase in micronucleus frequency, and only the highest concentration induced genotoxic damage (Schwarzbacherová et al., 2015). Three sublethal concentrations of difenoconazole, 0.037, 0.188, and 0.377 mg/L, were tested in *Pethia conchonius* fish (Ray et al., 2025). DNA damage in the exposed groups was significantly more serious than in the control group, increasing with concentration and exposure duration,

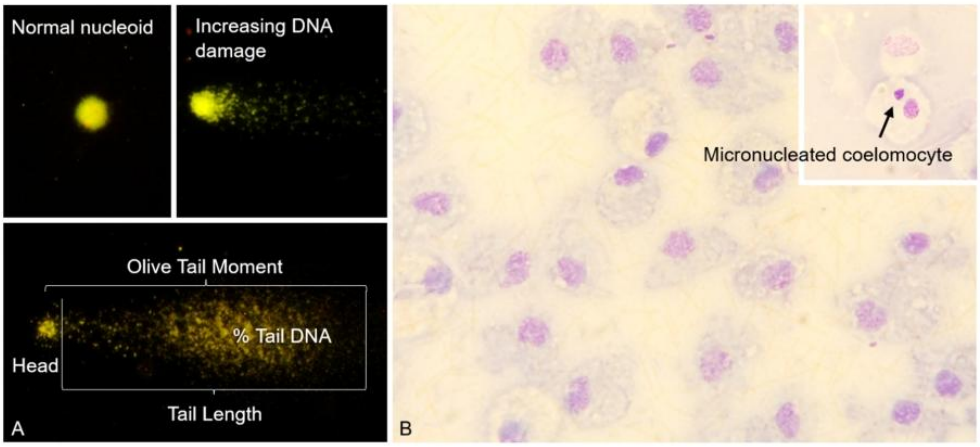

Fig. 2. Photomicrographs illustrating the genetic biomarkers analyzed in coelomocytes of *Eisenia fetida* earthworms: A) Comet assay; B) Micronucleus test.

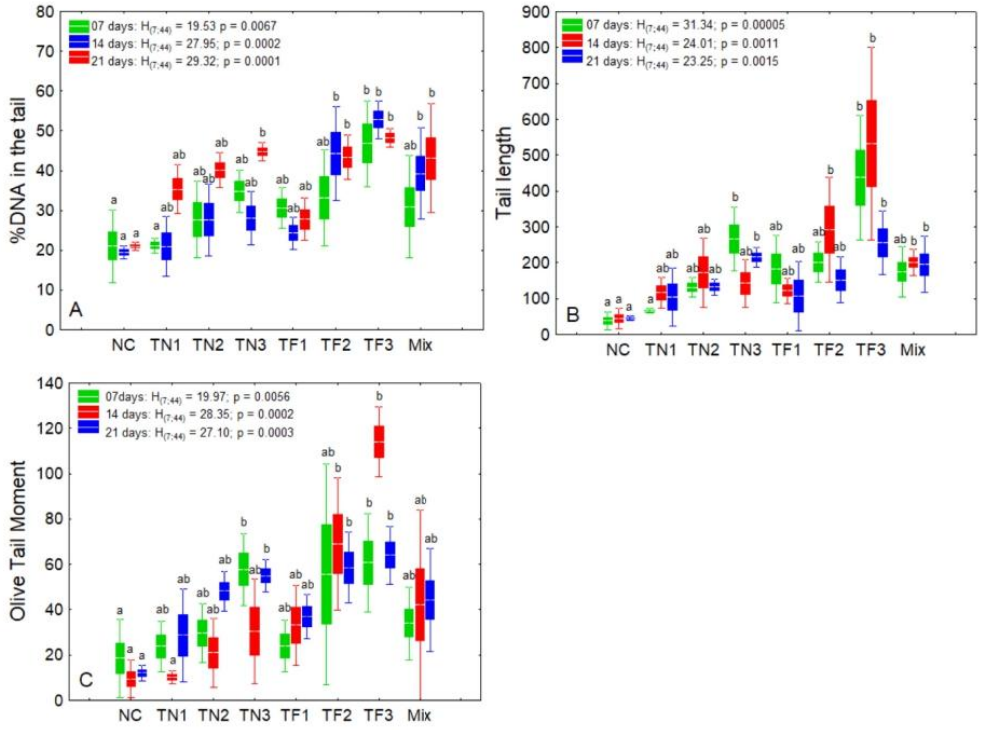

Fig. 3. Genotoxic effect of triadimefon, triadimenol, and their mixture in earthworms of the species *Eisenia fetida* exposed for 07, 14, and 21 days. Different letters compared to the control indicate a statistically significant difference; same letters or absence of letters indicate no significant difference. Kruskal-Wallis followed by Dunn's post hoc test. NC: Negative control; Triadimenol: TN1 (1.5 mg/kg); TN2 (3 mg/kg) and TN3 (6 mg/kg); Triadimefon: TF1 (0.06 mg/kg); TF2 (0.012 mg/kg) and TF3 (0.024 mg/kg); Mix: TN2 (3 mg/kg) + TF2 (0.012 mg/kg).

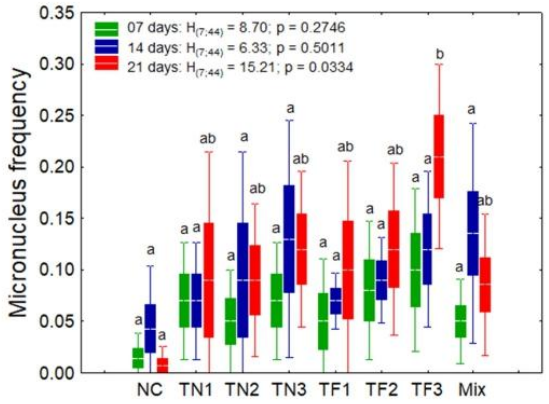

Fig. 4. Micronucleus frequency as a biomarker for *genotoxicity* of triadimefon, triadimenol, and their mixture in *Eisenia fetida* earthworms exposed for 07, 14, and 21 days. Absence of letters on the box plots indicates no significant difference. Kruskal-Wallis followed by Dunn's post hoc test. NC: Negative control; Triadimenol: TN1 (1.5 mg/kg); TN2 (3 mg/kg) and TN3 (6 mg/kg); Triadimefon: TF1 (0.06 mg/kg); TF2 (0.012 mg/kg) and TF3 (0.024 mg/kg); Mix: TN2 (3 mg/kg) + TF2 (0.012 mg/kg).

with a maximum increase of 73% in tail DNA (Ray et al., 2025). The triazole-based fungicide Prosaro® (tebuconazole 125 g/L and prothioconazole 125 g/L) acted directly on the DNA of *Eisenia fetida* earthworms (Campani et al., 2024). For rural workers exposed to triazoles, greater genotoxic damage was observed via the micronucleus test in exfoliated buccal mucosa cells (Costa et al., 2023). That study quantified the presence of cyproconazole, epoxiconazole, metconazole, propiconazole, and triadimenol in the urine of the rural workers.

Although triadimenol and triadimefon are widely used and detected in environmental matrices, studies on their genotoxic and mutagenic effects remain insufficient, particularly in earthworms. In the case of triadimefon, the review by Hou et al. (2022) also confirms that there are few studies with invertebrates and that more comprehensive investigations are needed. Therefore, this study highlights the genotoxic and mutagenic effects at low doses over different exposure times. Future studies are encouraged to combine these genetic biomarkers with biochemical ones such as Catalase, Superoxide Dismutase, Glutathione S-transferase, Malondialdehyde, Nitric oxide, Carbonylated proteins, and Total proteins. These analyses are critical because it is recognized that many pesticides can induce various reactions in animals, including the generation of Reactive Oxygen Species and alterations in antioxidant levels, leading to a state of redox imbalance and causing DNA damage (Sotero et al., 2024).

3.2.2. *Integrated results of genotoxicity (principal component analysis)*

Principal Component Analysis (PCA) was used to integrate genotoxicity biomarkers in *Eisenia fetida* in response to the triazoles triadimenol, triadimefon, and their mixture over exposure periods of 7, 14, and 21 days. The first two principal components jointly explained 60.07% of the total variance, with PC1 accounting for 48.57% and PC2 for 11.50% (Fig. 5; Supplementary Material 1). The negative control (NC), positioned opposite to the treatments, indicated low levels of

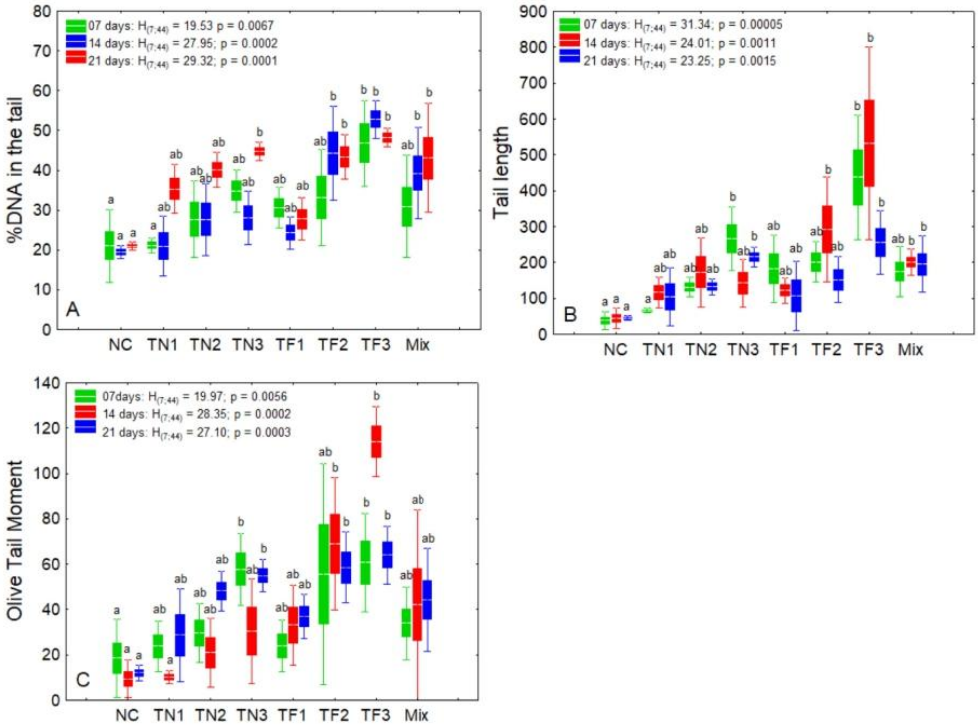

Fig. 3. Genotoxic effect of triadimefon, triadimenol, and their mixture in earthworms of the species *Eisenia fetida* exposed for 07, 14, and 21 days. Different letters compared to the control indicate a statistically significant difference; same letters or absence of letters indicate no significant difference. Kruskal-Wallis followed by Dunn's post hoc test. NC: Negative control; Triadimenol: TN1 (1.5 mg/kg); TN2 (3 mg/kg) and TN3 (6 mg/kg); Triadimefon: TF1 (0.06 mg/kg); TF2 (0.012 mg/kg) and TF3 (0.024 mg/kg); Mix: TN2 (3 mg/kg) + TF2 (0.012 mg/kg).

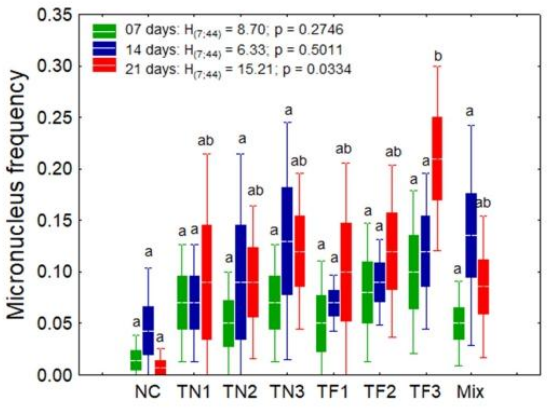

Fig. 4. Micronucleus frequency as a biomarker for *genotoxicity* of triadimefon, triadimenol, and their mixture in *Eisenia fetida* earthworms exposed for 07, 14, and 21 days. Absence of letters on the box plots indicates no significant difference. Kruskal-Wallis followed by Dunn's post hoc test. NC: Negative control; Triadimenol: TN1 (1.5 mg/kg); TN2 (3 mg/kg) and TN3 (6 mg/kg); Triadimefon: TF1 (0.06 mg/kg); TF2 (0.012 mg/kg) and TF3 (0.024 mg/kg); Mix: TN2 (3 mg/kg) + TF2 (0.012 mg/kg).

with a maximum increase of 73% in tail DNA (Ray et al., 2025). The triazole-based fungicide Prosaro® (tebuconazole 125 g/L and prothioconazole 125 g/L) acted directly on the DNA of *Eisenia fetida* earthworms (Campani et al., 2024). For rural workers exposed to triazoles, greater genotoxic damage was observed via the micronucleus test in exfoliated buccal mucosa cells (Costa et al., 2023). That study quantified the presence of cyproconazole, epoxiconazole, metconazole, propiconazole, and triadimenol in the urine of the rural workers.

Although triadimenol and triadimefon are widely used and detected in environmental matrices, studies on their genotoxic and mutagenic effects remain insufficient, particularly in earthworms. In the case of triadimefon, the review by Hou et al. (2022) also confirms that there are few studies with invertebrates and that more comprehensive investigations are needed. Therefore, this study highlights the genotoxic and mutagenic effects at low doses over different exposure times. Future studies are encouraged to combine these genetic biomarkers with biochemical ones such as Catalase, Superoxide Dismutase, Glutathione S-transferase, Malondialdehyde, Nitric oxide, Carbonylated proteins, and Total proteins. These analyses are critical because it is recognized that many pesticides can induce various reactions in animals, including the generation of Reactive Oxygen Species and alterations in antioxidant levels, leading to a state of redox imbalance and causing DNA damage (Sotero et al., 2024).

3.2.2. *Integrated results of genotoxicity (principal component analysis)*

Principal Component Analysis (PCA) was used to integrate genotoxicity biomarkers in *Eisenia fetida* in response to the triazoles triadimenol, triadimefon, and their mixture over exposure periods of 7, 14, and 21 days. The first two principal components jointly explained 60.07% of the total variance, with PC1 accounting for 48.57% and PC2 for 11.50% (Fig. 5; Supplementary Material 1). The negative control (NC), positioned opposite to the treatments, indicated low levels of

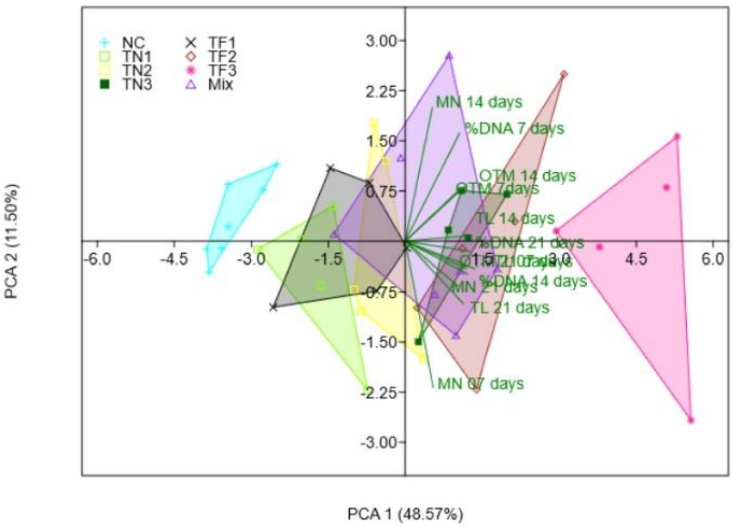

Fig. 5. Principal Component Analysis of genotoxicity and mutagenicity biomarkers for the effects of triazoles after 7, 14, and 21 days of exposure in *Eisenia fetida*. NC: negative control; Triadimenol: TN1 (1.5 mg/kg); TN2 (3 mg/kg) and TN3 (6 mg/kg); Triadimefon: TF1 (0.06 mg/kg); TF2 (0.012 mg/kg) and TF3 (0.024 mg/kg); Mix: TN2 (3 mg/kg) + TF2 (0.012 mg/kg).

genetic damage, as expected. In contrast, treatments with TN, TF, and the mixture showed displacement along PC1, evidencing the induction of genotoxic and mutagenic effects.

A concentration-dependent trend was observed for triadimenol, with treatments progressively distributed farther from the NC. This pattern suggests a dose–response relationship, in which increasing concentrations result in greater DNA damage intensity. For triadimefon, even intermediate concentrations (TF2) were already associated with genotoxic biomarkers, indicating higher toxicity compared to triadimenol. The TF3 treatment (0.024 mg/kg) showed the greatest separation from the control, reinforcing the high genotoxic and mutagenic potential of this compound. The triazole mixture was consistently positioned far from the control and close to the biomarker vectors, particularly at 14 and 21 days. This pattern suggests additive or possibly synergistic effects, indicating that simultaneous exposure to these compounds represents a higher genetic risk scenario than individual exposure.

Comet assay parameters (%DNA, TL, and OTM) showed strong positive correlations with each other, indicating the occurrence of primary DNA damage. These biomarkers were mainly associated with the 14- and 21-day exposures, suggesting an accumulation of genetic lesions over time. In contrast, the micronucleus test exhibited a distinct temporal response. While micronuclei at 7 days contributed less to group separation, micronuclei observed primarily at 21 days suggest that initial DNA damage evolved into fixed chromosomal alterations.

Overall, PCA demonstrates that triazoles induce genotoxic effects in *Eisenia fetida* in a manner dependent on concentration, compound type, and exposure time. Triadimefon stood out for its high toxicity even at lower concentrations, and the pesticide mixture represented a significant genetic risk. The consistency between comet assay biomarkers and the micronucleus test highlights the progression of genetic damage, from initial DNA lesions to permanent chromosomal alterations. Particular attention should be given to triadimefon due to its capacity to act synergistically with other pesticides, as previously reported. For example, the mixture of fludioxonil and triadimefon showed a synergistic response affecting zebrafish development (Wang et al., 2020). Similarly, binary mixtures of fenvalerate and triadimefon may simultaneously induce endocrine disruption and oxidative stress in a synergistic manner during embryonic development in medaka fish (Wu et al., 2018).

4. Conclusions

In summary, exposure of *Eisenia fetida* to the triazole fungicides triadimefon and triadimenol resulted in a significant reduction in biomass from day 14 onward, indicating sublethal effects associated with metabolic stress and potential alterations in nutrient assimilation. This stress likely impacts earthworm reproduction, survival, and ecological functions, though further investigation is required. Regarding cytogenetic biomarkers, both compounds induced genotoxic damage detected by the comet assay, particularly at higher concentrations and over prolonged exposure times. Triadimefon demonstrated greater toxicity, including mutagenicity in the micronucleus test after 21 days, while triadimenol did not significantly increase micronucleus frequency. The results highlight that, even with low mortality, triazoles compromise the physiological condition and genetic integrity of earthworms, underscoring potential ecological risks to soil and biota.

CRediT authorship contribution statement

Elisa Flávia Luiz Cardoso Bailão: Writing – original draft. **Luciane Madureira de Almeida:** Resources. **Leonardo Luiz Borges:** Writing – original draft, Project administration, Formal analysis. **Antônio Sérgio Nakao de Aguiar:** Writing – original draft, Supervision. **Marcelino Benvindo-Souza:** Validation, Investigation, Formal analysis, Data curation. **Áureo Barbosa de Souza:** Methodology, Investigation. **Amanda Silva Fernandes:** Writing – original draft, Visualization, Validation.

Consent to Publish

All authors agree to the publication.

Declaration of Competing Interest

The authors declare that they have no known competing financial interests or personal relationships that could have appeared to influence the work reported in this paper.

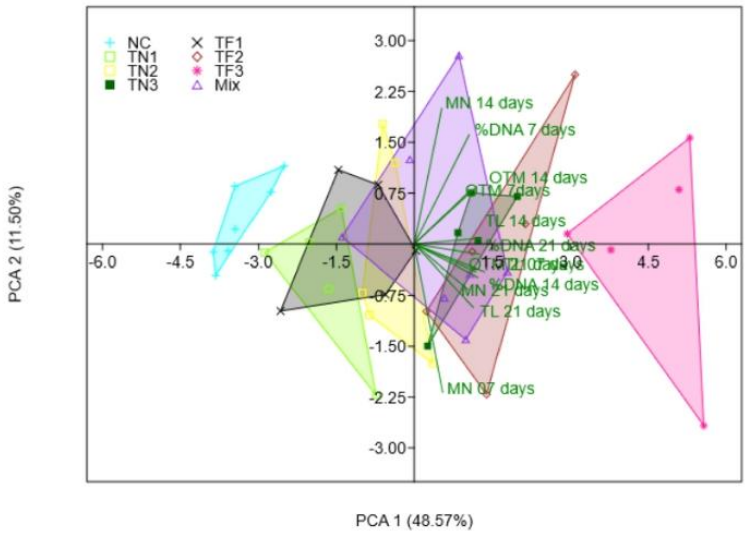

Fig. 5. Principal Component Analysis of genotoxicity and mutagenicity biomarkers for the effects of triazoles after 7, 14, and 21 days of exposure in *Eisenia fetida*. NC: negative control; Triadimenol: TN1 (1.5 mg/kg); TN2 (3 mg/kg) and TN3 (6 mg/kg); Triadimefon: TF1 (0.06 mg/kg); TF2 (0.012 mg/kg) and TF3 (0.024 mg/kg); Mix: TN2 (3 mg/kg) + TF2 (0.012 mg/kg).

genetic damage, as expected. In contrast, treatments with TN, TF, and the mixture showed displacement along PC1, evidencing the induction of genotoxic and mutagenic effects.

A concentration-dependent trend was observed for triadimenol, with treatments progressively distributed farther from the NC. This pattern suggests a dose–response relationship, in which increasing concentrations result in greater DNA damage intensity. For triadimefon, even intermediate concentrations (TF2) were already associated with genotoxic biomarkers, indicating higher toxicity compared to triadimenol. The TF3 treatment (0.024 mg/kg) showed the greatest separation from the control, reinforcing the high genotoxic and mutagenic potential of this compound. The triazole mixture was consistently positioned far from the control and close to the biomarker vectors, particularly at 14 and 21 days. This pattern suggests additive or possibly synergistic effects, indicating that simultaneous exposure to these compounds represents a higher genetic risk scenario than individual exposure.

Comet assay parameters (%DNA, TL, and OTM) showed strong positive correlations with each other, indicating the occurrence of primary DNA damage. These biomarkers were mainly associated with the 14- and 21-day exposures, suggesting an accumulation of genetic lesions over time. In contrast, the micronucleus test exhibited a distinct temporal response. While micronuclei at 7 days contributed less to group separation, micronuclei observed primarily at 21 days suggest that initial DNA damage evolved into fixed chromosomal alterations.

Overall, PCA demonstrates that triazoles induce genotoxic effects in *Eisenia fetida* in a manner dependent on concentration, compound type, and exposure time. Triadimefon stood out for its high toxicity even at lower concentrations, and the pesticide mixture represented a significant genetic risk. The consistency between comet assay biomarkers and the micronucleus test highlights the progression of genetic damage, from initial DNA lesions to permanent chromosomal alterations. Particular attention should be given to triadimefon due to its capacity to act synergistically with other pesticides, as previously reported. For example, the mixture of fludioxonil and triadimefon showed a synergistic response affecting zebrafish development (Wang et al., 2020). Similarly, binary mixtures of fenvalerate and triadimefon may simultaneously induce endocrine disruption and oxidative stress in a synergistic manner during embryonic development in medaka fish (Wu et al., 2018).

4. Conclusions

In summary, exposure of *Eisenia fetida* to the triazole fungicides triadimefon and triadimenol resulted in a significant reduction in biomass from day 14 onward, indicating sublethal effects associated with metabolic stress and potential alterations in nutrient assimilation. This stress likely impacts earthworm reproduction, survival, and ecological functions, though further investigation is required. Regarding cytogenetic biomarkers, both compounds induced genotoxic damage detected by the comet assay, particularly at higher concentrations and over prolonged exposure times. Triadimefon demonstrated greater toxicity, including mutagenicity in the micronucleus test after 21 days, while triadimenol did not significantly increase micronucleus frequency. The results highlight that, even with low mortality, triazoles compromise the physiological condition and genetic integrity of earthworms, underscoring potential ecological risks to soil and biota.

CRediT authorship contribution statement

Elisa Flávia Luiz Cardoso Bailão: Writing – original draft. **Luciane Madureira de Almeida:** Resources. **Leonardo Luiz Borges:** Writing – original draft, Project administration, Formal analysis. **Antônio Sérgio Nakao de Aguiar:** Writing – original draft, Supervision. **Marcelino Benvindo-Souza:** Validation, Investigation, Formal analysis, Data curation. **Áureo Barbosa de Souza:** Methodology, Investigation. **Amanda Silva Fernandes:** Writing – original draft, Visualization, Validation.

Consent to Publish

All authors agree to the publication.

Declaration of Competing Interest

The authors declare that they have no known competing financial interests or personal relationships that could have appeared to influence the work reported in this paper.

Acknowledgments

We appreciate the support of the Rede Hidro Cerrado: Rede de Pesquisa em Segurança Hídrica e Sociobiodiversidade para o Desenvolvimento Sustentável do Cerrado (CAPES and FAPEG, n.88881.986044/2024–01). We also thank the Fundação de Amparo à Pesquisa do Estado de Goiás (FAPEG) for funding through projects 21/2024. LMA acknowledges the grant of the Research Productivity Fellowship – CNPq, process no. 305180/2025-8 and the Fundação de Apoio ao Desenvolvimento do Ensino, Ciência e Tecnologia do Estado de Mato Grosso do Sul (Fundect-MS) for funding through projects 20/2023, process no. 202410267000982. EFLCB is granted with productivity fellowship from FAPEG (process no. 202510267001605). MBS also expresses gratitude for the CAPES research grant. We are also grateful for the financial support of the Fundação de Apoio ao Desenvolvimento do Ensino, Ciência e Tecnologia do Estado de Mato Grosso do Sul (Fundect-MS) and the research network on Desenvolvimento de Bioinsumos e Bioeconomia com foco na pecuária.

Appendix A. Supporting information

Supplementary data associated with this article can be found in the online version at doi:10.1016/j.etap.2026.105018.

Data availability

Data will be made available on request.

References

Aliste, M., Pérez-Lucas, G., Garrido, I., Fenoll, J., Navarro, S., 2021. Risk assessment of 1,2,4-triazole-typed fungicides for groundwater pollution using leaching potential indices. Water Air Soil Pollut. 232. https://doi.org/10.1007/S11270-021-05428-1.

Bart, S., Laurent, C., Pery, A.R., Mougin, C., Pelosi, C., 2017. Differences in sensitivity between earthworms and enchytraeids exposed to two commercial fungicides. Ecotoxicol. Environ. Saf. 140, 177–184. https://doi.org/10.1016/j.ecoenv.2017.02.052.

Benvindo-Souza, M., Araújo dos Santos, C.G., Alves de Assis, R., Borges, R.E., Raquel de Souza Santos, L., Salla, R.F., Luiz Cardoso Bailão, E.F., Mendonça do Prado, V.H., 2025. The impact of pollution from road runoff on lesser treefrogs, Dendropsophus minutus (Anura: Hylidae). Environmental Research 271, 121144. https://doi.org/10.1016/j.envres.2025.121144.

Campani, T., Casini, S., Maccantelli, A., Tosoni, F., D'Agostino, A., Caliani, I., 2024. Oxidative stress and DNA alteration on the earthworm Eisenia fetida exposed to four commercial pesticides. Environmental Science and Pollution Research 31 (24), 35969–35978. https://doi.org/10.1007/s11356-024-33511-7.

Cooper, E.L., Goven, A.J., Fitzpatrick, L.C., Venables, B.J., 1991. A non-invasive technique for sequential collection of earthworm (Lumbricus terrestris) leukocytes during subchronic immunotoxicity studies. Laboratory Animals 25, 61–67. https://doi.org/10.1258/002367791780808095.

Costa, L.F., Marciano, L.P.A, Feltrim, F., Freire, J.O., Silva, G.B., Silvério, A.C.P, Martins, I., 2023. Assessment of cellular damage with cytome assay among environmental/occupational triazole. Chemico-Biological Interactions 383, 110689. https://doi.org/10.1016/j.cbi.2023.110689.

Crowell, S.R., Henderson, W.M., Kenneke, J.F., Fisher, J.W., 2011. Development and application of a physiologically based pharmacokinetic model for triadimefon and its metabolite triadimenol in rats and humans. Toxicol. Lett. 205, 154–162. https://doi.org/10.1016/J.TOXLET.2011.05.1036.

Gao, M., Song, W., Zhang, J., Guo, J., 2013. Effect on enzymes and histopathology in earthworm (*Eisenia foetida*) induced by triazole fungicides. Environ. Toxicol. Pharm. 35, 427–433. https://doi.org/10.1016/j.etap.2013.02.003.

Garrison, A.W., Avants, J.K., Jones, W.J., 2011. Microbial transformation of triadimefon to triadimenol in soils: selective production rates of triadimenol stereoisomers affect exposure and risk. Environ. Sci. Technol. 45, 2186–2193. https://doi.org/10.1021/es103430s.

Hou, L., Jin, X., Liu, N., Luo, Y., Yan, Z., Chen, M., Liu, Y., Xie, H., Giesy, J.P., Wu, F., Xu, J., 2022. Triadimefon in aquatic environments: occurrence, fate, toxicity, and ecological risk, 34 Environ. Sci. Eur. 2022 34 (1), 12. https://doi.org/10.1186/S12302-022-00590-7.

Hou, L., Jin, X., Liu, N., Luo, Y., Liao, J., Guo, C., Xu, J., 2023. Effects of triadimefon fungicide on *Daphnia magna*: Multigenerational effect and population-level ecological risk. J. Environ. Manag. 339, 117822. https://doi.org/10.1016/j.jenvman.2023.117822.

How, C.M., Li, S.W., Liao, V.H.C., 2018. Chronic exposure to triadimenol at environmentally relevant concentration adversely affects aging biomarkers in Caenorhabditis elegans associated with insulin/IGF-1 signaling pathway. Sci. Total Environ. 485–492. https://doi.org/10.1016/J.SCITOTENV.2018.05.314, 640641.

Jovana, M., Tanja, M., Mirjana, S., 2014. Effects of three pesticides on the earthworm Eisenia fetida (Savigny 1826) under laboratory conditions: Assessment of mortality, biomass and growth inhibition. European Journal of Soil Biology 62, 127–131. https://doi.org/10.1016/j.ejsobi.2014.03.003.

Kevekordes, S., Gebel, T., Pav, K., Edenharder, R., Dunkelberg, H., 1996. Genotoxicity of selected pesticides in the mouse bone-marrow micronucleus test and in the sister-chromatid exchange test with human lymphocytes in vitro. Toxicology Letters 89, 35–42. https://doi.org/10.1016/s0378-4274(96)03779-4.

Kong, Z., Quan, R., Fan, B., Liao, Y., Chen, J., Li, M., Dai, X., 2020. Stereoselective behaviors of the fungicide triadimefon and its metabolite triadimenol during malt storage and beer brewing. J. Hazard Mater. 400, 123238. https://doi.org/10.1016/J.JHAZMAT.2020.123238.

Lammertyn, S., Magni, F.V., Durán, A., Repetti, M.R., Godoy, J.L., Zalazar, C.S., 2024. Earthworm injury test for in-situ biomonitoring of pesticides in biobeds. Chemosphere 363. https://doi.org/10.1016/j.chemosphere.2024.142923.

Li, Jitong, Wang, Y., Li, W., Xu, P., Guo, B., Li, Jianzhong, Wang, H., 2017. Tissue distribution and metabolism of triadimefon and triadimenol enantiomers in Chinese lizards (Eremias argus). Ecotoxicol. Environ. Saf. 142, 284–292. https://doi.org/10.1016/J.ECOENV.2017.04.035.

Li, Z., Zhang, Y., Li, Q., Wang, W., Li, J., 2011a. Enantioselective degradation, abiotic racemization, and chiral transformation of triadimefon in soils. Environ. Sci. Technol. 45, 2797–2803. https://doi.org/10.1021/ES103830Z.

Li, Z., Zhang, Y., Li, Q., Wang, W., Li, J., 2011b. Enantioselective degradation, abiotic racemization, and chiral transformation of triadimefon in soils. Environ. Sci. Technol. 45, 2797–2803. https://doi.org/10.1021/es103830z.

Liu, T., Diao, J., Di, S., Zhou, Z., 2014. Stereoselective Bioaccumulation and Metabolite Formation of Triadimefon in Tubifex tubifex. Environ. Sci. Technol. 48, 6687–6693. https://doi.org/10.1021/ES5000287.

Malik, N.A., Nazir, N., Manzoor, M., Gull, F., 2024. Fungicide-albumin interactions: unraveling the complex relationship—a comprehensive review. Biophys. Rev. 164 (16), 417439. https://doi.org/10.1007/S12551-024-01190-W.

Martyniuk, J., Goc Rasgele, P., 2025. Comparative Assessment of Short- and Long-Term Effects of Triadimenol Fungicide on Danio rerio Erythrocytes Using the Micronucleus and Erythrocyte Nuclear Abnormality Assays. Toxics 13 (3), 199. https://doi.org/10.3390/toxics13030199.

Mishra, C.S.K., Samal, S., Samal, R.R., 2022. Evaluating earthworms as candidates for remediating pesticide contaminated agricultural soil: a review. Front. Environ. Sci. 10, 924480. https://doi.org/10.3389/FENVS.2022.924480/XML.

Nasonov, A.I., Yakuba, G.V., 2024. Apple scab: resistance to chemical fungicides. BioBR 14, S17–S30. https://doi.org/10.1134/S2079086424600802.

OECD, 1984. Test No. 207: Earthworm, Acute Toxicity Tests | OECD [WWW Document]. URL https://www.oecd.org/en/publications/test-no-207-earthworm-acute-toxicity-tests_9789264070042-en.html (accessed 12.2.25).

Pelosi, C., Barot, S., Capowiez, Y., Hedde, M., Vandenbulcke, F., 2014. Pesticides and earthworms. A review. Agron. Sustain. Dev. 34, 199–228. https://doi.org/10.1007/s13593-013-0151-z.

Qiao, K., Fu, W., Jiang, Y., Chen, L., Li, S., Ye, Q., Gui, W., 2020. QSAR models for the acute toxicity of 1,2,4-triazole fungicides to zebrafish (Danio rerio) embryos. Environmental Pollution 265. https://doi.org/10.1016/j.envpol.2020.114837.

Ray, A., Dutta, D., Sarkar, A., Bahadur, M., 2025. Evaluation of toxic effects of a triazole fungicide, difenoconazole in a freshwater fish model. Ecotoxicology 2025 34:8 34, 1368–1383. https://doi.org/10.1007/S10646-025-02926-4.

Rico, A., Sabater, C., Castillo, M.Á., 2016. Lethal and sub-lethal effects of five pesticides used in rice farming on the earthworm *Eisenia fetida*. Ecotoxicol. Environ. Saf. 127, 222–229. https://doi.org/10.1016/j.ecoenv.2016.02.004.

Shao, Y., Hou, K., Du, Z., Li, B., Wang, J., Juhasz, A., Wang, I., Zhu, L., 2019. Evaluation of the toxicity of 1-butyl-3-methyl imidazolium tetrafluoroborate using earthworms (*Eisenia fetida*) in two soils. Sci. Total Environ. 686, 946–958. https://doi.org/10.1016/j.scitotenv.2019.06.010.

Silva, H.E., Benvindo-Souza, M., e Silva, D.D.M., Antoniosi Filho, N.R., 2023. Genotoxic and mutagenic evaluation in *Eisenia foetida* annelids exposed to iron ore tailings from the region of Brumadinho, MG, Brazil. Environ. Toxicol. Pharmacol. 102, 104247. https://doi.org/10.1016/j.etap.2023.104247.

Singh, N., 2005. Factors affecting triadimefon degradation in soils. J. Agric. Food Chem. 53, 70–75. https://doi.org/10.1021/JF048884J.

Sotero, D.F., de Freitas, R.M.P., Virote, A.J.P.P., Benvindo-Souza, M., Tavares, G.R.G., Bastos, R.P., Carvalho, P., Silva, D.D.M., 2024. Can Salvinia auriculata bioremediate the toxic effects of Fipronil 800wg on the tadpoles of *Dendropsophus minutus*? Aquat. Toxicol. 271, 106926. https://doi.org/10.1016/j.aquatox.2024.106926.

Sun, S., Yan, J., Tai, L., Chai, J., Hu, H., Han, L., Lu, A., Yang, C., Chen, M., 2023. Novel (Z)/(*E*)-1,2,4-triazole derivatives containing oxime ether moiety as potential ergosterol biosynthesis inhibitors: design, preparation, antifungal evaluation, and molecular docking. Mol. Divers 27, 145–157. https://doi.org/10.1007/S11030-022-10412-W.

Tang, Y., Liu, Y., Jin, Y., Zhang, F., Zhang, W., Luo, S., Zang, J., Yang, W., Chen, Y., 2024. Toxicological risk assessment of triadimenol for human exposure, broiler health, and food safety. Food Chem. Toxicol. 194. https://doi.org/10.1016/j.fct.2024.115071.

Wang, Y., Xu, C., Wang, D., Weng, H., Yang, G., Guo, D., Yu, R., Wang, X., Wang, Q., 2020. Combined toxic effects of fludioxonil and triadimefon on embryonic development of zebrafish (*Danio rerio*). Environ. Pollut. 260, 114105. https://doi.org/10.1016/j.envpol.2020.114105.

Wu, S., Hu, G., Zhao, X., Wang, Q., Jiang, J., 2018. Synergistic potential of fenvalerate and triadimefon on endocrine disruption and oxidative stress during rare minnow embryo development. Environ. Toxicol. 33 (7), 759–769. https://doi.org/10.1002/tox.22563.

Xue, P., Liu, X., Shi, X., Yuan, H., Wang, J., Zhang, J., He, Z., 2023. Stereoselective accumulation and biotransformation of chiral fungicide epoxiconazole and oxidative stress, detoxification, and endogenous metabolic disturbance in earthworm (Eisenia foetida). Science of The Total Environment 858, 159932. https://doi.org/10.1016/j.scitotenv.2022.159932.

Yasmin, S., D'Souza, D., 2007. Effect of pesticides on the reproductive output of *Eisenia fetida*. Bull. Environ. Contam. Toxicol. 79, 529–532. https://doi.org/10.1007/s00128-007-9269-5.

Zhang, W., Deng, Y., Chen, L., Zhang, L., Wang, Z., Liu, R., Diao, J., Zhou, Z., 2020. Effect of triadimefon and its metabolite on adult amphibians *Xenopus laevis*. Chemosphere 243. https://doi.org/10.1016/j.chemosphere.2019.125288.

Zhang, W., Lu, Y., Huang, L., Cheng, C., Di, S., Chen, L., Zhou, Z., Diao, J., 2018. Comparison of triadimefon and its metabolite on acute toxicity and chronic effects during the early development of *Rana nigromaculata* tadpoles. Ecotoxicol. Environ. Saf. 156, 247–254. https://doi.org/10.1016/j.ecoenv.2018.03.009.

Zhou, D., Ning, Y., Wang, B., Wang, G., Su, Y., Li, L., Wang, Y., 2016. Study on the influential factors of Cd2+ on the earthworm *Eisenia fetida* in oxidative stress based on factor analysis approach. Chemosphere 157, 181–189. https://doi.org/10.1016/j.chemosphere.2016.05.045.

Zhuo, Y., Yang, Y., Zhang, H., Wang, X., Cao, M., Wang, Y., 2025. Toxicological evaluation and metabolic profiling of earthworms (*Eisenia fetida*) after exposure to microplastics and acetochlor. Environ. Res. 276, 121546. https://doi.org/10.1016/J.ENVRES.2025.121546.